CHIRAL MAGNETIC AND VORTICAL EFFECTS IN RELATIVISTIC HEAVY ION COLLISIONS

A Dissertation

by

YIFENG SUN

Submitted to the Office of Graduate and Professional Studies of
Texas A&M University
in partial fulfillment of the requirements for the degree of

DOCTOR OF PHILOSOPHY

Chair of Committee,	Che-Ming Ko
Committee Members,	Charles M. Folden III
	Rainer Fries
	Carl A. Gagliardi
	Ralf Rapp
Head of Department,	Peter McIntyre

December 2017

Major Subject: Physics

ABSTRACT

In the present dissertation, the derivation of the chiral magnetic effect (CME) and chiral separation effect (CSE) from the Hamiltonian of Dirac fermions in a magnetic field is given. It is shown that the CSE is related to the spin polarization vector of massless fermions and becomes less important when fermions are massive. The chiral kinetic equations for massless fermions in a magnetic field are also derived from the Lagrangian of a massless fermion either using the semiclassical approximation or by solving the Dirac equation. The chiral vortical effect (CVE) and chiral vortical separation effect (CVSE) are similarly derived as for the case of the CME and CSE. The interplay between the vector and axial vector charge densities can generate two kinds of gapless collective modes, called the chiral magnetic wave (CMW) and the chiral vortical wave (CVW), and both can be derived in the hydrodynamic and kinetic approaches. Effects of the CMW and CVW in relativistic heavy ion collisions are then studied by solving the chiral kinetic equations numerically using the test-particle method. It is found that, the CMW generated by the magnetic field in a quark matter with its initial conditions modeled by the Bjorken boost-invariant model can lead to different elliptic flows for particles of positive and negative charges if the chirality changing scattering (CCS) between massless quarks and antiquarks is included. Neglecting the Lorentz force acting on quarks and antiquarks as in other studies, it is found that the obtained elliptic flow splitting depends linearly on the charge asymmetry of the quark matter, similar to that measured in experiments at RHIC. The magnitude of the splitting is, however, less than the experimental results even if the magnetic field is taken to have a long lifetime. The presence of a vorticity field in the quark matter is found to only lead to an axial dipole moment in the

transverse plane but not an elliptic flow splitting between particles of positive and negative charges. Including effects from both the magnetic field and the vorticity field can, on the other hand, leads to the splitting between the elliptic flows of positively and negatively charged particles even for quark matter of zero charge asymmetry. However, the inclusion of the Lorentz force changes the sign of the slope of the charge asymmetry dependence of the elliptic flow splitting, leading to a result opposite to that from the experiments and thus making it unlikely that the observed elliptic flow splitting between charged particles is due to the CMW. Including in quark scattering the correction to the phase-space measure due to the vorticity field, the chiral kinetic equations are also used to study the spin polarization of light quarks in a rotating quark matter with its initial conditions taken from a multiphase transport (AMPT) model. Converting the spin-polarized light quarks to hadrons using the quark coalescence model leads to the spin polarizations of Λ and $\overline{\Lambda}$ hyperons that are comparable with experimental results both in magnitude and trend as a function of collision energy.

DEDICATION

This dissertation is dedicated to my parents, Fengcai Wang and Shaoying Sun, and my younger sister, Hanxiao Sun, for their unconditional love and support.

ACKNOWLEDGEMENTS

First of all, I would like to thank my dissertation advisor, Prof. Che-Ming Ko, who gave me so much support and guidance throughout the course of my research with patience and dedication. He gave the best guidance I ever had with his endless enthusiasm and immense knowledge. I am also grateful to my committee members, Prof. Charles M. Folden III, Prof. Rainer Fries, Prof. Carl A. Gagliardi, Prof. Jeremy W. Holt and Prof. Ralf Rapp for giving me insightful comments and suggestions.

I would like to express my sincere gratitude to my former colleague in Prof. Ko's group, Dr. Feng Li, who gave me much help, feedback and valuable suggestions throughout my research. I also give my gratitude to my former colleague in Prof. Ko's group, Dr. Kyong Chol Han, who gave me valuable feedback and suggestions.

Thanks also go to the faculty, staff and fellow graduate students at the Cyclotron Institute, Prof. Saskia Mioduszewski, Ms. Paula Barton, Shuai Liu, Yanfang Liu, Zhidong Yang and Xiaojian Du.

CONTRIBUTORS AND FUNDING SOURCES

Contributors

This work was supervised by a dissertation committee consisting of Professor Che-Ming Ko and Professors Rainer Fries, Carl A. Gagliardi and Ralf Rapp of the Department of Physics and Professor Charles M. Folden III of the Department of Chemistry.

All work for the dissertation was completed by the student, under the advisement of Che-Ming Ko of the Department of Physics.

Funding Sources

This material is based upon work supported in part by the US Department of Energy under Contract No. DE-SC0015266 and the Welch Foundation under Grant No. A-1358.

NOMENCLATURE

QCD	Quantum Chromodynamics
CME	Chiral Magnetic Effect
CVE	Chiral Vortical Effect
CSE	Chiral Separation Effect
CVSE	Chiral Vortical Separation Effect
CMW	Chiral Magnetic Wave
CVW	Chiral Vortical Wave
CKM	Chiral Kinetic Motion
LF	Lorentz Force
CCS	Chirality Changing Scattering

TABLE OF CONTENTS

Page

LIST OF FIGURES

FIGURE Page

1. INTRODUCTION

The fundamental force that governs the dynamics of quarks and gluons, which are the smallest building blocks of all matter known to date, is described by the SU(3) gauge theory called quantum chromodynamics (QCD). Because of its non-abelian nature, QCD differs from quantum electrodynamics (QED) that governs the dynamics of particles carrying electric charge and photons, particularly in its two unique features of asymptotic freedom [8, 9] and color confinement. The former refers to the fact that interactions between quarks and gluons become increasingly weaker at high energy and small distance, while the latter implies that no colored quarks and anitquarks can exist in isolation and they form instead bound hadrons when their energies are low and separations become large. A transition from confined hadrons to deconfined quarks and gluons, called the quark-gluon plasma (QGP), is expected to occur at high temperature and density, such as in the matter produced in collisions of heavy ions at relativistic energies and the interior of neutron stars. Together with the deconfinement transition, the hot dense matter produced in relativistic heavy ion collisions also undergoes the chiral transition from the broken phase of massive light quarks and antiquarks [10] to the restored phase of almost massless quarks and antiquarks. Studying the deconfinement and chiral phase transitions in hot dense matter is a major goal of the experiments at the BNL Relativistic Heavy Ion Collider (RHIC) [11, 12, 13, 14] and the CERN Large Hadron Collider (LHC) [15].

In the chirally restored phase, light quarks become almost massless and thus have definite chirality or helicity that their spins point either along or opposite to the directions of their momenta, called right-handed or left-handed, respectively. Many novel phenomena as a result of this transition have recently attracted a lot

of interest. Among them is the existence of a non-trivial gauge field configuration in QCD vacuum that can be characterized by a non-zero winding number [16, 17] and the frequent transition between these different vacua [18, 19] by sphalerons [20, 21] in the QGP produced in relativistic heavy ion collisions. In the presence of a magnetic field, which is produced in non-central heavy ion collisions, this can lead to a finite vector current in the QGP, called the chiral magnetic effect (CME) [22, 23, 24]. It is shown in Ref. [22] that the magnetic field can further lead to the separation of right-handed and left-handed particles in the transverse plane of a heavy ion collision, a phenomenon called the chiral separation effect (CSE) [25, 26]. Furthermore, through the interplay between the axial charge density and the vector (baryon) charge density, a gapless collective excitation called the chiral magnetic wave (CMW) can be generated [27]. In heavy ion collisions, the CMW can lead to the splitting between the elliptic flows of positively and negatively charged pions after the transverse expansion of the system [27]. The vector and axial vector currents can also be generated in a rotating QGP in non-central heavy ion collisions, when there are non-vanishing axial and vector chemical potentials [28], and they are called, respectively, the chiral vortical effect (CVE) and chiral vortical separation effect (CVSE). The resulting gapless collective excitation from the interplay between the vector and axial vector charge densities is called the chiral vortical wave (CVW) and may be found by studying the elliptic flow splitting between baryons and anti-baryons [29].

Spin polarization of Λ hyperons in non-central heavy ion collisions is another phenomenon that is related to the effect of the vorticity field in the produced QGP on the dynamics of massless quarks. An earlier study [30, 31] has attributed the global spin polarization of Λ hyperons along the direction of the total angular momentum to their constitute quarks, which are polarized due to their spin-orbit interactions in the

QGP. Since the vorticity field generated in relativistic heavy ion collisions can have local structures, similar structures are expected in the spin polarization density of Λ hyperons. This has indeed been seen from the single-particle distribution function after a hydrodynamic [32, 33, 34] or kinetic [35] evolution of heavy ion collisions by assuming that they are in thermal equilibrium with the rotating matter. However, there is a lack of connections between the final spin polarization of hadrons to that of quarks in these approaches.

As mentioned above, an interesting property of QCD is its non-trivial gauge field configurations [17], which are characterized by the Chern-Simons topological charge or winding number Q_w [36]. For a pure gauge field $A_\mu(x)$, the topological charge Q_w is given by

$$Q_w = \frac{g^2}{32\pi^2}\int d^4x F_{\mu\nu}\tilde{F}^{\mu\nu}, \tag{1.1}$$

where $F_{\mu\nu} = \partial_\mu A_\nu - \partial_\nu A_\mu + ig[A_\mu, A_\nu]$ is the gauge field strength tensor and $\tilde{F}^{\mu\nu} = \frac{1}{2}\epsilon^{\mu\nu\rho\sigma}F_{\rho\sigma}$.

Based on either the evaluation of the triangular diagram involving the correlation of an axial vector current with two vector currents [37] or the change in the path integral measure of the fermion fields in gauge-invariant theories under a local chiral transformation [38], i.e., multiplied by the phase factor $e^{i\gamma_5\theta(x)}$ with γ_5 being the Dirac matrix and $\theta(x)$ is an arbitrary function of space and time, it can be shown that the axial charge current is not conserved and satisfies the following equation,

$$\partial^\mu J^5_\mu = 2i\sum_f m_f \left\langle \overline{\psi}_f \gamma^5 \psi_f \right\rangle - \frac{N_f g^2}{16\pi^2} F_{\mu\nu}\tilde{F}^{\mu\nu}. \tag{1.2}$$

In the limit of massless fermions, i.e., $m_i = 0$, this leads to a difference between

right-handed and left-handed fermions,

$$\Delta(N_L - N_R) = 2N_f Q_w. \tag{1.3}$$

It has been suggested in Ref. [22] that the signature of the non-trivial gauge field configuration of QCD vacuum can be found by looking at the separation between positively and negatively charged particles via the chiral magnetic effect. In non-central heavy ion collisions, a large magnitude of magnetic field is created in the transverse plane [39, 40]. This magnetic field can lead to a current along or opposite to the direction of magnetic field when the axial charge chemical potential μ_5 is non-zero due to non-zero topological charge in the produced QGP, and this effect can be tested by studying the separation between particles of different charges. Several experiments [41, 42, 43] from the STAR Collaboration at BNL and the ALICE Collaboration at CERN have found the signal of charge separation, but its physical explanation is still under debate. For example, this charge separation can be attributed to resonance decays [44] or transverse momentum conservation [45] and charge conservation [46]. Also, the similarities between the charge separation signals in p+Pb and Pb+Pb collisions observed by the CMS Collaboration at LHC put more challenge on the interpretation of CME [47].

The CMW is a gapless collective mode generated from the interplay between the vector charge density and axial charge density due to the CME and CSE, respectively [48, 27]. As a result, the finite charge density created in heavy ion collisions can fluctuate and generate an electric quadrupole moment in the transverse plane of the QGP [27], which can be seen by the difference in the elliptic flows of positively and negatively charged particles. The elliptic flow difference between π^+ and π^- as a function of charge asymmetry has been measured in many experiments

from the STAR Collaboration and the ALICE Collaboration [3, 49], and the results seem to agree with the interpretation of CMW. However, there are still other above-mentioned background effects that may contribute to the signal [50, 51], such as local charge conservation and the conformal hydrodynamic evolution with non-zero shear viscosity to entropy density ratio η/s. The similarities in the charge asymmetry dependence of the elliptic flow difference in p+Pb and Pb+Pb collisions also challenge the interpretation of CMW [52].

For the spin polarization of fermions in a vorticity field, which has recently been extensively studied in heavy ion collisions, it can be understood using the statistical-hydrodynamic model by considering the spin-vorticity coupling of massive fermions at the kinetic freeze-out [32, 33, 34]. In the quantum kinetic approach [35], the spin polarization of a massive particle is, however, obtained from the spin vector density in the colliding system. In both approaches, the results on the spin polarization of Λ hyperons are comparable to the experimental data from the STAR Collaboration both in its magnitude and dependence on the collision energy [7].

In some studies of the chiral effects, schematic models are used by assuming a non-expanding system [27, 29]. A more realistic anomalous hydrodynamics [28] has also been used to study the effect of CMW on elliptic flows in heavy ion collisions assuming a strong and long-lived external magnetic field [53, 54]. The study of CME has also been carried out in Refs. [55, 56] using anomalous hydrodynamics, and the results are comparable to the experimental data. The spin polarization of Λ hyperons has been studied based on the information about the vorticity field after a hydrodynamic or transport evolution [57, 58, 59, 60, 61, 62, 63, 64, 65, 66, 67, 68, 69, 70, 71].

In all above studies of CME, CMW and the Λ spin polarization, thermal equilibrium has been assumed in the produced matter. To include the non-equilibrium effect, chiral kinetic theory has been developed by including in the usual kinetic the-

ory the chiral effects due to the smallness of quark masses [72, 73, 74, 75, 76, 77, 1]. In this dissertation, the chiral kinetic theory and its extension, the chiral or anomalous transport model, are developed and used to study the above discussed chiral effects. This thesis is an attempt to quantitatively understand these chiral effects under various conditions and to see if they can explain the experimental data as well as to point out new possibilities for improving the chiral kinetic equations. The remaining chapters are organized as follows. In Chapter 2, the CME, CSE, CVE, CVSE, CMW and CVW are discussed by studying the response of an equilibrated fermion system to magnetic and vorticity fields and deriving the related transport phenomena. Also shown is the dependence of the chiral effects on temperature, vector and axial charge chemical potentials, and the masses of fermions. Various methods for deriving the chiral kinetic equations are presented in Chapter 3. This will be followed in Chapter 4 by a study of the CMW effect on the elliptic flow splitting between positively and negatively charged particles in heavy ion collisions. Chapter 5 is about the discussion on the elliptic flow splitting of charged particles in the presence of a vorticity field as well as both magnetic and vorticity fields. Chapter 6 includes the effect of CVSE on the spin polarization of quarks. A coalescence model will then be used to convert quarks to Λ hyperons to study their spin polarization [78, 79]. Finally, a summary is given in Chapter 7. Four appendices are included to show the derivation of CMW and CVW from hydrodynamics (Appendix A), the derivation of the Berry curvature and chiral kinetic equations from the path integral method (Appendix B), the derivation of CMW and CVW in chiral kinetic theory (Appendix C), and the time evolution of the magnetic field in relativistic heavy ion collisions (Appendix D).

Some of the results in this dissertation, particularly those in Chapters 4-6, have been published in Refs. [1, 4, 5].

2. THEORY OF CHIRAL MAGNETIC AND VORTICAL EFFECTS

2.1 Chiral magnetic effects

In normal electromagnetism, the charge or vector current is generated by applying an electric field to charged particles, leading to Ohm's law

$$\mathbf{J}^V = \sigma \mathbf{E}, \tag{2.1}$$

where σ is the electric conductivity. In the presence of a magnetic field $\mathbf{B}$, a vector current can also be generated if there is a nonzero axial charge chemical potential μ_5 [23], i.e., non-equal numbers of right-handed (with spin along the direction of momentum) and left-handed (with spin opposite to the direction of momentum) charged particles. In the case that these charged particles are massless, the vector current is related to the magnetic field by

$$\mathbf{J}^V = \frac{Q^2 \mu_5}{2\pi^2} \mathbf{B}. \tag{2.2}$$

where Q is the charge of the particle. The magnetic field can also generate an axial charge current if the charge chemical potential μ is nonzero [26], i.e.,

$$\mathbf{J}^A = \frac{Q^2 \mu}{2\pi^2} \mathbf{B}. \tag{2.3}$$

Eqs.(2.2) and (2.3) are called the chiral magnetic effect (CME) and the chiral separation effect (CSE), respectively.

The chiral magnetic and separation effects can be derived in various ways, e.g., from solving the Dirac equation in a magnetic field. A simple way to derive the CME

based on the chiral anomaly and energy conservation is given in Ref. [23]. According to this study, the equation for the chiral anomaly in Eq. (1.2) of Chapter 1 due to the electromagnetic field can be expressed in terms of the field strength tensor of the photon field and thus the electric field $\mathbf{E}$ and the magnetic field $\mathbf{B}$. For massless quarks, it becomes

$$\partial^\mu J^5_\mu = -\frac{e^2}{16\pi^2} F_{\mu\nu}\tilde{F}^{\mu\nu} = \frac{e^2}{2\pi^2}\mathbf{E}\cdot\mathbf{B}. \tag{2.4}$$

Integrating over space gives

$$\frac{dN^5}{dt} \equiv \int d^3\mathbf{x}\partial^\mu J^5_\mu = -\frac{e^2}{16\pi^2}\int d^3\mathbf{x} F_{\mu\nu}\tilde{F}^{\mu\nu} = \frac{e^2}{2\pi^2}\int d^3\mathbf{x}\mathbf{E}\cdot\mathbf{B}. \tag{2.5}$$

According to the above equation, increasing N_5 by two by converting a particle from negative helicity to positive helicity increases the energy by $2\mu_5$ if the chemical potentials for right and left chirality particles are $\mu+\mu_5$ and $\mu-\mu_5$, respectively. The rate of energy flow in the electric field $\mathbf{E}$ is thus given by

$$\int d^3\mathbf{x}\mathbf{J}^V\cdot\mathbf{E} = \mu_5\frac{dN^5}{dt} = \frac{e^2\mu_5}{2\pi^2}\int d^3\mathbf{x}\mathbf{E}\cdot\mathbf{B}, \tag{2.6}$$

where $\mathbf{J}^V$ is the charge current. Since the above equality holds for any electric field, one thus obtains the CME that the magnetic field can generate a charge current in a medium of finite axial charge chemical potential,

$$\mathbf{J}^V = \frac{e^2\mu_5}{2\pi^2}\mathbf{B}. \tag{2.7}$$

2.1.1 *Vector and axial vector currents from the Dirac equation*

The expression derived above for the CME can be obtained more systematically by solving the Dirac equation in a magnetic field. Besides showing how the CME and CSE and the resulting spin polarization can be obtained, this method also allows one to include the effect of finite particle mass.

In the presence of a constant magnetic field $\mathbf{B}$, which is chosen to point along the z-axis and thus can be obtained from the gauge potential $\mathbf{A} = \{0, Bx, 0\}$, the time-independent Dirac equation for a spin-1/2 fermion of mass m, charge Q, and energy E is given by

$$\gamma^0[\boldsymbol{\gamma}\cdot(\mathbf{p} - Q\mathbf{A}) + m]\Psi = E\Psi, \tag{2.8}$$

where the Dirac Gamma matrices are

$$\gamma^0 = \begin{bmatrix} I & 0 \\ 0 & -I \end{bmatrix}, \quad \gamma^i = \begin{bmatrix} 0 & \sigma^i \\ -\sigma^i & 0 \end{bmatrix},$$

with σ^i being the Pauli matrices,

$$\sigma^1 = \begin{bmatrix} 0 & 1 \\ 1 & 0 \end{bmatrix}, \quad \sigma^2 = \begin{bmatrix} 0 & -i \\ i & 0 \end{bmatrix}, \quad \sigma^3 = \begin{bmatrix} 1 & 0 \\ 0 & -1 \end{bmatrix}.$$

In terms of the two components of the wave function $\Psi = \begin{pmatrix} \Psi_L \\ \Psi_S \end{pmatrix}$, the Dirac

equation changes to the following two equations:

$$\boldsymbol{\sigma}\cdot(\mathbf{p}-Q\mathbf{A})\Psi_S + m\Psi_L = E\Psi_L, \tag{2.9}$$

$$\boldsymbol{\sigma}\cdot(\mathbf{p}-Q\mathbf{A})\Psi_L - m\Psi_S = E\Psi_S. \tag{2.10}$$

Inserting the relation $\Psi_S = \frac{\boldsymbol{\sigma}\cdot(\mathbf{p}-Q\mathbf{A})}{E+m}\Psi_L$ obtained from Eq. (2.10) into Eq. (2.9) leads to

$$[\boldsymbol{\sigma}\cdot(\mathbf{p}-Q\mathbf{A})][\boldsymbol{\sigma}\cdot(\mathbf{p}-Q\mathbf{A})]\Psi_L + m^2\Psi_L = E^2\Psi_L. \tag{2.11}$$

Using the identity $(\boldsymbol{\sigma}\cdot\mathbf{A})(\boldsymbol{\sigma}\cdot\mathbf{B}) = \mathbf{A}\cdot\mathbf{B} + i\boldsymbol{\sigma}\cdot\mathbf{A}\times\mathbf{B}$, Eq. (2.11) can be rewritten as

$$[(\mathbf{p}-Q\mathbf{A})^2 + m^2 - Q\boldsymbol{\sigma}\cdot\mathbf{B}]\Psi_L = E^2\Psi_L. \tag{2.12}$$

Taking the wave function Ψ_L to be $\begin{pmatrix}\chi_+\\0\end{pmatrix}$ or $\begin{pmatrix}0\\\chi_-\end{pmatrix}$ for the spin pointing along or opposite to the direction of the magnetic field, one then has

$$[(\mathbf{p}-Q\mathbf{A})^2 + m^2 \mp QB]\chi_\pm = E_\pm^2\chi_\pm. \tag{2.13}$$

It is straightforward to show that the eigenvalues of the above equation are given by the Landau levels

$$E_{n,\pm} = \sqrt{m^2 + p_z^2 + (2n+1)|Q|B \mp QB}, \tag{2.14}$$

where n are integers, with corresponding wave functions

$$\chi_{n,\pm} = e^{ip_y y + ip_z z}\phi_n\left(x - \frac{p_y}{QB}\right), \quad \phi_n(x) = \frac{H_n(x/l_c)}{\sqrt{2^n n!\sqrt{\pi}l_c}}e^{(-\frac{1}{2}(\frac{x}{l_c})^2)}, \tag{2.15}$$

where $l_c = 1/\sqrt{|Q|B}$.

Using

$$\begin{aligned}
(p_x - QA_x)\chi_n &= -i\sqrt{\frac{|Q|B}{2}}[\sqrt{n}\chi_{(n-1)} - \sqrt{n+1}\chi_{(n+1)}] \\
(p_y - QA_y)\chi_n &= -\text{sign}(QB)\sqrt{\frac{|Q|B}{2}}[\sqrt{n}\chi_{(n-1)} + \sqrt{n+1}\chi_{(n+1)}] \\
(p_z - QA_z)\chi_n &= p_z\chi_n,
\end{aligned} \tag{2.16}$$

then $\Psi_S = \frac{\boldsymbol{\sigma}\cdot(\mathbf{p}-Q\mathbf{A})}{E+m}\Psi_L$ leads to

$$\begin{pmatrix} \frac{p_z}{E+m}\chi_n \\ -\frac{i\sqrt{2n|QB|}}{E+m}\chi_{n-1} \end{pmatrix} \quad \text{or} \quad \begin{pmatrix} \frac{i\sqrt{2(n+1)|QB|}}{E+m}\chi_{n+1} \\ -\frac{p_z}{E+m}\chi_n \end{pmatrix} \tag{2.17}$$

for positively charged particles and

$$\begin{pmatrix} \frac{p_z}{E+m}\chi_n \\ \frac{i\sqrt{2(n+1)|QB|}}{E+m}\chi_{n+1} \end{pmatrix} \quad \text{or} \quad \begin{pmatrix} -\frac{i\sqrt{2n|QB|}}{E+m}\chi_{n-1} \\ -\frac{p_z}{E+m}\chi_n \end{pmatrix} \tag{2.18}$$

for negatively charged particles. For systems consisting of both particles and antiparticles, one can choose positively charged ($Q > 0$) particles to have the wave

function

$$\chi_{n,+} = e^{ip_y y + ip_z z} \begin{pmatrix} \phi_n(x - l_c) \\ 0 \\ \frac{p_z}{E_{n,+}+m}\phi_n(x - l_c) \\ -\frac{i\sqrt{2nQB}}{E_{n,+}+m}\phi_{n-1}(x - l_c) \end{pmatrix} \tag{2.19}$$

if its spin is up, where, $E_{n,+} = \sqrt{m^2 + p_z^2 + 2nQB}$, and

$$\chi_{n,-} = e^{ip_y y + ip_z z} \begin{pmatrix} 0 \\ \phi_n(x - l_c) \\ \frac{i\sqrt{2(n+1)QB}}{E_{n,-}+m}\phi_{n+1}(x - l_c) \\ -\frac{p_z}{E_{n,-}+m}\phi_n(x - l_c) \end{pmatrix} \tag{2.20}$$

if its spin is down, where $E_{n,-} = \sqrt{m^2 + p_z^2 + 2(n+1)QB}$.

For a spin up particle, the expectation value for its velocity is given by $\mathbf{v} = \frac{\overline{\Psi}\boldsymbol{\gamma}\Psi}{\overline{\Psi}\gamma^0\Psi}$. Using the above wave function gives $v_x = 0$, $v_y = 0$ and $v_z = \frac{p_z}{E}$. One can also obtain the expectation value for the spin of the particle, which is defined as

$$\mathbf{S} = \frac{1}{2}\frac{\Psi^\dagger \begin{pmatrix} \boldsymbol{\sigma} & 0 \\ 0 & \boldsymbol{\sigma} \end{pmatrix} \Psi}{\overline{\Psi}\gamma^0\Psi}. \tag{2.21}$$

One then has $S_x = 0$ and $S_y = 0$, and $S_z = \frac{1}{2} - \frac{nQB}{E(E+m)}$ for a spin up particle and $S_z = -\frac{1}{2} + \frac{(n+1)QB}{E(E+m)}$ for a spin down particle.

Consider a system of particles and antiparticles, which is assumed to have positive and negative charges, respectively, for simplicity, and to be in thermal equilibrium with the single particle energy distribution $f(E)$. If it has a chemical potential μ_R for

particles of right chirality, i.e., particles with momentum along the direction of spin and antiparticles with momentum opposite to spin, the charge current for positively charged particles of right chirality is then

$$\begin{aligned} J_z &= Q\frac{QB}{2\pi}\sum_{n=0}^{\infty}\int_0^{\infty}\frac{dp_z}{2\pi}\frac{p_z}{E_{n,+}}f(E_{n,+}-\mu_R)+Q\frac{QB}{2\pi}\sum_{n=0}^{\infty}\int_{-\infty}^{0}\frac{dp_z}{2\pi}\frac{p_z}{E_{n,-}}f(E_{n,-}-\mu_R) \\ &= \frac{Q^2B}{4\pi^2}\sum_{n=0}^{\infty}\int_0^{\infty}dp_z\left[\frac{p_z}{E_{n,+}}f(E_{n,+}-\mu_R)-\frac{p_z}{E_{n,-}}f(E_{n,-}-\mu_R)\right] \\ &= \frac{Q^2B}{4\pi^2}\int_0^{\infty}dp_z\frac{p_z}{\sqrt{m^2+p_z^2}}f(\sqrt{m^2+p_z^2}-\mu_R), \end{aligned} \tag{2.22}$$

where $E_{n,+}=\sqrt{m^2+p_z^2+2nQB}$ and $E_{n,-}=\sqrt{m^2+p_z^2+2(n+1)QB}$, and the charge current for negatively charged (-Q) antiparticles of right chirality (negative helicity) is

$$\begin{aligned} J_z &= -Q\frac{QB}{2\pi}\sum_{n=0}^{\infty}\int_0^{\infty}\frac{dp_z}{2\pi}\frac{p_z}{E_{n,-}}f(E_{n,-}+\mu_R) \\ &- Q\frac{QB}{2\pi}\sum_{n=0}^{\infty}\int_{-\infty}^{0}\frac{dp_z}{2\pi}\frac{p_z}{E_{n,+}}f(E_{n,+}+\mu_R) \\ &= -\frac{Q^2B}{4\pi^2}\sum_{n=0}^{\infty}\int_0^{\infty}dp_z\left[\frac{p_z}{E_{n,-}}f(E_{n,-}+\mu_R)-\frac{p_z}{E_{n,+}}f(E_{n,+}+\mu_R)\right] \\ &= -\frac{Q^2B}{4\pi^2}\int_0^{\infty}dp_z\frac{p_z}{\sqrt{m^2+p_z^2}}f(\sqrt{m^2+p_z^2}+\mu_R), \end{aligned} \tag{2.23}$$

where $E_{n,-}=\sqrt{m^2+p_z^2+2nQB}$ and $E_{n,+}=\sqrt{m^2+p_z^2+2(n+1)QB}$. The charge current for right chirality particles and antiparticles is thus

$$\mathbf{J}_R^V=\frac{Q^2\mathbf{B}}{4\pi^2}\int_0^{\infty}dp_z\frac{p_z}{\sqrt{m^2+p_z^2}}[f(\sqrt{m^2+p_z^2}-\mu_R)-f(\sqrt{m^2+p_z^2}+\mu_R)]. \tag{2.24}$$

For the axial charge current, which is defined as

$$\mathbf{J}^A = \overline{\Psi}\boldsymbol{\gamma}\gamma^5\Psi = \Psi^\dagger \begin{pmatrix} \boldsymbol{\sigma} & 0 \\ 0 & \boldsymbol{\sigma} \end{pmatrix} \Psi, \tag{2.25}$$

it is

$$\begin{aligned} J_z^A &= Q\frac{QB}{2\pi}\sum_{n=0}^{\infty}\int_0^\infty \frac{dp_z}{2\pi}\left[1-\frac{2nQB}{E_{n,+}(E_{n,+}+m)}\right] f(E_{n,+}-\mu_R) \\ &+ Q\frac{QB}{2\pi}\sum_{n=0}^{\infty}\int_{-\infty}^0 \frac{dp_z}{2\pi}\left[1-\frac{2(n+1)QB}{E_{n,-}(E_{n,-}+m)}\right) f(E_{n,-}-\mu_R\Big] \\ &= \frac{Q^2B}{4\pi^2}\int_0^\infty dp_z f(\sqrt{m^2+p_z^2}-\mu_R) \end{aligned} \tag{2.26}$$

for positively charged particles of right chirality and

$$J_z^A = -\frac{Q^2B}{4\pi^2}\int_0^\infty dp_z f(\sqrt{m^2+p_z^2}+\mu_R) \tag{2.27}$$

for negatively charged antiparticles of right chirality. The axial charge current for right chirality particles and antiparticles is then

$$\mathbf{J}_R^A = \frac{Q^2\mathbf{B}}{4\pi^2}\int_0^\infty dp_z[f(\sqrt{m^2+p_z^2}-\mu_R) - f(\sqrt{m^2+p_z^2}+\mu_R)]. \tag{2.28}$$

Similarly, the charge current and the axial charge current for left chirality particles and antiparticles are

$$\mathbf{J}_L^V = -\frac{Q^2\mathbf{B}}{4\pi^2}\int_0^\infty dp_z \frac{p_z}{\sqrt{p_z^2+m^2}}[f(\sqrt{m^2+p_z^2}-\mu_L) - f(\sqrt{m^2+p_z^2}+\mu_L)], \tag{2.29}$$

and

$$\mathbf{J}_L^A = \frac{Q^2\mathbf{B}}{4\pi^2}\int_0^\infty dp_z[f(\sqrt{m^2+p_z^2}-\mu_L) - f(\sqrt{m^2+p_z^2}+\mu_L)], \tag{2.30}$$

respectively, where μ_L is the chemical potential for particles of left chirality, i.e., particles with momentum opposite to and antiparticles with momentum along the direction of spin. Similar results can be found in Ref. [80].

2.1.2 Chiral magnetic effect and chiral separation effect

In the massless limit $m \to 0$ and with the Fermi-Dirac distribution for $f(E)$, one has from Eqs.(2.24), (2.29)-(2.30)

$$\begin{aligned}
\mathbf{J}_R^V &= \frac{Q^2\mathbf{B}}{4\pi^2}\int_0^\infty dp_z[f(p_z-\mu_R) - f(p_z+\mu_R)] \\
&= \frac{Q^2\mathbf{B}}{4\pi^2}\int_0^\infty dp_z\left[\frac{1}{e^{(p_z-\mu_R)/T}+1} - \frac{1}{e^{(p_z+\mu_R)/T}+1}\right] \\
&= \frac{Q^2T\mathbf{B}}{4\pi^2}[-\ln(1+e^{(\mu_R-p_z)/T})|_0^\infty + \ln(1+e^{(-\mu_R-p_z)/T})|_0^\infty] \\
&= \frac{Q^2\mu_R}{4\pi^2}\mathbf{B}, \qquad (2.31) \\
\mathbf{J}_R^A &= \frac{Q^2\mu_R}{4\pi^2}\mathbf{B}, \qquad (2.32) \\
\mathbf{J}_L^V &= -\frac{Q^2\mu_L}{4\pi^2}\mathbf{B}, \qquad (2.33) \\
\mathbf{J}_L^A &= \frac{Q^2\mu_L}{4\pi^2}\mathbf{B}. \qquad (2.34)
\end{aligned}$$

Combining the above equations leads to

$$\begin{aligned}
\mathbf{J}^V &= \mathbf{J}_R^V + \mathbf{J}_L^V = \frac{Q^2\mu_5}{2\pi^2}\mathbf{B}, \qquad (2.35) \\
\mathbf{J}^A &= \mathbf{J}_R^A + \mathbf{J}_L^A = \frac{Q^2\mu}{2\pi^2}\mathbf{B}, \qquad (2.36)
\end{aligned}$$

where $\mu = (\mu_R + \mu_L)/2$ and $\mu_5 = (\mu_R - \mu_L)/2$, which are seen to be the same CME and CSE given in the beginning of this Chapter. It is interesting to note that the conductivity coefficients in these equations depend only on the chemical potential and not on the temperature.

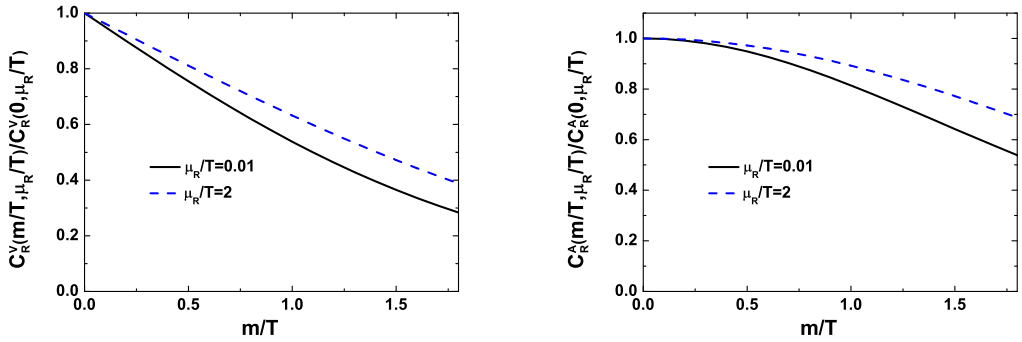

Figure 2.1: Fermion mass dependence of CME (left window) and CSE (right window) coefficients.

For fermions of non-zero mass, the conductivity coefficients in CME and CSE become mass-dependent. To see this dependence, one introduces a dimensionless CME coefficient $C_R^V = \frac{J_R^V}{TB}$, which is a function of m/T and μ_R/T, that is

$$C_R^V = \frac{Q^2}{4\pi^2 T}\int_0^\infty dp_z \frac{p_z}{\sqrt{m^2+p_z^2}}[f(\sqrt{m^2+p_z^2}-\mu_R) - f(\sqrt{m^2+p_z^2}+\mu_R)]. \quad (2.37)$$

Shown in the left window of Fig. 2.1 is the fermion mass dependence of the CME coefficient using the Fermi-Dirac distribution function and the two values of 0.01 (solid line) and 2 (dashed line) for μ_R/T. It shows that the CME coefficient decreases with increasing fermion mass, and the decrease is slower for a larger chemical potential. Similarly, one can also define the dimensionless CSE coefficient $C_R^A = \frac{J_R^A}{TB}$.

The results shown in the right window of Fig.2.1 indicate that it also decreases with increasing fermion mass but at a slower rate than the CME coefficient C_R^V.

2.1.3 Spin polarization in a magnetic field

The above results allows one to study the spin polarization of charged particles in a magnetic field. According to Eq. (2.25), the axial charge current is related to the spin density $\mathbf{S}$ by $\mathbf{J}^A = 2|Q|\mathbf{S}$. The spin polarization vector is then defined by $\mathbf{P} = \frac{2\mathbf{S}}{n}$, where n is the particle number density. For a system with zero axial charge chemical potential, the spin polarization of positively and negatively charged particles along the direction of the magnetic field, i.e., $\hat{\mathbf{B}} = \mathbf{B}/B$, are

$$\mathbf{P}_+ = \frac{\int_0^\infty dp_z f(\sqrt{m^2+p_z^2}-\mu)}{I_+}\hat{\mathbf{B}}, \tag{2.38}$$

$$\mathbf{P}_- = -\frac{\int_0^\infty dp_z f(\sqrt{m^2+p_z^2}+\mu)}{I_-}\hat{\mathbf{B}}, \tag{2.39}$$

respectively, where

$$I_+ = \sum_{n=0}^{\infty}\int_0^\infty dp_z[f(\sqrt{m^2+p_z^2+2nQB}-\mu) + f(\sqrt{m^2+p_z^2+2(n+1)QB}-\mu)], \tag{2.40}$$

$$I_- = \sum_{n=0}^{\infty}\int_0^\infty dp_z[f(\sqrt{m^2+p_z^2-2nQB}+\mu) + f(\sqrt{m^2+p_z^2-2(n+1)QB}+\mu)]. \tag{2.41}$$

For a small magnetic field, i.e., $\sqrt{QB} \ll T$, one can replace the summation $\sum_{n=0}^{\infty}$ by $\int_0^\infty \frac{d\mathbf{p}_T^2}{2QB}$, where $\mathbf{p}_T$ is the momentum in the transverse plane perpendicular to $\hat{\mathbf{B}}$,

and simplify the above equations to

$$\mathbf{P}_{+} = 2\pi Q \frac{\int_0^\infty dp f(\sqrt{m^2+p^2}-\mu)}{\int d^3\mathbf{p} f(\sqrt{m^2+p^2}-\mu)}\mathbf{B}, \tag{2.42}$$

$$\mathbf{P}_{-} = -2\pi Q \frac{\int_0^\infty dp f(\sqrt{m^2+p^2}+\mu)}{\int d^3\mathbf{p} f(\sqrt{m^2+p^2}+\mu)}\mathbf{B}. \tag{2.43}$$

In the limit of vanishing mass $m \to 0$, $P_{\pm} = \frac{QB}{4T^2}\frac{\mathrm{Li}_1(-e^{\pm\mu/T})}{\mathrm{Li}_3(-e^{\pm\mu/T})}$, where $\mathrm{Li}_j(x)$ is the Polylogarithm function, which shows a monotonically decreasing polarization with increasing charge chemical potential and has a maximum value of $\frac{QB}{4T^2}$ when $\mu \to -\infty$. For $m \to \infty$, the spin polarization is $P = \frac{QB}{2mT}$, corresponding to its classical limit.

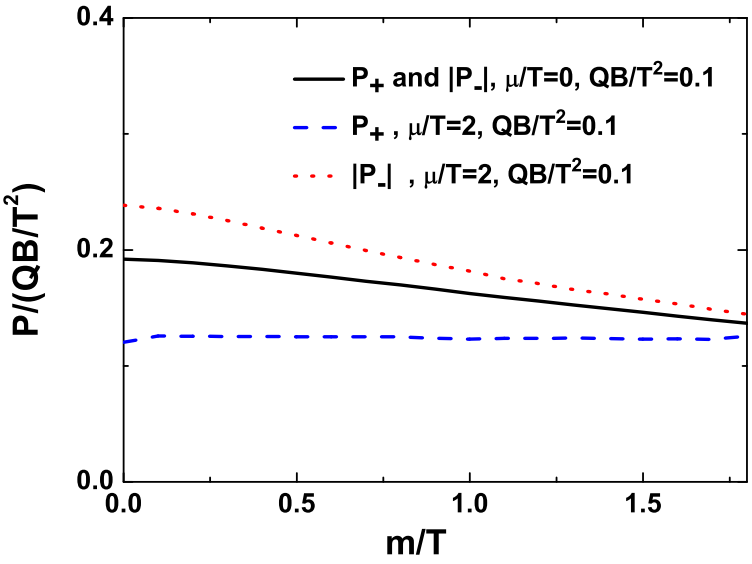

Figure 2.2: Fermion mass dependence of the magnitude of spin polarization of positively and negatively charged particles divided by QB/T^2 for a small magnetic field.

Fig. 2.2 shows the magnitude of spin polarization of positively and negatively

charged particles, whose spin polarization directions are opposite, for a small magnetic field. As shown by the solid line, the magnitude of spin polarization at zero chemical potential is the same for positively and negatively charged particles. Starting with a value of $0.19\frac{QB}{T^2}$ at zero mass, it decreases with increasing mass. At finite chemical potential, the magnitude of the spin polarization of negatively charged particles (dotted line) increases while that of positively charged particles (dashed line) decreases with increasing chemical potential.

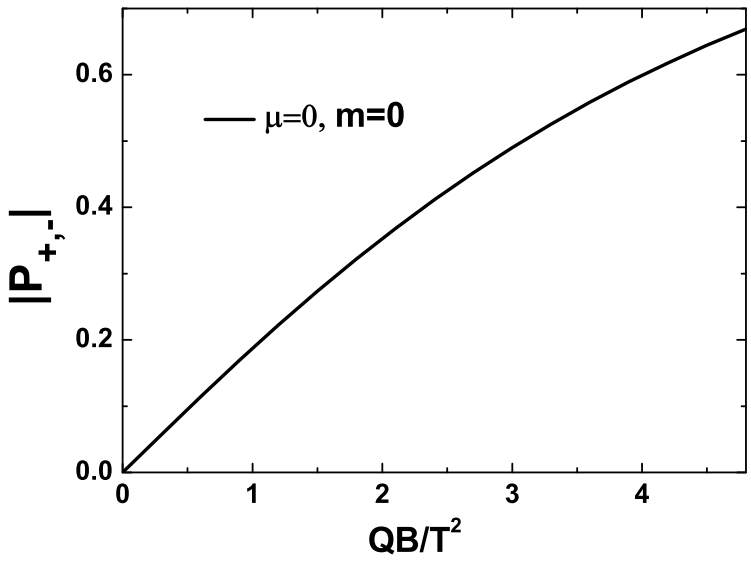

Figure 2.3: Magnetic field dependence of the magnitude of spin polarization of massless positively and negatively charged particles at zero charge chemical potential $\mu = 0$.

If the magnetic field is large, i.e., $\sqrt{QB} \gg T$, one needs to evaluate the summation in Eqs. (2.40) and (2.41) explicitly. As shown in Fig. 2.3 for the magnetic field dependence of the spin polarization in the case of massless fermions, it initially

increases linearly with the strength of the magnetic field when it is small but the increase becomes slower when the strength of the magnetic field is large.

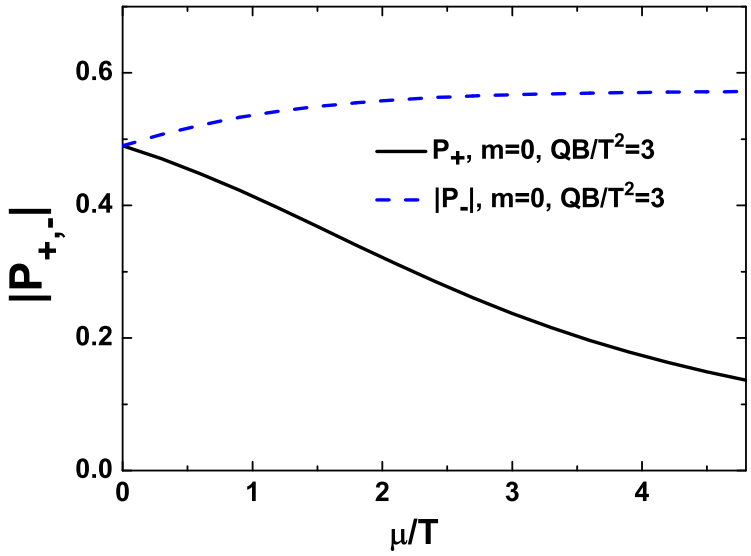

Figure 2.4: Chemical potential dependence of the magnitude of spin polarization of massless positively and negatively charged particle at $QB/T^2 = 3$.

As to the chemical potential dependence of the spin polarization, it is shown in Fig. 2.4 for the case of massless limit $m \to 0$. It is seen that the spin polarization of positively charged particles (solid line) decreases with the increase of chemical potential, and this is because the contribution from the lowest Landau level is smaller when the chemical potential is larger. As to the spin polarization for negatively charged particles (dashed line), it increases with the increase of chemical potential as a result of increasing dominance of the lowest Landau level. The above behavior of the spin polarization holds for both small and large strength of the magnetic field. In the massive limit $m \to \infty$, the magnitude of spin polarization becomes independent

of the chemical potential and is simply given by

$$|P| = \frac{1}{\sum_{n=0} e^{-\frac{nQB}{mT}} + \sum_{n=1} e^{-\frac{nQB}{mT}}} = \tanh\left(\frac{QB}{2mT}\right)$$

for both positively and negatively charged particles.

2.1.4 The chiral magnetic wave

Through the interplay between the CME and the CSE, a new form of gapless collective excitation, called the chiral magnetic wave (CMW), emerges from the coupling of the density waves for the axial and electric charges [48, 27]. According to Ref. [27], the chiral magnetic wave can induce in a heavy ion collision a charge quadrupole moment in the transverse plane perpendicular to the beam direction and lead to the splitting of the elliptic flows of positively and negatively charged particles during the expansion of the produced QGP. In Chapters 4 and 5, the chiral kinetic equations will be used to study if the CMW can indeed lead to a splitting between the elliptic flows of negatively and positively charged particles.

The velocity of the CMW can be found using the magnetohydrodynamics [48, 27], which is shown in Appendix A, and the resulting magnitude of the velocity of CMW is $|\frac{Q\mathbf{B}}{4\pi^2\alpha}|$. For particles and antiparticle described by the Fermi-Dirac distribution, one has, for small chemical potential,

$$\alpha = -2\int \frac{d^3\mathbf{p}}{(2\pi)^3}\frac{\partial f}{\partial p} = \frac{2}{\pi^2}\int_0^\infty f p dp = \frac{T^2}{6},$$

which gives the magnitude of the velocity of CMW as $|\frac{6QB}{4\pi^2T^2}|$.

The expression given in the above for the velocity of CMW shows a linear dependence on the strength of the magnetic field and is thus not valid for very large magnetic field as the velocity then can exceed one or the velocity of light. In this

case, fermions are frozen in the lowest Landau level [48], which is also shown in section 2.1.1. Taking into account this effect leads to $\rho = \frac{|QB|\mu}{4\pi^2}$, which then results in the velocity of CMW being one.

2.2 Chiral vortical effects

Another interesting anomalous chiral effect is associated with the rotation of a fermion system, which can be quantified by the vorticity field $\boldsymbol{\omega} = \frac{1}{2}\boldsymbol{\nabla} \times \mathbf{u}$, where $\mathbf{u}$ is the flow field. Similar to the CME and CSE due to the magnetic field, the vorticity field can induce vector and axial vector currents in a system with nonzero charge and axial charge chemical potentials, that is

$$\mathbf{J}^V = \frac{\mu\mu_5}{\pi^2}\boldsymbol{\omega} \quad \text{and} \quad \mathbf{J}^A = \left(\frac{T^2}{6} + \frac{\mu^2 + \mu_5^2}{2\pi^2}\right)\boldsymbol{\omega}, \tag{2.44}$$

called, respectively, the chiral vortical effect (CVE) and the chiral vortical separation effect (CVSE).

These anomalous currents due to the vorticity field were first derived in Refs. [81, 82, 83] using the method of gauge/gravity duality. Based on the hydrodynamic approach, it was later shown that the CVE and CVSE are consistent with the second law of thermodynamics [28]. Calculating the anomalous vortical conductivity at weak coupling using the Kubo formula, it was found in Refs. [84, 85] that it gives rise to anomalous vortical effects even in an uncharged fluid, which was not included in previous studies. There is also the derivation of CVE and CVSE from the kinetic theory based on the quantum Winger approach [75] or the Coriolis force [72]. The latter further shows explicitly the role of the Berry curvature in chiral vortical effects.

2.2.1 Chiral vortical effect and chiral vortical separation effect from the Dirac equation

Similar to the derivation of the CME and CSE in the previous section for fermions in a magnetic field, the Dirac equation can also be used to derive the CVE and CVSE for fermions in a vorticity field. Unlike the electromagnetic field, the vorticity field is not a gauge field and thus cannot be included in the Hamiltonian of the system in the usual way. Comparing the derivation of vortical conductivity from the Kubo formula [84, 85],

$$\sigma_\omega = \lim_{k_n \to 0} \epsilon_{ijn} \frac{-i}{2k_n} \langle J^i T^{0j} \rangle|_{\omega=0}, \tag{2.45}$$

where $T^{\mu\nu}$ is the energy-momentum tensor, which is similar to the derivation of chiral magnetic conductivity [86]

$$\sigma_B = \lim_{k_n \to 0} \epsilon_{ijn} \frac{-i}{2k_n} \langle J^i J^j \rangle|_{\omega=0}, \tag{2.46}$$

indicates that there is a coupling between the momentum and the fluid field $\mathbf{p}\cdot\mathbf{u}dt$ in the action for a single particle, similar to the action $Q\mathbf{A}\cdot d\mathbf{x}$ for a charged particle in an electromagnetic field. Because $\mathbf{p}\cdot\mathbf{u}dt = p^0\dot{\mathbf{x}}\cdot\mathbf{u}dt = p^0\mathbf{u}\cdot d\mathbf{x}$, the term involving the gauge field $Q\mathbf{A}$ in the Hamiltonian of section 2.1.1 can be replaced by $p^0\mathbf{u}$ when there is a vorticity field, which is similar to the result from Ref. [87] in the non-relativistic limit.

Since the above gauge field induces an equivalent magnetic field $2p^0\omega$, one can use the results of section 2.1.1 and finds that $E_{n,\pm} = \sqrt{m^2 + p_z^2 + (2n+1)2E_{n,\pm}\omega \mp 2E_{n,\pm}\omega}$,

which gives the energy

$$E_{n,\pm} = (2n + 1 \mp 1)\omega + \sqrt{m^2 + p_z^2 + (2n + 1 \mp 1)^2\omega^2}. \tag{2.47}$$

One can then show that the vector charge currents are

$$\begin{aligned} \mathbf{J}_R^V &= \frac{\boldsymbol{\omega}}{2\pi^2}\int_0^\infty p_z dp_z[f(\sqrt{m^2+p_z^2}-\mu_R) + f(\sqrt{m^2+p_z^2}+\mu_R)], & (2.48)\\ \mathbf{J}_L^V &= -\frac{\boldsymbol{\omega}}{2\pi^2}\int_0^\infty p_z dp_z[f(\sqrt{m^2+p_z^2}-\mu_L) + f(\sqrt{m^2+p_z^2}+\mu_L)], & (2.49) \end{aligned}$$

and the axial charge currents are

$$\begin{aligned} \mathbf{J}_R^A &= \frac{\boldsymbol{\omega}}{2\pi^2}\int_0^\infty \sqrt{m^2+p_z^2} dp_z[f(\sqrt{m^2+p_z^2}-\mu_R) + f(\sqrt{m^2+p_z^2}+\mu_R)], & (2.50)\\ \mathbf{J}_L^A &= \frac{\boldsymbol{\omega}}{2\pi^2}\int_0^\infty \sqrt{m^2+p_z^2} dp_z[f(\sqrt{m^2+p_z^2}-\mu_L) + f(\sqrt{m^2+p_z^2}+\mu_L)]. & (2.51) \end{aligned}$$

In the massless limit, the above equations reduce to $\mathbf{J}_R^V = \boldsymbol{\omega}(\frac{T^2}{12} + \frac{\mu_R^2}{4\pi^2}) = \mathbf{J}_R^A$ and $\mathbf{J}_L^V = -\boldsymbol{\omega}(\frac{T^2}{12} + \frac{\mu_L^2}{4\pi^2}) = -\mathbf{J}_L^A$, which gives $\mathbf{J}^V = \frac{\mu\mu_5\boldsymbol{\omega}}{\pi^2}$ and $\mathbf{J}^A = (\frac{T^2}{6} + \frac{\mu^2+\mu_5^2}{2\pi^2})\boldsymbol{\omega}$, same as shown in Eq. (2.44).

Since the axial charge current is equal to twice the spin polarization density, one can further show that the spin polarization density from the Dirac equation is exactly the same as the result obtained from the quantum Wigner approach [35]. Using the result

$$\boldsymbol{\Pi} = \frac{\boldsymbol{\omega}}{4\pi^2 T}\int_0^\infty p^2 dp \frac{e^{\beta(E_p \mp \mu)}}{(e^{\beta(E_p \mp \mu)}+1)^2} \tag{2.52}$$

from the quantum Wigner approach and the identity $\frac{e^{\beta(E_p\mp\mu)}}{(e^{\beta(E_p\mp\mu)}+1)^2} = -T\frac{\partial f}{\partial p}$, where $\boldsymbol{\Pi}$ is the spin-polarization density, one can show that $\boldsymbol{\Pi} = \frac{\boldsymbol{\omega}}{2\pi^2}\int_0^\infty pf dp$, which is the

same as the result from solving the Dirac equation.

In the non-relativistic limit, the spin polarization probability is found to be

$$P = 4\pi m\omega \frac{\int_0^\infty dpf}{\int_0^\infty f d^3\mathbf{p}} = m\omega/mT = \omega/T.$$

This result is twice the result from the quantum Wigner approach [35] and the statistical-hydrodynamic approach [32, 33, 34], and the reason for this difference is not yet clear and needs to be further studied.

2.2.2 The chiral vortical wave

For a fermion system in thermal equilibrium, one can use the results for the CVE and CVSE to derive the wave equations for the charge density of right and left chirality particles and antiparticles as well as their velocities. The derivation of the CVW is then similar to that of the CMW [29] and is also shown in Appendix A. Using the Fermi-Dirac distribution for massless quarks leads to $\frac{3\omega\mu}{\pi^2 T^2}$ for the velocity of the chiral vortical wave (CVW), which is zero for zero chemical potential. In Chapter 5, the effect of the CVW on the elliptic flow splitting between negatively and positively charged particles in a heavy ion collision will also be studied.

It is worthy to note that in the literature, there are also studies of CMW and CVW based on different considerations as well as of other wave modes [88, 89].

3. CHIRAL KINETIC EQUATIONS *

The chiral magnetic and vortical effects discussed in the previous chapter are for fermion systems in thermal equilibrium, which are useful for studying these effects in heavy ion collisions based on the hydrodynamic model. To include possible non-equilibrium effects, microscopic chiral kinetic equations have been developed [72, 73, 74, 75, 76, 77]. In Ref. [72], the chiral kinetic equations are derived from considering the Berry phase associated with the action of a quantum system in an external magnetic field. The resulting chiral kinetic equations reproduce the chiral anomaly as well as the CME and CSE in equilibrated systems. However, these equations are not manifestly Lorentz covariant and require the introduction of a modified Lorentz transformation [90]. The same chiral kinetic equations can be derived from the Landau Fermi liquid theory by taking into account the Berry curvature flux through the Fermi surface [73, 74] or from the semiclassical Foldy-Wouthuysen diagonalization of the quantum Dirac Hamiltonian for massless fermions and antifermions [77]. On the other hand, the manifestly Lorentz covariant chiral kinetic equations have been derived in Refs. [75, 76] based on the consideration of the covariant Wigner function for massless spin-1/2 fermions, which reproduce the non-covariant chiral kinetic equation after integrating over the zeroth component of the four-momentum.

*Part of this chapter is reprinted with permissions from "Anomalous transport model study of chiral magnetic effects in heavy ion collisions" by Yifeng Sun, Che Ming Ko and Feng Li, 2016, Phys. Rev. C **94**, 045204, Copyright 2016 by APS, and "Λ hyperon polarization in relativistic heavy ion collisions from a chiral kinetic approach" by Yifeng Sun and Che Ming Ko, 2017, Phys. Rev. C **96**, 024906, Copyright 2017 by APS.

3.1 Chiral kinetic equations from the semiclassical method

The classical equations of motion for a massless spin-1/2 particle in an external electromagnetic field can be simply derived from the semiclassical method that considers the conservation of the total angular momentum [1]. For a massless spin-1/2 fermion, its total angular momentum $\mathbf{J}$ is given by the sum of its orbital $\mathbf{L}$ and spin $\mathbf{S}$ angular momenta, i.e., $\mathbf{J} = \mathbf{L} + \mathbf{S} = \mathbf{r} \times \mathbf{p} + \lambda \hat{\mathbf{p}}/2$, where $\lambda = \pm$ is the helicity of the particle with the plus and minus signs for particles with spin parallel (positive helicity) and antiparallel (negative helicity) to the momentum, respectively. The convention $\hbar = c = 1$ has been used in the above. Under the influence of an external force $\mathbf{F}$, the rate of change in the total momentum is then

$$\begin{aligned} \frac{d\mathbf{J}}{dt} &= \frac{d\left(\mathbf{r} \times \mathbf{p} + \lambda \frac{\hat{\mathbf{p}}}{2}\right)}{dt} \\ &= \frac{d\mathbf{r}}{dt} \times \mathbf{p} + \mathbf{r} \times \frac{d\mathbf{p}}{dt} + \lambda \left[\frac{\dot{\mathbf{p}}}{2p} - \mathbf{p}\left(\frac{\mathbf{p}}{2p^3} \cdot \dot{\mathbf{p}}\right)\right] \\ &= \left(\dot{\mathbf{r}} - \lambda \dot{\mathbf{p}} \times \frac{\mathbf{p}}{2p^3}\right) \times \mathbf{p} + \mathbf{r} \times \mathbf{F}, \end{aligned} \tag{3.1}$$

where the relation $d\mathbf{p}/dt = \mathbf{F}$ and the identity $(\mathbf{A} \times \mathbf{B}) \times \mathbf{C} \equiv (\mathbf{A} \cdot \mathbf{C})\mathbf{B} - (\mathbf{B} \cdot \mathbf{C})\mathbf{A}$ have been used. Using the fact that $d\mathbf{J}/dt = \mathbf{r} \times \mathbf{F}$, one then has $\dot{\mathbf{r}} - \lambda \dot{\mathbf{p}} \times \frac{\mathbf{p}}{2p^3} = f(p)\hat{\mathbf{p}}$, where $f(p)$ is a function of the magnitude p of the momentum and $\hat{\mathbf{p}}$ is a unit vector along the direction of the momentum. In the absence of external force, $\mathbf{F} = 0$, one has $\dot{\mathbf{r}} = \hat{\mathbf{p}}$, which then requires $f(p) = 1$. This thus leads to $\dot{\mathbf{r}} = \hat{\mathbf{p}} + \lambda \dot{\mathbf{p}} \times \frac{\mathbf{p}}{2p^3} = \hat{\mathbf{p}} + \lambda \dot{\mathbf{p}} \times \mathbf{b}$, where $\mathbf{b} = \frac{\mathbf{p}}{2p^3}$.

Including the Lorentz force in the presence of an external electromagnetic field, $\mathbf{F} = Q(\mathbf{E} + \dot{\mathbf{r}} \times \mathbf{B}) = \dot{\mathbf{p}}$, the equations of motion for massless spin-1/2 fermions are

thus

$$\dot{\mathbf{r}} = \frac{\hat{\mathbf{p}} + \lambda Q \mathbf{E} \times \mathbf{b} + \lambda \mathbf{Q}(\hat{\mathbf{p}} \cdot \mathbf{b})\mathbf{B}}{1 + \lambda Q(\mathbf{B} \cdot \mathbf{b})}, \tag{3.2}$$

$$\dot{\mathbf{p}} = \frac{Q(\mathbf{E} + \hat{\mathbf{p}} \times \mathbf{B}) + \lambda \mathbf{Q^2 b}(\mathbf{E} \cdot \mathbf{B})}{1 + \lambda Q(\mathbf{B} \cdot \mathbf{b})}. \tag{3.3}$$

These equations include the effect of CME, CSE and the anomalous Hall effect, and are the same as those given in Refs. [72, 75, 76, 77].

3.2 Chiral kinetic equations from the path integral method

The quantity $\mathbf{b} = \frac{\mathbf{p}}{2p^3}$ in the previous section has a topological origin and is related to the Berry curvature of a massless spin 1/2 fermion in a magnetic field as shown in Ref. [72] from the path-integral formulation of quantum mechanics. Following Ref. [72], the Hamiltonian of a massless fermion of helicity $\lambda = 1$ is given by $H = \boldsymbol{\sigma} \cdot \mathbf{p}$. The transition amplitude for the particle from the initial spin state $|i\rangle$ at t_i to the final spin state $|f\rangle$ at time t_f is given by

$$\langle f|e^{-iH(t_f - t_i)}|i\rangle = \int \mathcal{D}x\mathcal{D}p\mathcal{P}e^{i\int_{t_i}^{t_f}(\mathbf{p}\cdot\dot{\mathbf{x}} - \boldsymbol{\sigma}\cdot\mathbf{p})\mathbf{dt}}, \tag{3.4}$$

where the integration of the path-ordered matrix $(\mathbf{p}\cdot\dot{\mathbf{x}} - \boldsymbol{\sigma}\cdot\mathbf{p})\Delta t$ is over the classical path $(\mathbf{x}(t), \mathbf{p}(t))$ in the phase space.

Since the massless fermion has only one helicity state $\lambda = 1$ (the opposite one corresponds to its antiparticle), the above matrix must be diagonalized in the helicity basis. For each point of phase space on the trajectory, there is always a unitary matrix $V_{\mathbf{p}}$ to diagonalize this matrix, i.e., $V_{\mathbf{p}}^{\dagger}\boldsymbol{\sigma}\cdot\mathbf{p}V_{\mathbf{p}} = p\sigma_3$. For two neighboring points t_1 and t_2 with momenta $\mathbf{p_1}$ and $\mathbf{p_2}$, one can then transform the second part of the

transition amplitude as

$$\begin{aligned} e^{-i\boldsymbol{\sigma}\cdot\mathbf{p}\Delta t} &= V_{\mathbf{p_2}}V_{\mathbf{p_2}}^{\dagger}e^{-i\boldsymbol{\sigma}\cdot\mathbf{p_2}\Delta t}V_{\mathbf{p_2}}V_{\mathbf{p_2}}^{\dagger}V_{\mathbf{p_1}}V_{\mathbf{p_1}}^{\dagger} \\ &= V_{\mathbf{p_2}}e^{-ip_2\sigma_3\Delta t}V_{\mathbf{p_2}}^{\dagger}V_{\mathbf{p_1}}V_{\mathbf{p_1}}^{\dagger} \\ &= V_{\mathbf{p_2}}e^{-ip_2\sigma_3\Delta t}e^{i\hat{\mathbf{a}}_{\mathbf{p_2}}\cdot\dot{\mathbf{p}}_2\Delta t}V_{\mathbf{p_1}}^{\dagger}, \end{aligned} \tag{3.5}$$

with $\hat{\mathbf{a}}_{\mathbf{p_2}} = iV_{\mathbf{p}}^{\dagger}\boldsymbol{\nabla}_{\mathbf{p}}V_{\mathbf{p}}|_{\mathbf{p}=\mathbf{p_2}}$. From its definition, $\hat{\mathbf{a}}_{\mathbf{p}}$ is a pure real number and is thus given by $\hat{\mathbf{a}}_{\mathbf{p_2}} = -\mathrm{Im}(V_{\mathbf{p}}^{\dagger}\boldsymbol{\nabla}_{\mathbf{p}}V_{\mathbf{p}})$. In this adiabatic approximation, the Lagrangian for a single particle of positive energy is then $\mathcal{L} = \mathbf{p}\cdot\dot{\mathbf{x}} - p - \mathbf{a}_{\mathbf{p}}\cdot\dot{\mathbf{p}}$ with $\mathbf{a}_{\mathbf{p}} = \mathrm{Im}(V_{\mathbf{p}}^{\dagger}\boldsymbol{\nabla}_{\mathbf{p}}V_{\mathbf{p}})_{11}$. In the presence of a gauge field, the Lagrangian becomes $\mathcal{L} = (\mathbf{p}+Q\mathbf{A})\cdot\dot{\mathbf{x}} - p - Q\phi - \mathbf{a}_{\mathbf{p}}\cdot\dot{\mathbf{p}}$. The equations of motion of the massless spin 1/2 fermion can be obtained by the method of variation, and they are $\dot{\mathbf{r}} = \hat{\mathbf{p}} + \lambda\dot{\mathbf{p}}\times\mathbf{b}$ and $\dot{\mathbf{p}} = Q(\mathbf{E} + \dot{\mathbf{x}}\times\mathbf{B})$ with $\mathbf{b} = \boldsymbol{\nabla}_{\mathbf{p}}\times\mathbf{a}_{\mathbf{p}} = \frac{\mathbf{p}}{2p^3}$. Substituting the second equation to the first one leads to the chiral kinetic equations in the previous section. Details on the above derivation is given in appendix B.

3.3 Chiral kinetic equations from the Dirac equation

In the above two approaches, the spin of a massless fermion is assumed to be either along or opposite to its momentum. Since this may not always be the case, a more general method without this assumption is used in this section to derive the equations of motion of massless fermions in a magnetic field. This method further allows one to see that the chiral kinetic equations derived in the previous section are the first-order quantum correction $\mathcal{O}(\hbar)$ to the classical equations of motion. Since one is dealing with massless fermions, one can use the two-component Weyl representation of spinors to describe particles of right chirality and left chirality with the Hamiltonian $H = \pm\boldsymbol{\sigma}\cdot\mathbf{p}$. Without losing generality, only right chirality

particles as in the previous section are considered. In the presence of a gauge field $A = (\mathbf{A}, \phi)$, the Hamiltonian changes to $H = \boldsymbol{\sigma} \cdot (\boldsymbol{\pi} - Q\mathbf{A}) + \mathbf{Q}\phi$, where $\boldsymbol{\pi}$ is the canonical momentum. Since the evolution of the average value of any physical observable can be described by $\dot{A} = \frac{1}{i\hbar}[A, H]$, one has

$$\begin{aligned}
\frac{dx^i}{dt} &= \frac{1}{i\hbar}[x^i, H] = \frac{\partial H}{\partial \pi^i} = \sigma^i, && (3.6)\\
\frac{d\pi^i}{dt} &= \frac{1}{i\hbar}[\pi^i, H] = -\frac{\partial H}{\partial x^i} = Q\sigma^j \frac{\partial A^j}{\partial x^i} - Q\frac{\partial \phi}{\partial x^i}, && (3.7)\\
\frac{d\sigma^i}{dt} &= \frac{1}{i\hbar}[\sigma^i, H] = \frac{1}{i\hbar}[\sigma^i, \sigma^j(\pi^j - QA^j)] \\
&= \frac{1}{i\hbar} 2i\epsilon_{ijk}(\pi^j - QA^j)\sigma^k = \frac{2}{\hbar}\epsilon_{ijk}(\pi^j - QA^j)\sigma^k. && (3.8)
\end{aligned}$$

Using the relation $\mathbf{p} = \boldsymbol{\pi} - \mathbf{QA}$ between the kinetic momentum and canonical momentum, one obtains the equation of motion for the kinetic momentum,

$$\begin{aligned}
\frac{dp^i}{dt} &= \frac{d\pi^i}{dt} - Q\frac{dA^i}{dt}, \\
&= Q\sigma^j \frac{\partial A^j}{\partial x^i} - Q\frac{\partial \phi}{\partial x^i} - Q\frac{\partial A^i}{\partial t} - Q\frac{\partial A^i}{\partial x^j}\dot{x}^j, \\
&= Q\sigma^j \frac{\partial A^j}{\partial x^i} - Q\frac{\partial A^i}{\partial x^j}\sigma^j + QE^i \\
&= Q\epsilon_{ijk}\sigma^j B^k + QE^i, && (3.9)
\end{aligned}$$

where the relations $E^i = -\frac{\partial \phi}{\partial x^i} - \frac{\partial A^i}{\partial t}$ and $B^i = -\frac{1}{2}\epsilon_{ijk}(\frac{\partial A^j}{\partial x^k} - \frac{\partial A^k}{\partial x^j})$ are used. The three equations in the previous paragraph can be rewritten as

$$\dot{\mathbf{r}} = \boldsymbol{\sigma}, \tag{3.10}$$

$$\dot{\mathbf{p}} = Q(\mathbf{E} + \boldsymbol{\sigma} \times \mathbf{B}), \tag{3.11}$$

$$\dot{\boldsymbol{\sigma}} = \frac{2}{\hbar}\mathbf{p} \times \boldsymbol{\sigma}. \tag{3.12}$$

It is seen from Eq. (3.11) that for a massless fermion of right chirality or positive helicity with the direction of its momentum different from that of the magnetic field, its spin acquires a component that is perpendicular to its momentum according to Eq. (3.12). As a result, the particle no longer has a definite helicity. The reason that helicity is not a good quantum number in the presence of magnetic field is because components of the kinetic momentum in the perpendicular direction do not commute.

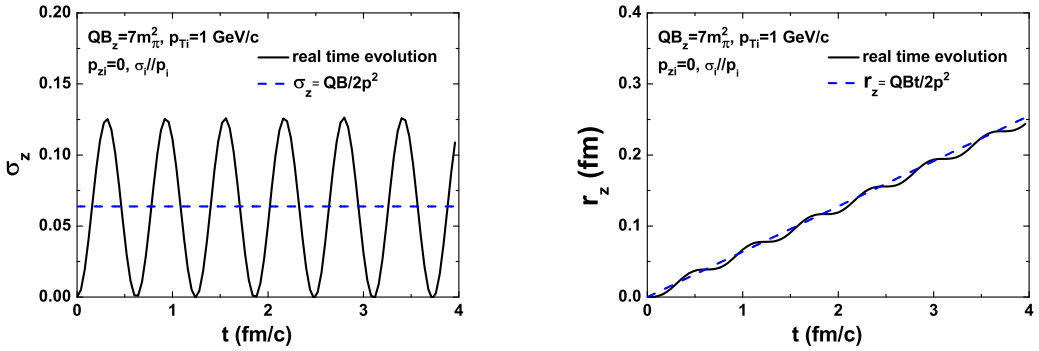

Figure 3.1: Time evolution of the z-component of the spin of a massless fermion (left window) and its displacement (right window) in a magnetic field along the z direction. The initial spin and momentum of the particle are along the same direction in the $x-y$ plane.

To illustrate the above results, one considers a massless fermion with initial kinetic momentum of magnitude 1 GeV/c in the $x-y$ plane and in a magnetic field of magnitude $7m_\pi^2$ in the z direction, and the initial spin direction is taken to be along the kinetic momentum. Results obtained from solving the above equations are shown in Fig. 3.1. It is seen from the solid line in the left window that the spin of the particle in the z-direction oscillates in time with an average value of $\frac{QB}{2p^2}$ given by the dashed

line. According to Eq. (3.10), the velocity of the particle is given by its spin, and this leads to the time dependence of its displacement in the z-direction shown by the solid line in the right window, with its average value shown by the dashed line.

The above equations can be reduced to the chiral kinetic equations of previous sections by using

$$\frac{\hbar}{2}\dot{\boldsymbol{\sigma}} \times \mathbf{p} = (\mathbf{p} \times \boldsymbol{\sigma}) \times \mathbf{p} = \mathbf{p^2}\boldsymbol{\sigma} - (\mathbf{p} \cdot \boldsymbol{\sigma})\mathbf{p}, \tag{3.13}$$

which can be rewritten as

$$\boldsymbol{\sigma} = \frac{\hbar}{2p^2}\dot{\boldsymbol{\sigma}} \times \mathbf{p} + (\hat{\mathbf{p}} \cdot \boldsymbol{\sigma})\hat{\mathbf{p}}. \tag{3.14}$$

The first-order quantum correction to the above equation can be obtained by iteration, and the result is given by

$$\begin{aligned} \boldsymbol{\sigma} &= \hat{\mathbf{p}} + \frac{\hbar}{2p^2}\dot{\hat{\mathbf{p}}} \times \mathbf{p} + (\hat{\mathbf{p}} \cdot \hat{\mathbf{p}})\hat{\mathbf{p}} - \hat{\mathbf{p}} + \mathcal{O}(\hbar^{\mathbf{2}}) \\ &= \hat{\mathbf{p}} + \hbar\dot{\mathbf{p}} \times \frac{\mathbf{p}}{2p^3} + \mathcal{O}(\hbar^2). \end{aligned} \tag{3.15}$$

Using this equation in Eqs.(3.10) and (3.11) and the convention of $\hbar = 1$, one then obtains the chiral kinetic equations in previous sections.

Results obtained from solving the chiral kinetic equations for the example discussed in the above are shown by the dashed lines in Fig. 3.1, which thus correspond to the average values of the exact results obtained from solving Eqs.(3.10)-(3.12).

3.4 Phase-space modification due to chiral kinetic motions

The Berry curvature not only changes the equations of motion of massless fermions but also modifies the volume of their phase space from $d^3\mathbf{x}d^3\mathbf{p}$ to $\sqrt{G}d^3\mathbf{x}d^3\mathbf{p}$, where

$\sqrt{G} = 1 + \lambda Q(\mathbf{B} \cdot \mathbf{b})$ [91, 92, 93]. This can be understood either by considering the change in the volume of the phase space of a particle during a short time interval [91] or that in the Poisson brackets for different combinations of $\mathbf{x}$ and $\mathbf{p}$ [93]. In this section, some details of the derivation, which are missing in Ref. [91], are given. Following Ref. [91], the change in the volume of the phase space is

$$\begin{aligned} d(\mathbf{x} + \Delta\mathbf{x}) d(\mathbf{p} + \Delta\mathbf{p}) &= d(\mathbf{x} + \dot{\mathbf{x}} dt) d(\mathbf{p} + \dot{\mathbf{p}} dt) \\ &\approx d\mathbf{x} d\mathbf{p} [1 + dt(\boldsymbol{\nabla}_{\mathbf{x}} \cdot \dot{\mathbf{x}} + \boldsymbol{\nabla}_{\mathbf{p}} \cdot \dot{\mathbf{p}})]. \end{aligned} \tag{3.16}$$

In terms of $\Delta V = d\mathbf{x} d\mathbf{p}$, the above equation becomes $d\Delta V = \Delta V dt(\boldsymbol{\nabla}_{\mathbf{x}} \cdot \dot{\mathbf{x}} + \boldsymbol{\nabla}_{\mathbf{p}} \cdot \dot{\mathbf{p}})$. Using the identity

$$\boldsymbol{\nabla}_{\mathbf{x}} \cdot \dot{\mathbf{x}} + \boldsymbol{\nabla}_{\mathbf{p}} \cdot \dot{\mathbf{p}} = \frac{\boldsymbol{\nabla}_{\mathbf{x}} \cdot (\sqrt{G}\dot{\mathbf{x}}) + \boldsymbol{\nabla}_{\mathbf{p}} \cdot (\sqrt{G}\dot{\mathbf{p}})}{\sqrt{G}} - \frac{\dot{\mathbf{x}} \cdot \boldsymbol{\nabla}_{\mathbf{x}} \sqrt{G} + \dot{\mathbf{p}} \cdot \boldsymbol{\nabla}_{\mathbf{p}} \sqrt{G}}{\sqrt{G}}, \tag{3.17}$$

and Eqs.(3.2) and (3.3), one finds

$$
\begin{aligned}
&\boldsymbol{\nabla}_{\mathbf{x}} \cdot \dot{\mathbf{x}} + \boldsymbol{\nabla}_{\mathbf{p}} \cdot \dot{\mathbf{p}} \\
&= \frac{Q\lambda(\boldsymbol{\nabla}_{\mathbf{x}} \times \mathbf{E}) \cdot \mathbf{b} + Q\lambda \frac{\boldsymbol{\nabla}_{\mathbf{x}} \cdot \mathbf{B}}{2p^2} + Q(\boldsymbol{\nabla}_{\mathbf{p}} \times \hat{\mathbf{p}}) \cdot \mathbf{B} + Q^2\lambda 2\pi\delta^{(3)}(\mathbf{p})(\mathbf{E} \cdot \mathbf{B})}{\sqrt{G}} \\
&\quad - \frac{\dot{\mathbf{x}}\boldsymbol{\nabla}_{\mathbf{x}}\sqrt{G} + \dot{\mathbf{p}}\boldsymbol{\nabla}_{\mathbf{p}}\sqrt{G}}{\sqrt{G}} \\
&= \frac{-Q\lambda \frac{\partial \mathbf{B}}{\partial t} \cdot \mathbf{b} + Q^2\lambda 2\pi\delta^{(3)}(\mathbf{p})(\mathbf{E} \cdot \mathbf{B})}{\sqrt{G}} - \frac{\dot{\mathbf{x}}\boldsymbol{\nabla}_{\mathbf{x}}\sqrt{G} + \dot{\mathbf{p}}\boldsymbol{\nabla}_{\mathbf{p}}\sqrt{G}}{\sqrt{G}} \\
&= \frac{-Q\lambda \frac{d(\mathbf{B}\cdot\mathbf{b})}{dt} + Q\lambda \frac{\partial(\mathbf{B}\cdot\mathbf{b})}{\partial \mathbf{x}} \cdot \dot{\mathbf{x}} + Q\lambda \frac{\partial(\mathbf{B}\cdot\mathbf{b})}{\partial \mathbf{p}} \cdot \dot{\mathbf{p}} + Q^2\lambda 2\pi\delta^{(3)}(\mathbf{p})(\mathbf{B} \cdot \mathbf{E})}{\sqrt{G}} \\
&\quad - \frac{\dot{\mathbf{x}}\boldsymbol{\nabla}_{\mathbf{x}}\sqrt{G} + \dot{\mathbf{p}}\boldsymbol{\nabla}_{\mathbf{p}}\sqrt{G}}{\sqrt{G}} \\
&= \frac{-Q\lambda \frac{d(\mathbf{B}\cdot\mathbf{b})}{dt} + Q^2\lambda 2\pi\delta^{(3)}(\mathbf{p})(\mathbf{B} \cdot \mathbf{E})}{\sqrt{G}},
\end{aligned}
\tag{3.18}
$$

after using the Maxwell equations $\boldsymbol{\nabla} \cdot \mathbf{B} = 0$ and $\boldsymbol{\nabla} \times \mathbf{E} = -\frac{\partial \mathbf{B}}{\partial t}$ as well as the relation $\nabla \cdot \mathbf{b} = 2\pi\delta^{(3)}(\mathbf{p})$. Therefore, one has

$$
\frac{d\Delta V}{\Delta V} = -\frac{d\sqrt{G}}{\sqrt{G}} + \frac{Q^2\lambda 2\pi\delta^3(\mathbf{p})(\mathbf{E} \cdot \mathbf{B})}{\sqrt{G}} dt.
$$

For particles of non-zero momentum, the second term is zero, and one has $\Delta V = \frac{\Delta V_0}{\sqrt{G}}$, which shows that the phase-space volume is no longer conserved during the time evolution of the particle. Since the phase-space volume is a local function of state variables and should not have a memory of the past, one can thus introduce a modified phase-space volume $\sqrt{G}d^3\mathbf{x}d^3\mathbf{p}$ such that it remains the same as it moves in a magnetic field.

One can also obtain the above result from the Boltzmann equation $\frac{\partial f}{\partial t} + \dot{\mathbf{x}} \cdot \frac{\partial f}{\partial \mathbf{x}} +$

$\dot{\mathbf{p}} \cdot \frac{\partial f}{\partial \mathbf{p}} = 0$ in the collisionless limit. Using the equation

$$\frac{\partial \sqrt{G}}{\partial t} + \frac{\partial \sqrt{G}\dot{\mathbf{x}}}{\partial \mathbf{x}} + \frac{\partial \sqrt{G}\dot{\mathbf{p}}}{\partial \mathbf{p}} = 2Q^2\lambda\pi \mathbf{E}\cdot\mathbf{B}\delta^3(\mathbf{p}),$$

which can be derived by using the Maxwell equations and the definition of $\sqrt{G}$, one has

$$\frac{\partial \sqrt{G}f}{\partial t} + \frac{\partial \sqrt{G}f\dot{\mathbf{x}}}{\partial \mathbf{x}} + \frac{\partial \sqrt{G}f\dot{\mathbf{p}}}{\partial \mathbf{p}} = 2Q^2\lambda\pi f\mathbf{E}\cdot\mathbf{B}\delta^3(\mathbf{p}).$$

The charge current for right chirality particles and antiparticles is then

$$\begin{aligned} \mathbf{J}^V_R &= Q\int \frac{d^3\mathbf{p}}{(2\pi)^3} f(p-\mu_R)\sqrt{G}\dot{\mathbf{x}} - Q\int \frac{d^3\mathbf{p}}{(2\pi)^3} f(p+\mu_R)\sqrt{G}\dot{\mathbf{x}} \\ &= \frac{Q^2\mathbf{B}}{4\pi^2}\int_0^\infty dp[f(p-\mu_R) - f(p+\mu_R)], \end{aligned} \tag{3.19}$$

which is the same as that from solving the Dirac equation. The same holds for the charge current of left chirality particles and antiparticles obtained from these two approaches.

One can also obtain the chiral anomaly from the chiral kinetic equations. For right chirality particles and antiparticles, one finds

$$\frac{dn_R}{dt} = \int \frac{d^3\mathbf{p}}{(2\pi)^3} 2Q^2\pi f(p-\mu_R)\mathbf{E}\cdot\mathbf{B}\delta^3(\mathbf{p}) = \frac{Q^2\mathbf{E}\cdot\mathbf{B}}{4\pi^2} f(-\mu_R), \tag{3.20}$$

$$\frac{dn_{\bar{R}}}{dt} = -\int \frac{d^3\mathbf{p}}{(2\pi)^3} 2Q^2\pi f(p+\mu_R)\mathbf{E}\cdot\mathbf{B}\delta^3(\mathbf{p}) = -\frac{Q^2\mathbf{E}\cdot\mathbf{B}}{4\pi^2} f(\mu_R), \tag{3.21}$$

which gives

$$\frac{d(n_R - n_{\bar{R}})}{dt} = \frac{Q^2\mathbf{E}\cdot\mathbf{B}}{4\pi^2}[f(-\mu_R) + f(\mu_R)] = \frac{Q^2\mathbf{E}\cdot\mathbf{B}}{4\pi^2}. \tag{3.22}$$

The above equation shows that the chiral anomaly does not depend on the temperature and chemical potential of the system and thus is valid for any systems of massless Dirac fermions. A similar equation can be obtained for left chirality particles and antiparticles. Combining the two equations then leads to the chiral anomaly equation $\frac{dn^5}{dt} = \frac{Q^2\mathbf{E}\cdot\mathbf{B}}{2\pi^2}$. It is noted that although the chiral anomaly can be derived from the geometric phase as described above, it is generically a topological effect [94, 95] and can be verified from a more general consideration such as the Fujikawa method [38].

3.5 Chiral magnetic wave in chiral kinetic theory

The CMW can also be described in chiral kinetic theory [96], which is valid for a weak magnetic field, and the derivation in Ref. [96] is given in Appendix C for completeness. It is shown in section 2.1.4 that the velocity of the CMW is $\frac{6QB}{4\pi^2T^2}$ when the massless fermions are described by the Fermi-Dirac distribution. In contrast, using the classical Boltzmann distribution gives $\omega = \mathbf{k}\cdot\frac{Q\mathbf{B}}{4T^2}$, which leads to a larger velocity for the CMW than that from the Fermi-Dirac distribution. This is because more particles have higher momentum in the latter case as a result of the Pauli principle, which then leads to a smaller velocity according to $\mathbf{v} = \frac{e\mathbf{B}}{2p^2}$.

3.6 Chiral vortical effects in chiral kinetic theory

Chiral vortical effects can also be studied in chiral kinetic theory. Although the chiral kinetic equations for fermions in a vorticity field can be derived from the quantum Wigner functions [75, 76], the effect of the vorticity field on the motions of massless fermions can also be included in the chiral kinetic equation through the Coriolis force [72] as shown in Ref. [5] and to be followed in this section. In the absence of mean-field potentials, such as those in Refs. [79, 97, 98, 99] based on the Nambu-Jona-Lasinio model, the momentum $\mathbf{p}$ of a particle in the center-of-mass or fireball frame of a heavy ion collision is a constant between scatterings, that is $\dot{\mathbf{p}} = 0$.

Its momentum $\mathbf{p}'$ in the frame that rotates with an angular velocity given by the vorticity field $\boldsymbol{\omega}$ is, however, affected by the Coriolis force,

$$\dot{\mathbf{p}}' = -2p'\boldsymbol{\omega} \times \dot{\mathbf{r}}', \tag{3.23}$$

where p' is the magnitude of $\mathbf{p}'$ and $\dot{\mathbf{r}}'$ is the velocity of the particle in the rotating frame.

From the adiabatic approximation to the motion of a massless spin-$\frac{1}{2}$ particle that the direction of its spin follows instantaneously the direction of its momentum [72] or from considering the conservation of the total angular momentum of the particle [1] in this rotating frame, its velocity $\dot{\mathbf{r}}'$ is given by,

$$\dot{\mathbf{r}}' = \hat{\mathbf{p}}' + \lambda \dot{\mathbf{p}}' \times \mathbf{b}', \tag{3.24}$$

where $\lambda = \pm 1$ is the helicity of the particle, $\hat{\mathbf{p}}'$ is a unit vector along $\mathbf{p}'$, and $\mathbf{b}' = \frac{\hat{\mathbf{p}}'}{2p'^2}$ is the Berry curvature resulting from the adiabatic approximation [72] or the conservation of the total angular momentum [1]. Substituting Eq. (3.23) to Eq. (3.24) leads to

$$\dot{\mathbf{r}}' \;=\; \frac{\hat{\mathbf{p}}' + 2\lambda p'(\hat{\mathbf{p}}' \cdot \mathbf{b}')\boldsymbol{\omega}}{1 + 2\lambda p'(\boldsymbol{\omega} \cdot \mathbf{b}')}. \tag{3.25}$$

In the absence of collective flow, the origin of the rotational frame is stationary in the fireball frame. In this case, $\dot{\mathbf{r}} = \dot{\mathbf{r}}'$ and $\mathbf{p} = \mathbf{p}'$, and the chiral kinetic equations of motion for massless spin-$\frac{1}{2}$ particles are thus

$$\dot{\mathbf{r}} = \frac{\hat{\mathbf{p}} + 2\lambda p(\hat{\mathbf{p}} \cdot \mathbf{b})\boldsymbol{\omega}}{1 + 2\lambda p(\boldsymbol{\omega} \cdot \mathbf{b})}, \quad \dot{\mathbf{p}} = 0. \tag{3.26}$$

The two equations in Eq. (3.26) are similar to those derived in Ref. [76] from consideration of the covariant Wigner distribution function of massless spin 1/2 particles in a vorticity field, except that the numerical factor 2 in the denominator is 4 instead. Although applying the usual Lorentz transformation to Eq. (3.25) does not lead to Eq. (3.26), it is known that the chiral kinetic equations satisfy a nontrivial Lorentz transformation [100]. Therefore Eq. (3.26) is also assumed to be valid for the case with collective flow. As to the numerical factor in the denominator, later considerations based on the covariant Wigner distribution function of massless spin 1/2 particles have indicated that its value is not uniquely determined [101]. One therefore has in general the equations of motion for massless particles in the presence of a vortical field are

$$\begin{aligned} \dot{\mathbf{r}} &= \frac{\hat{\mathbf{p}} + 2\lambda p(\hat{\mathbf{p}}\cdot\mathbf{b})\boldsymbol{\omega}}{\sqrt{G}}, \\ \dot{\mathbf{p}} &= 0 \end{aligned}$$

with $\sqrt{G} = 1 + a\lambda p(\boldsymbol{\omega}\cdot\mathbf{b})$ and $\mathbf{b} = \frac{\hat{\mathbf{p}}}{2p^3}$.

Since the phase-space measure is also changed by the vorticity field, the vector charge currents of right and left chirality particles and antiparticles are given by

$$\begin{aligned} \mathbf{J}_{R,L} &= \int \frac{d^3\mathbf{p}}{(2\pi)^3}\sqrt{G}\dot{\mathbf{x}} f(p-\mu_{R,L}) - \int \frac{d^3\mathbf{p}}{(2\pi)^3}\sqrt{G}\dot{\mathbf{x}} f(p+\mu_{R,L}) \\ &= \boldsymbol{\omega}\left(\frac{T^2}{12} + \frac{\mu_{R,L}^2}{4\pi^2}\right), \end{aligned} \tag{3.27}$$

the same as those obtained from solving the Dirac equation.

The CVW can also be derived in chiral kinetic theory in a similar way as that for the CMW [29], which is also shown in Appendix C. It is of interest to note that there are also studies of the chiral vortical effects by taking into consideration of the

scattering between spin-polarized particles and antiparticles [90, 102].

4. ANOMALOUS TRANSPORT MODEL STUDY OF CHIRAL MAGNETIC EFFECTS IN HEAVY ION COLLISIONS *

In the present chapter, the chiral kinetic equations for massless quarks and antiquarks are solved using the test particle method [103] and also the scatterings of these particles is included by assuming that they are not affected by the magnetic field. With initial conditions taken from a Bjorken boost-invariant model without initial transverse flow, this anomalous transport model is then used to study the elliptic flow in heavy ion collisions at the highest energy from RHIC and the results are compared with those obtained from anomalous hydrodynamics [54] and with the experimental data [3].

4.1 The anomalous transport model

As discussed in previous chapters, the dynamics of massless spin-1/2 fermions in a magnetic field can be described by the anomalous transport equation for the phase-space distribution functions f_R and f_L of right chirality and left chirality ones, that is

$$\partial_t f_{R/L} + \dot{\mathbf{x}} \cdot \nabla_{\mathbf{x}} f_{R/L} + \dot{\mathbf{p}} \cdot \nabla_{\mathbf{p}} f_{R/L} = I_C, \tag{4.1}$$

where

$$\frac{d\mathbf{r}}{dt} = \frac{\hat{\mathbf{p}} + \lambda Q(\hat{\mathbf{p}} \cdot \mathbf{b})\mathbf{B}}{1 + \lambda Q \mathbf{B} \cdot \mathbf{b}}, \tag{4.2}$$

$$\frac{d\mathbf{p}}{dt} = \frac{Q\hat{\mathbf{p}} \times \mathbf{B}}{1 + \lambda Q \mathbf{B} \cdot \mathbf{b}}, \tag{4.3}$$

*Reprinted with permission from "Anomalous transport model study of chiral magnetic effects in heavy ion collisions"by Yifeng Sun, Che Ming Ko and Feng Li, 2016, Phys. Rev. C **94**, 045204, Copyright 2016 by APS.

with $\lambda = 1$ for particles and antiparticles of positive helicity and $\lambda = -1$ for particles and antiparticles of negative helicity, and the Berry curvature $\mathbf{b} = \frac{\mathbf{p}}{2p^3}$.

The term I_C on the right-hand side of the transport equation is the collision term that takes into account the effect due to scattering of massless quarks and antiquarks. In most studies, this effect is addressed in the relaxation time approach either for quark-quark scattering [104] or for quark-gluon scattering [105]. Since the interaction Lagrangian of massless quarks and antiquarks with gluons in QCD is $\mathcal{L} = ig\bar{q}_R \not{A} q_R + ig\bar{q}_L \not{A} q_L$, where g is the strong coupling constant, q_R and q_L are the field operators for quarks of right and left chiralities, respectively, and $\not{A} = \gamma^\mu A_\mu$ with A_μ being the gluon filed, there are no changes in the chiralities of quarks in quark-quark scattering and of antiquarks in antiquark-antiquark scattering. For the scattering between quark and antiquark, their chiralities can, however, change through the s-channel annihilation process. The processes $q_R\bar{q}_R \to q_L\bar{q}_L$ and $q_L\bar{q}_L \to q_R\bar{q}_R$ conserve axial charge density, which is given by $n_5 = \left\langle \bar{\Psi}\gamma^0\gamma^5\Psi \right\rangle = \left\langle \bar{\Psi}_R\gamma^0\Psi_R \right\rangle - \left\langle \bar{\Psi}_L\gamma^0\Psi_L \right\rangle = (n_R - n_{\bar{R}}) - (n_L - n_{\bar{L}})$, and are thus allowed in QCD, which is chirally invariant in the massless quark limit. This process ensures both local charge and axial charge conservations in an equilibrated quark matter and is essential for generating a splitting of the elliptic flows of positively and negatively charged particles in the kinetic approach. The reason for this is as follows. Although the chiral kinetic motion can lead to a separation of particles of right chiralities from those of left chiralities in space, the effect is the same for positively and negatively charged particles. However, including quark-antiquark scatterings that change their chiralities can result in a charge quadrupole moment in the transverse plane of a heavy ion collision. For simplicity, only massless quarks and antiquarks are allowed to undergo chirality changing scattering in quark-antiquark scattering.

The combined effects due to the chiral kinetic motion (CKM) and the chirality

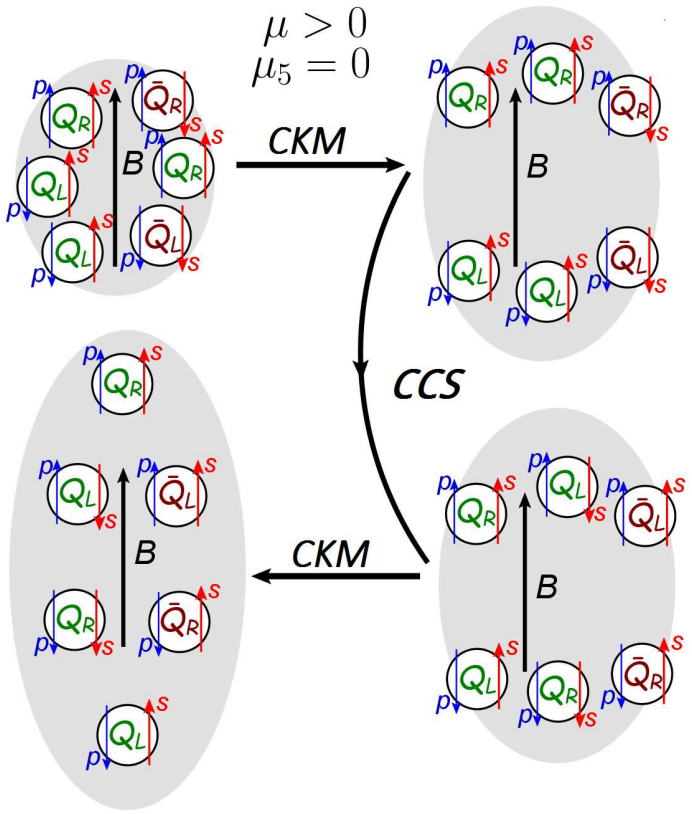

Figure 4.1: Effects of chiral kinetic motion (CKM) and chirality changing scattering between quark and antiquark (CCS) on the distribution of massless quarks and antiquarks in the transverse plane of a heavy ion collision with initial positive charge chemical potential $\mu > 0$ and vanishing axial charge chemical potential $\mu_5 = 0$. Reprinted from Ref. [1]

changing scattering (CCS) between quark and antiquark in heavy ion collisions in the presence of a magnetic field are illustrated in Fig. 4.1. The upper left picture shows the initial distribution of quarks and antiquarks in the transverse plane for the case of positive charge chemical potential $\mu > 0$ and vanishing axial charge chemical potential $\mu_5 = 0$, corresponding to more quarks than antiquarks but with equal number of right and left chiralities. In the above, one has $\mu = (\mu_R + \mu_L)/2$ and $\mu_5 = (\mu_R - \mu_L)/2$, where $\mu_R/T = (N_R - N_{\bar{R}})/(N_R + N_{\bar{R}})$ and $\mu_L/T = (N_L - N_{\bar{L}})/(N_L + N_{\bar{L}})$ with N_R and N_L denoting the numbers of particles with right and left chiralities,

respectively, while $N_{\bar{R}}$ and $N_{\bar{L}}$ denoting corresponding numbers for antiparticles. The temperature of the quark matter is denoted by T. Equation (4.2) then indicates that quarks and antiquarks of right chiralities would move upward along the direction of the magnetic field, while those of left chiralities would move in the opposite direction, leading to a positive axial charge dipole moment in the transverse plane, as shown in the upper right picture of Fig. 4.1. The lower right picture shows the effect of the chirality changing quark-antiquark scattering $q_R\bar{q}_R \to q_L\bar{q}_L$ and $q_L\bar{q}_L \to q_R\bar{q}_R$. Further upward and downward motions of quarks and antiquarks of right and left chiralities, respectively, according to Eq. (4.2) result in the lower left picture, which clearly shows a positive axial charge dipole moment and a positive charge quadrupole moment in the transverse plane. The latter can then lead to a splitting of the elliptic flows of positively charged quarks and negatively charged antiquarks as shown in Refs. [27, 106].

In the above discussion, the effect of gluons in the system is not considered. Since gluons have spin one, they will not change the chiralities of the quarks or antiquarks that they scatter with [105]. Including these scatterings will thus not affect the picture discussed in the above. Also, the magnetic field affects the scattering of quarks and antiquarks through the change of the phase-space integral in the collision term of the chiral transport model [104, 105], i.e., replacing the usual $d^3\mathbf{x}d^3\mathbf{p}/(2\pi)^3$ by $(1 + \lambda Q\mathbf{B}\cdot\mathbf{b})d^3\mathbf{x}d^3\mathbf{p}/(2\pi)^3$, which is needed to ensure the correct equilibrium distribution in the presence of the magnetic field. Since it was not known how this effect could be included in the chiral transport model when the study in Ref. [1] was carried out, it had been neglected in that study.

To implement particle scatterings in the chiral or anomalous transport model, the geometric method of Ref. [107] is generalized by using the scattering cross section σ in the fireball frame to check whether the impact parameter between two colliding

particles is smaller than $\sqrt{\sigma/\pi}$ and if the two colliding particles pass through each other at the next time step during the evolution of the system. For the three-momenta of the two particles after their scattering, they are taken to be isotropic in their center-of-mass frame. The Pauli blocking effect on the final states is, however, neglected because of the high temperature of the partonic matter produced in heavy ion collisions.

4.2 Heavy ion collisions in the presence of magnetic field

To apply the anomalous transport model to heavy ion collisions, a Bjorken boost-invariant model is used for the initial conditions. Specifically, the cubic power of temperature distribution, which is proportional to the particle number density distribution, in the transverse plane of the collision is taken to have a Woods-Saxon form

$$T(x,y) = \frac{T_0}{(1+e^{\frac{\sqrt{x^2+y^2/c^2}-R}{a}})^{\frac{1}{3}}}, \tag{4.4}$$

where c describes the spatial anisotropy of produced partonic matter in the transverse plane of non-central heavy ion collisions, R is the radius, and a is surface thickness. The transverse momentum distributions of quarks and antiquarks are then given by the corresponding Boltzmann distributions with a charge chemical potential μ. For simplicity, quarks and antiquarks are taken to have same electric charge of $e/2$ and $-e/2$[2], respectively, and assume that the ratio μ/T is uniform in space. For distributions in the z direction, it is assumed to be boost invariant, i.e., $z = \tau_0 \sinh y$ and $p_z = m_T \sinh y$, where τ_0, $m_T = \sqrt{m_q^2 + p_x^2 + p_y^2} = \sqrt{p_x^2 + p_y^2} = p_T$, and y are the thermalization time, transverse mass, and rapidity, respectively. For the initial

[2]Although this would underestimate the effect on u and $\bar{u}$ quarks and overestimate that on d and $\bar{d}$ quarks, the net effect would be minimal for flavor-symmetric quark matter.

axial charge chemical potential μ_5/T, it is taken to be zero everywhere.

To study the chiral magnetic effect in heavy ion collisions, the magnetic field **B** generated in these collisions is assumed to be uniform along the y axis, which is perpendicular to the reaction plane, as in Ref. [108] and to have the following time dependence:

$$eB = \frac{eB_0}{1 + (t/\tau)^2} \tag{4.5}$$

with B_0 and τ being its maximum strength and lifetime, respectively. According to Ref. [40], the magnitude of the magnetic field in a heavy ion collision can be as large as several 10^{14} T in noncentral Au+Au collisions at $\sqrt{s} = 200$ GeV, although it lasts for only about 0.1 fm/c. However, including the electric conductivity effect could increase the lifetime of the magnetic field in a heavy ion collision to several fm/c [109]. More discussions about the time evolution of magnetic field can be found in Refs. [110, 111, 40, 109] as well as in Appendix B.

With above initial conditions and magnetic field, the anomalous transport equations are solved using the parameters $T_0 = 300$ MeV, $R = 3.5$ fm, $a = 0.5$ fm, $c = 1.5$, and $\tau_0 = 0.4$ fm/c that are appropriate for Au+Au collisions at center-of-mass energy $\sqrt{s} = 200$ GeV and impact parameter $b = 9$ fm, which approximately corresponds to collisions at the 30–40% centrality. The total number of quarks and antiquarks is then approximately 1500 if one considers only rapidities $|y| \leq 2$. As in the AMPT model [112] and the Nambu-Jona-Lasinio model [113], it is assumed that only quarks and antiquarks are present in the partonic phase of a heavy ion collision. For the magnetic field, the values $eB_0 = 7m_\pi^2$ and $\tau = 6$ fm/c are used. For the value of μ/T, which is the same as the charge asymmetry $A_\pm = \frac{N_+ - N_-}{N_+ + N_-}$ of the partonic matter, where N_+ and N_- are the numbers of positively and negatively charged

quarks, respectively, a number of values between 0 and 0.16 are considered. For the parton scattering cross section, it is taken to have the temperature dependence $\sigma = \sigma_0(T_0/T)^3$ in order to be consistent with that calculated in the NJL model [114] and the shear viscosity to entropy density ratio extracted from the measured elliptic flow using the viscous hydrodynamics [115]. For the value of σ_0, it is chosen to reproduce the measured elliptic flow of pions and is taken to be isotropic and independent of the momenta and energy of the colliding particles. As to the temperature of the local medium where two partons scatter, it is determined from taking the local energy density to be the same as that of an equilibrated noninteracting massless quarks and antiquarks. Because of the smaller number of partons in a local cell, the energy density is evaluated by using partons from a large ensemble of events, although only partons in the same event are allowed to scatter with each other [107].

Since partons in a local cell are expected to convert to hadrons when their temperature drops below the chirality restoration temperature T_χ, which is taken to be 150 MeV, the duality ansatz is used by simply relabelling quarks as pions and letting them follow the normal equations of motion with the velocity given by $\mathbf{p}/E$ and to scatter with known hadronic cross sections given in Ref. [116]. One could import these quarks and antiquarks to the AMPT model to convert them to hadrons and let the latter undergo further hadronic scattering as in Ref. [97]. Since most quarks and antiquarks are converted to resonances such as the ρ meson, which subsequently decay to pions, using the quark-hadron duality by converting a quark to a pion is thus a reasonable approximation. In the present study, particles after T_χ are evolved until they freeze-out kinetically, which is defined locally when the temperature of a cell drops to $T_f = 120$ MeV. Note that the effect from switching from the chiral kinetic equation to the normal equation of motion at T_χ is similar to the freeze-out hole effect discussed in Ref. [54].

4.3 Results

In the present section, the time evolution of the partonic matter is studied by following the motions of quarks and antiquarks according to the chiral kinetic equations [Eqs. (4.2) and (4.3)] with and without the Lorentz force as well as with and without including the chirality changing scattering between quark and antiquark. These different studies allow us to investigate the relative importance among the effects due to the chiral kinetic motion (CKM), the Lorentz force (LF), and the chirality changing scattering (CCS).

4.3.1 Pion elliptic flow

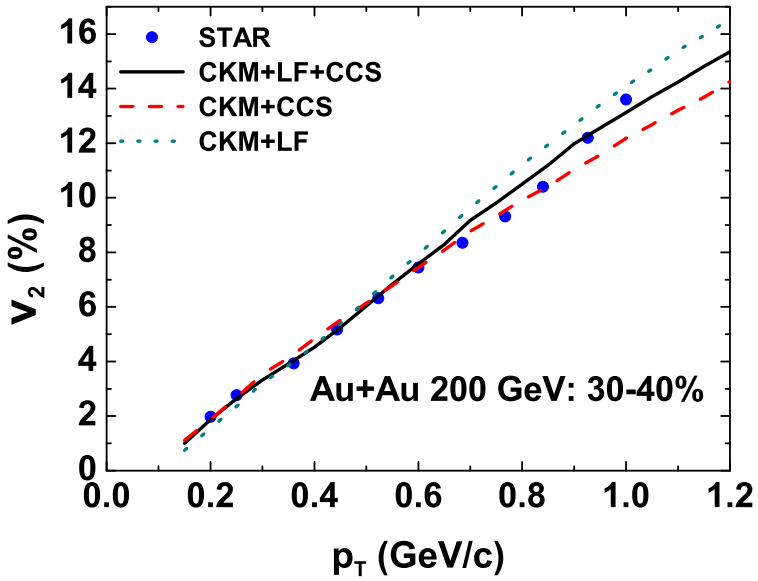

Figure 4.2: Elliptic flow of all kinetically freeze-out pions as a function of their transverse momentum for the three cases of chiral kinetic motion with Lorentz force and chirality changing scattering (CKM+LF+CCS), without chirality changing scattering (CKM+LF), and without Lorentz force (CKM+CCS). Experimental data (solid circles) are from Ref. [2]. Reprinted from Ref. [1]

The dashed line in Fig. 4.2 shows the elliptic flow v_2 of all kinetically freeze-out pions as a function of their transverse momentum in midrapidity ($|y| \leq 1$) from solving the chiral kinetic equation with Lorentz force and including the chirality changing scattering (CKM+LF+CCS). It is obtained with a coefficient $\sigma_0 = 13.7$ mb in the parton scattering cross section and is seen to agree with the experimental data (solid circles) from the STAR Collaboration [2]. The result obtained without the chirality changing scattering (CKM+LF), using $\sigma_0 = 13.1$ mb and shown by the dotted line as well as that obtained without the Lorenz force (CKM+CCS), using $\sigma_0 = 15.5$ mb and shown by the dashed line, also agree reasonably with the experimental data, particularly for momentum below 0.5 GeV. The integrated v_2 of these pions with transverse momenta in the range $0.15 \leq p_T \leq 0.5$ GeV/c is 0.036 in all three cases, which reproduces surprisingly well the experimental value.

4.3.2 Time evolution of eccentricity difference

Figure 4.3 shows the time evolution of the difference $\Delta\epsilon_2 = \epsilon_{2-} - \epsilon_{2+}$ between the eccentricities ($\epsilon_2 = \langle (x^2-y^2)/(x^2+y^2) \rangle$) of negatively and positively charged particles for the total charge asymmetry $A_\pm = 0.16$ of these particles. It is noted that this value of $A_\pm$ is much larger than the value $-0.03 < A_\pm^{ex} < 0.03$ in the experimental measurements [3], and it is used in order to amplify the effect of the chiral magnetic wave. The momentum range included in the calculation is again $0.15 \leq p_T \leq 0.5$ GeV/c. The solid line shows the results obtained by following the motions of quarks and antiquarks via the chiral kinetic equation including both the Lorentz force and the chirality changing scattering, i.e., CKM+LF+CCS. The eccentricity difference between negatively and positively charged particles in this case is seen to increase with time, but decreases after reaching a maximum value. This increase is due to both the chiral kinetic effect, which leads to the fluctuation of axial charge, and the effect

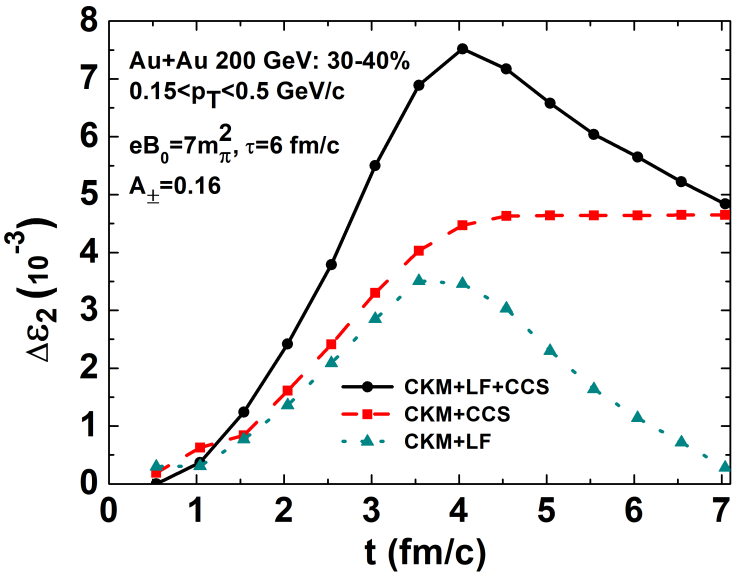

Figure 4.3: Eccentricity difference between negatively and positively charged particles as a function of time for different scenarios of parton dynamics as in Fig. 4.2 when the total charge asymmetry of the quark matter is $A_{\pm} = 0.16$. Reprinted from Ref. [1]

of chirality change in parton scattering, which converts the axial charge fluctuation to the charge fluctuation. How the eccentricity difference between negatively and positively charged particles changes in time in the case neglecting the Lorentz force but including the chirality changing scattering (CKM+CCS), which includes the same physics as in Refs. [53, 54], is shown by the dashed line. The eccentricity difference between positively and negatively charged particles in this case is seen to increase with time until it reachs a plateau. As shown by the dotted line, including the Lorentz force but without the chirality changing scattering (CKM+LF) leads to an eccentricity difference that has a similar time dependence as the CKM+LF+CCS case except a smaller maximum value.

4.3.3 Time evolution of elliptic flow difference

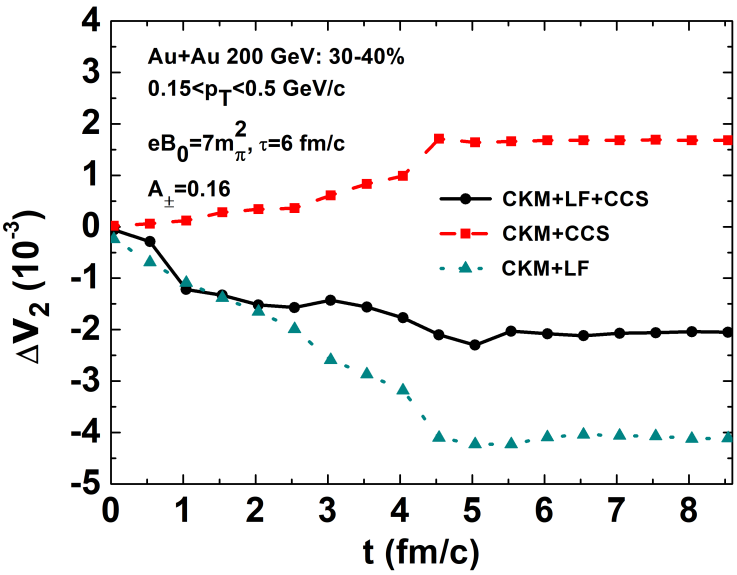

Figure 4.4: Same as Fig. 4.3 for the elliptic flow difference Δv_2 between negatively and positively charged particles. Reprinted from Ref. [1]

Because of their different spatial eccentricities, the elliptic flows of positively and negatively charged particles become different in heavy ion collisions. Fig. 4.4 shows the results for the difference $\Delta v_2 = v_{2-} - v_{2+}$ between the elliptic flows of negatively and positively charged particles with their transverse momenta between 0.15 and 0.5 GeV as a function of time for charge asymmetries $A_\pm = 0.16$. For the case from solving the chiral kinetic equation with Lorentz force and including the chirality changing scattering (CKM+LF+CCS), the elliptic flow difference is seen to decrease with time, which is in contrast with the expectation from the evolution of the eccentricity difference shown in Fig. 4.3. As shown below, this unexpected result

is due to the competition between the effects of the CMW and the Lorentz force.

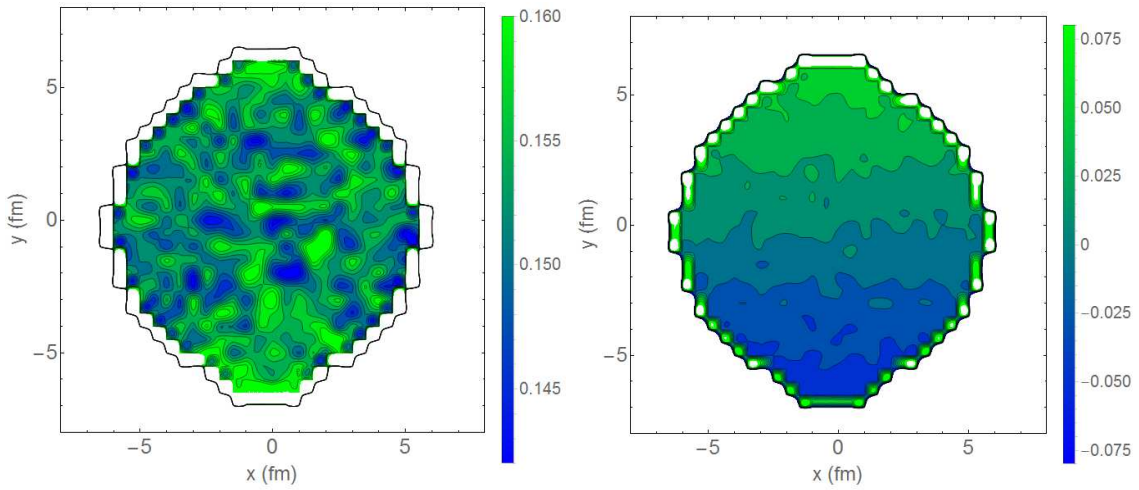

Figure 4.5: Charge chemical potential μ/T (left window) and axial charge chemical potential μ_5/T (right window) distributions in the transverse plane $z = 0$ at time $t =$ 5 fm/c for events with charge asymmetry $A_\pm = 0.16$ for the case of including chiral kinetic motion and chirality changing scattering but no Lorentz force. Reprinted from Ref. [1]

For the case neglecting the Lorentz force (CKM+CCS), the elliptic flow difference shown by the dashed line is seen to increase with time as a result of the larger eccentricity of negatively charged particles compared to positively charged particles. To better understand the reason for the elliptic flow difference between positively and negatively charged partons, we show in Fig. 4.5 the charge chemical potential μ/T (left window) and axial charge chemical potential μ_5/T (right window) distributions of particles in the transverse plane ($z = 0$) at time $t = 5$ fm/c. It is seen that the charge chemical potential is small in the equator and large in the pole of the transverse plane of the collision, similar to that found in Ref. [27] based on the CMW consideration. It also confirms the schematic pictures illustrated in Fig. 4.1. The

charge quadrupole moment resulting from such a distribution would then lead to an elliptic flow that is larger for negatively charged particles than for positively charged particles as demonstrated in Ref. [106] using the AMPT model by giving a finite electric quadrupole moment in the initial parton distribution. The distribution of μ_5/T in the transverse plane of the collision shows, on the other hand, a finite dipole moment. These results thus clearly demonstrate that the chiral kinetic equation leads to the separation of partons with different chiralities in the transverse plane of a heavy ion collision, which leads at the same time to a separation of partons of different charges by the chirality changing scattering between massless positively and negatively charged partons, reminiscent of the effect due to the CMW. If the change of the chiralities of these partons during their scattering is not allowed in the anomalous transport model, both μ/T and μ_5/T would be uniform in space with the values $\mu/T = 0.16$ and $\mu_5/T = 0$. This agrees with the results based only on the chiral kinetic equation, which is same for both positively and negatively charged partons but different for partons of different chiralities.

Shown in Fig. 4.4 by the dotted line are the results obtained with the inclusion of the Lorentz force but not allowing the chiralities to change in the quark-antiquark scattering (CKM+LF). It shows that this further reduces the elliptic flow difference between negatively and positively charged particles. This is because the Lorentz force has an opposite effect from that due to the chiral kinetic motion and the chirality changing quark-antiquark scattering. This can be understood as follows. Because of the cylindrical initial distribution, particles have a larger flow in the z direction than in the x direction. With the magnetic field along the y direction, the Lorentz force then deflects positively and negatively charged particles moving in the positive z-direction to the negative and positive x-axis, respectively. In the case that the charge asymmetry $A_\pm$ is larger than zero, this would lead to more particles in the second and

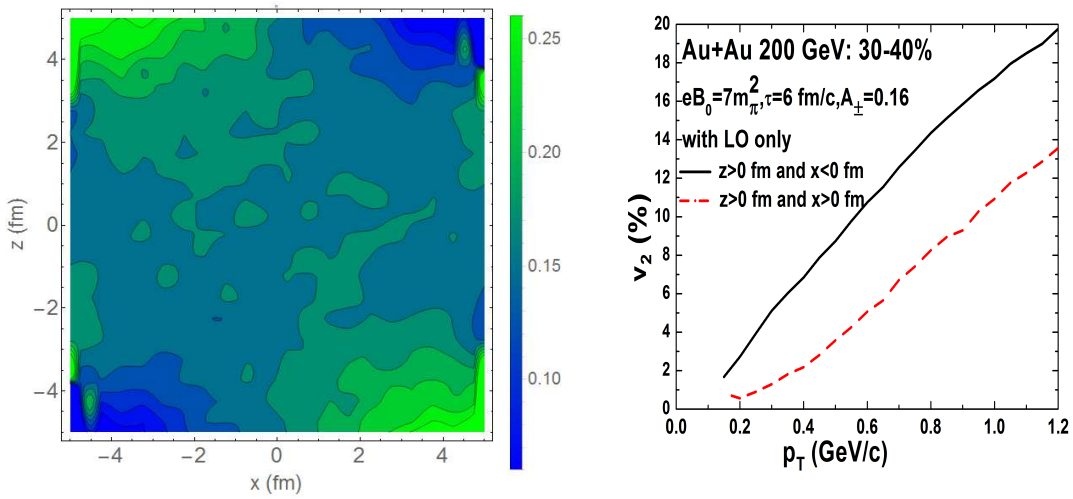

Figure 4.6: Lorentz force effect on charge chemical potential μ/T (left window) and elliptic flow of all particles in the first and second quadrants of $x-z$ plane (right window) at time $t = 5$ fm/c for events with charge asymmetry $A_{\pm} = 0.16$.

fourth quadrants than in the first and third quadrants of the x-z plane as shown in the left window of Fig. 4.6. Due to their more frequent collisions, positively charged particles then acquire a larger elliptic flow than the negatively charged particles as shown in the right window of Fig. 4.6. More specifically, denoting the charge chemical potential and elliptic flow in the first quadrant by μ_r and v_{2r}, respectively, and in the second quadrant by μ_l and v_{2l}, respectively, then one has $\mu_l > \mu_r$ and $v_{2l} > v_{2r}$ as a result of the Lorentz force. The elliptic flows of negatively and positively charged particles are then, respectively,

$$\frac{v_{2l}e^{-\mu_l/T} + v_{2r}e^{-\mu_r/T}}{e^{-\mu_l/T} + e^{-\mu_r/T}} = \frac{v_{2l}}{1+e^{\frac{\mu_l-\mu_r}{T}}} + \frac{v_{2r}}{1+e^{-\frac{\mu_l-\mu_r}{T}}} \tag{4.6}$$

$$\frac{v_{2l}e^{\mu_l/T} + v_{2r}e^{\mu_r/T}}{e^{\mu_l/T} + e^{\mu_r/T}} = \frac{v_{2l}}{1+e^{-\frac{\mu_l-\mu_r}{T}}} + \frac{v_{2r}}{1+e^{\frac{\mu_l-\mu_r}{T}}}. \tag{4.7}$$

Their difference is thus

$$(v_{2l} - v_{2r}) \left(\frac{1}{1 + e^{\frac{\mu_l - \mu_r}{T}}} - \frac{1}{1 + e^{-\frac{\mu_l - \mu_r}{T}}} \right) < 0 \tag{4.8}$$

and is negative. This conclusion is not affected by the inclusion of the third and fourth quadrants.

The above effect due to the Lorentz force will not be present if there is no asymmetry in the initial distribution of particles in the $x - z$ plane. For example, if the initial particle distribution is isotropic in the x-z plane, the charge distribution would remain isotropic in the presence of the Lorentz force, and there would be no elliptic flow difference between the positively and negatively charged particles even for $A_\pm \neq 0$.

It is noted that the axial charge and charge chemical potential distributions in the transverse plane for the case of CKM+LF+CCS also show finite dipole and quadrupole moments, similar to those shown in Figs. 4.5 and 4.6 for the case of CKM+CCS. Without the chirality changing scattering, i.e., for the case of CKM+LF, both the axial charge and charge chemical potential distributions become uniform in the transverse plane, i.e., vanishing dipole and quadrupole moments.

4.3.4 Charge asymmetry dependence of the elliptic flow difference

Shown in Fig. 4.7 by the solid line is the elliptic flow difference Δv_2 between negatively and positively charged particles at freeze-out as a function of the charge asymmetry $A_\pm$ for the case of CKM+LF+CCS. Again, the transverse momenta of these particles are taken to be $0.15 \leq p_T \leq 0.5$ GeV/c. It is seen that the final elliptic flow difference Δv_2 is almost linearly dependent on the total charge asymmetry but with a slope opposite to that found in experiments [3] and in the theoretical study based on the CMW [27]. For the case neglecting the Lorentz force

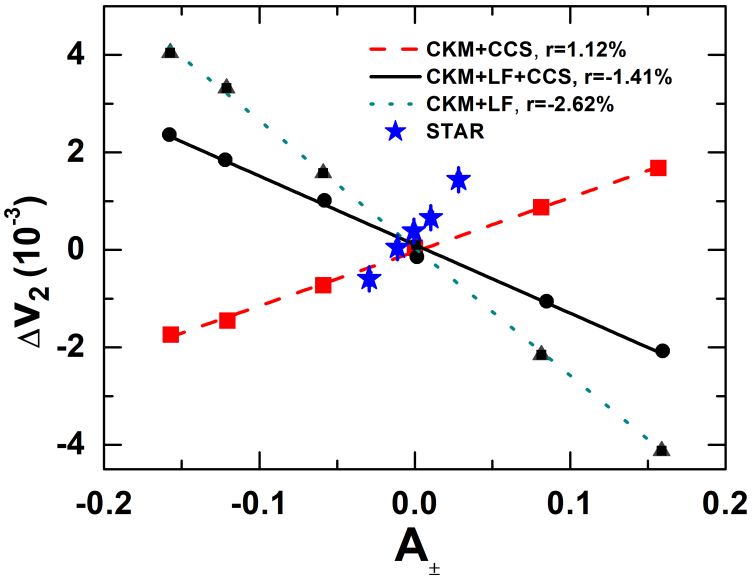

Figure 4.7: Elliptic flow difference Δv_2 as a function of charge asymmetry $A_\pm$ for different scenarios of parton dynamics as in Fig. 4.2. Experimental data (solid stars) are from Ref. [3]. Reprinted from Ref. [1]

but including chirality changing scattering (CKM+CCS), shown by dashed line, the slope of the $A_\pm$ dependence of Δv_2 in the present study is $r = 0.0112$, which gives a value $r/v_2 = 0.31$ that is about a factor of three smaller than the experimental value of 0.85 but is comparable to the value $r/v_2 = 0.27$ from a study based on the anomalous hydrodynamics [54]. For the charge asymmetry dependence of the elliptic flow difference between negatively and positively charged particles in the case including the Lorentz force but neglecting the chirality changing quark-antiquark scattering (CKM+LF), the slope of the elliptic flow differences between negatively and positively charged particles is seen to be more negative than in the other two cases.

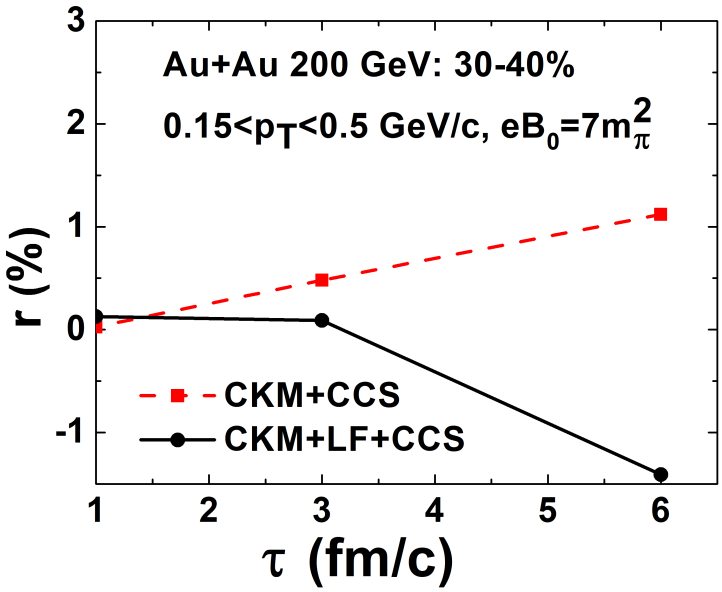

Figure 4.8: Lifetime τ of magnetic field dependence of the slope parameter r of the charge asymmetry dependence of the elliptic flow difference between negatively and positively charges particles for the cases of including chiral kinetic motion and chirality changing scattering with and without the Lorentz force.

4.3.5 The lifetime of magnetic field dependence of the elliptic flow difference

In the above discussions, a long-lived magnetic field, treated as an external field, of a lifetime $\tau = 6$ fm/c, has been used to study the elliptic flow splitting between negatively and positively charged particles for different values of charge asymmetry. In this section, how the elliptic splitting is affected by the lifetime of the magnetic field is studied. The solid line in Fig. 4.8 shows the parameter r, which is the slope of the charge asymmetry dependence of the elliptic flow difference between negatively and positively charges particles, as a function of the lifetime τ of the magnetic field for the case of CKM+LF+CCS. The slope parameter is seen to be very small at $\tau = 1$ fm/c and decreases with increasing lifetime of the magnetic field, and it becomes

negative after $\tau = 3$ fm/c. Neglecting the Lorentz force (CKM+CCS), on the other hand, leads to a slope parameter that is essentially zero at $\tau = 1$ fm/c and increases with the lifetime of the magnetic field. Compared to the measured slope parameter of 3.06%, the theoretical result is a factor of three smaller even for a magnetic field of lifetime $\tau = 6$ fm/c.

In Appendix D, the time evolution of the magnetic field in heavy ion collisions is studied in a transport model using initial conditions from the AMPT model and including the dynamics of the electromagnetic field and partons as well as their interactions. It is found that the lifetime of the magnetic field never exceeds 0.1 fm/c no matter how the conductivity of the quark matter is increased by decreasing the parton scattering cross section. Using this realistic magnetic field, it is found that the effects from both the CMW and the Lorentz force on the elliptic flow splitting between negatively and positively charged particles become negligible.

4.4 Summary

Based on the anomalous transport model, which includes the propagation of massless quarks and antiquarks according to the chiral kinetic equation and allows the change of chiralities during the scattering between positively and negatively charged partons, the elliptic flow of charged particles in non-central relativistic heavy ion collisions has been studied. Using initial conditions from the Bjorken boost invariant model and assuming the presence of a strong and long-lived magnetic field, an appreciable charge quadrupole moment in the transverse plane of the collision has been obtained. Although the latter leads to different elliptic flows for particles of negative and positive charges as the system expands, the resulting elliptic flow difference shows a linear dependence on the total charge asymmetry of the partonic matter with a slope that is negative and has a small magnitude, which is in contrast

to the experimental results. Neglecting the Lorentz force as in the anomalous hydrodynamics of Ref. [54], the resulting elliptic flow splitting behaves similarly as that found from studies based on anomalous hydrodynamics using similar initial conditions and assuming similar strength and lifetime for the magnetic field. Compared to the experimental data on the elliptic flow difference between negatively and positively charged particles, results in this case are still much smaller. Decreasing the lifetime of the magnetic field further reduces the magnitude of the slope parameter. Because of the opposite effect of the Lorentz force to that of the CMW, it is thus unlikely that the elliptic flow splitting observed in experiments is due to the CMW.

A larger elliptic flow difference could be obtained if one allows in the initial state a positive μ_5/T in $y > 0$ and negative μ_5/T in $y < 0$ besides a positive charge asymmetry, and vice versa, instead of generating such a distribution dynamically as in the present study. Also, the different elliptic flows between charged particles could be partly due to the different mean-field potentials between particles and antiparticles in the partonic [117] and the hadronic [118] matter of finite baryon chemical potential [97].

The justification for the existence of a long-lived magnetic field in relativistic heavy ion collisions remains missing, although its strength is known to be sufficiently strong [119, 120, 39]. Calculations based on the transport model show that the lifetime of the magnetic field in heavy ion collisions at $\sqrt{s_{NN}} = 200$ GeV cannot exceed 0.1 fm/c even when one uses a very large conductivity for the quark matter. As a result, effects due to the CMW or the Lorentz force are too small to be seen experimentally.

5. CHIRAL VORTICAL AND MAGNETIC EFFECTS IN THE ANOMALOUS TRANSPORT MODEL *

In the present chapter, the study in the previous chapter is extended to include also the vorticity field in the partonic matter and investigate how the results, particularly the splitting between the elliptic flows of negatively and positively charged particles, are affected.

5.1 Anomalous transport model with both magnetic and vorticity fields

The anomalous transport model for massless fermions in a magnetic field described in the previous section can be generalized to include also a vorticity field by using the chiral kinetic equation that includes both the magnetic and vorticity fields, which are taken from Ref. [76] using the covariant Wigner function approach for massless spin-1/2 fermions in four dimensions. After integrating over the energy in the Lorentz covariant chiral kinetic equation, a chiral kinetic equation in three dimensions is obtained. The resulting chiral equations of motion for massless quarks and antiquarks are given by

$$\sqrt{G}\dot{\mathbf{r}} = \hat{\mathbf{p}} + \lambda Q(\hat{\mathbf{p}}\cdot\mathbf{b})\mathbf{B} + \lambda\frac{\boldsymbol{\omega}}{p}, \tag{5.1}$$

$$\sqrt{G}\dot{\mathbf{p}} = Q\hat{\mathbf{p}}\times\mathbf{B}, \tag{5.2}$$

$$\sqrt{G} = 1 + \lambda Q\mathbf{b}\cdot\mathbf{B} + 4\lambda p(\mathbf{b}\cdot\boldsymbol{\omega}). \tag{5.3}$$

In the above, $\mathbf{b} = \frac{\mathbf{p}}{2p^3}$ is the Berry curvature due to a vector potential in the momentum space, λ is the helicity of the particle, and $\boldsymbol{\omega} = \frac{1}{2}\boldsymbol{\nabla}\times\mathbf{u}$ is the vorticity with $\mathbf{u}$

*Reprinted with permission from "Chiral vortical and magnetic effects in the anomalous transport model" by Yifeng Sun and Che Ming Ko, 2017, Phys. Rev. C **95**, 034909, Copyright 2017 by APS.

being the velocity field.

As shown in the study of CMW in the previous chapter based on the anomalous transport model [1], the chirality-changing scattering (CCS) between quark and antiquark is essential for generating the elliptic flow difference between negatively and positively charged particles. One thus also allows in the present study massless quarks and antiquarks of the same chiralities to undergo the CCS scattering. The effect from the change of phase space measure due to the magnetic field and/or the vorticity field is again neglected.

5.2 Initial conditions of non-central heavy ion collisions

For the initial conditions of a heavy ion collision, the same ones in the previous chapter, i.e., a fireball with geometry corresponding to collisions of Au+Au at $\sqrt{s_{NN}} = 200$ GeV at centralities of 30-40%, are used. Similar to the magnetic field introduced in previous chapter, the vorticity field is taken to have a direction along the y-axis perpendicular to the reaction plane and a uniform strength in space with the time dependence,

$$\omega = \frac{\omega_0}{1 + (t/\tau_\omega)^2}. \tag{5.4}$$

Results shown later are based on $\omega_0 = 0.1$ fm^{-1} and $\tau_\omega = 2.7$ fm/c for the vorticity field, similar to those of Ref. [58] based on a multipase tranport (AMPT) model [112] for Au+Au collisions at 200 GeV and centrality 30-40%, except that the vorticity field in heavy ion collisions is taken as a spatially uniform external field for simplicity.

5.3 Results

In the present section, the time evolution of the partonic matter is studied by following the trajectories of massless quarks and antiquarks according to the chiral

equations of motion [Eqs. (5.1) and (5.2)]. As in the previous chapter, three cases are considered, and they are: including only the vorticity field (CVE), both magnetic and vorticity fields without the Lorentz force (CVE+CME), and both magnetic field and vorticity fields with the Lorentz force (CVE+CME+LF). In all cases, the chirality-changing scattering (CCS) between quark and antiquark of the same chirality is included, although it has no effect in the case of CVE only.

5.3.1 Pion elliptic flow

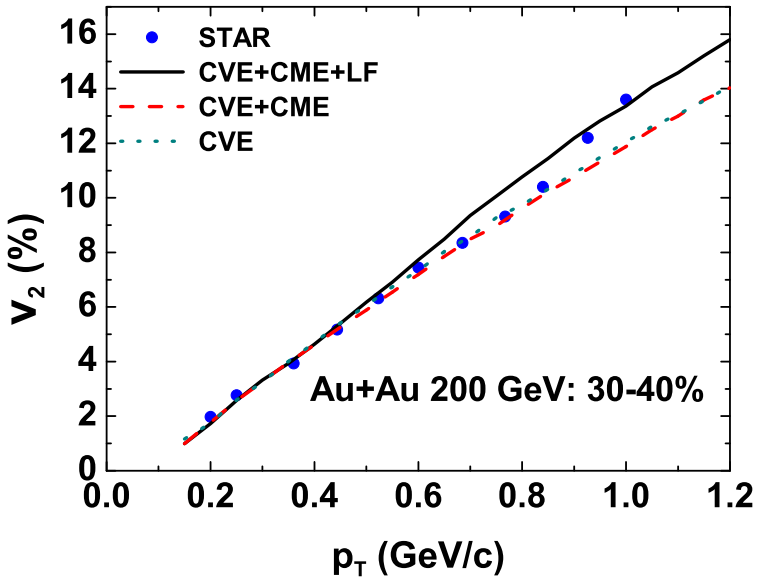

Figure 5.1: Elliptic flow of kinetically freeze-out pions in midrapidity ($|y| \leq 1$) as a function of transverse momentum for the three cases of including both chiral vortical and magnetic effects and the effect due to the Lorentz force (CVE+CME+LF), without the Lorentz force (CVE+CME), and with only the vortical effect (CVE). Experimental data (solid circles) are from Ref. [2]. Reprinted from Ref. [4]

Fig. 5.1 shows the elliptic flow of kinetically freeze-out pions in midrapidity

($|y| \leq 1$) as a function of transverse momentum. The solid line is obtained with the coefficient $\sigma_0 = 13.6$ mb in the parton scattering cross section for the case of including the chiral effects due to both the vorticity and magnetic fields as well as the Lorentz force (CVE+CME+LF). The result obtained without the Lorentz force (CVE+CME) and using $\sigma_0 = 15.5$ mb is shown by the dashed line, while the result including only the chiral vortical effect (CVE) and using $\sigma_0 = 13.3$ mb is shown by the dotted line. The transverse momentum dependence of the pion elliptic flow is seen to agree with the experimental data from the STAR Collaboration [2] for all three cases. The integrated v_2 of pions with transverse momenta in the range of $0.15 \leq p_T \leq 0.5$ GeV/c is 0.036 in all three cases, which also agrees with the experimental value.

5.3.2 Effect of the vorticity field

In Ref. [29], it is argued that the chiral vortical wave (CVW) generated in a rotating fluid system can lead to a splitting between the elliptic flows of baryons and anti-baryons if the baryon chemical potential of the system is non-zero. Similarly, for non-zero charge chemical potential, one expects the CVW to lead to a splitting between the elliptic flows of negatively and positively charged particles. In this section, the anomalous transport model is used to study the effect of the vorticity field on the elliptic flow splitting of π^+ and π^- for different values of charge chemical potential by taking the magnetic field to be zero, i.e., $B_0 = 0$.

Figure 5.2 shows the time evolution of the differences $\Delta\epsilon_2 = \epsilon_{2-} - \epsilon_{2+}$ between the eccentricities $[\epsilon_2 = \langle (x^2-y^2)/(x^2+y^2) \rangle]$ and $\Delta v_2 = v_{2-} - v_{2+}$ between the elliptic flows $[v_2 = \langle (p_x^2-p_y^2)/(p_x^2+p_y^2) \rangle]$ of negatively and positively charged particles for the total charge asymmetry $A_\pm = 0.16$ of these particles. The transverse momenta are again in the range of $0.15 \leq p_T \leq 0.5$ GeV/c. These differences are consistent with

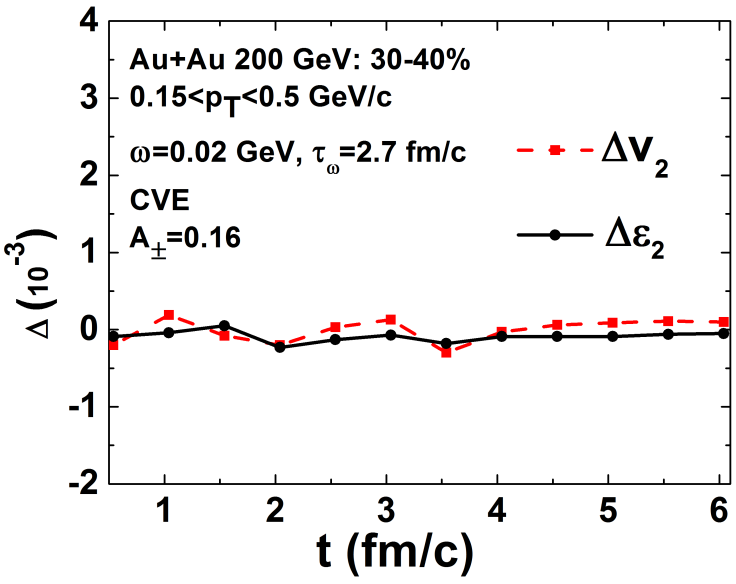

Figure 5.2: Eccentricity and elliptic flow difference between negatively and positively charged particles as functions of time for total charge asymmetry of quark matter $A_\pm = 0.16$. Reprinted from Ref. [4]

zero, indicating that the CVW alone does not lead to any eccentricity and elliptic flow differences between charged particles.

The above result can be understood as follows. According to the chiral equation of motion [Eq. (5.1)] for the case without a magnetic field, the vorticity field modifies the velocities of particles of opposite helicities by the same amount but with opposite sign. As a result, nonzero positive and negative axial charge chemical potentials μ_5 appear in the positive and negative y regions of the transverse plane, respectively. However, the average change in the velocity of positively charged particles is the same as that of negatively charged particles with both given by $\Delta v = v\frac{e^{\mu_R/T}-e^{\mu_L/T}}{e^{\mu_R/T}+e^{\mu_L/T}}$, where v is the magnitude of the average modified velocity of particles of right or left helicity, and μ_R and μ_L are chemical potentials of right and left chiralities, respectively.

Negatively and positively charged particles thus have same spatial distributions if their initial spatial distributions are the same. Therefore, no eccentricity difference between negatively and positively charged particle appears even though an additional charge quadrupole moment is generated in the transverse plane by the CVW. The effect of CVW is thus different from that of CMW, which causes the average change in the velocities of negatively and positively charged particles to have the opposite sign given by Δv and $-\Delta v$, respectively, and can thus result in a larger eccentricity for negatively charged particles than for positively charged particles.

The above result obtained with only the vorticity field differs from that of Ref. [29] based on schematic considerations. Using the argument for the effect of the chiral magnetic wave introduced in Ref. [27] based on consideration of the net charge distribution, it is argued in Ref. [29] that the additional charge quadrupole moment generated by the vorticity field would lead to an elliptic flow splitting between negatively and positively charged particles. As discussed in the previous paragraph, since the spatial distributions of negatively and positively charged particles remain the same, the additional charge quadrupole moment does not lead to different eccentricities between negatively and positively charged particles and thus cannot generate a splitting between their elliptic flows. This is different from the case with only the magnetic field, where the additional quadrupole momentum generated by the chiral magnetic wave can indeed lead to different eccentricities and thus elliptic flows between negatively and positively charged particles as shown in the previous chapter [1].

Although the CVW does not lead to the eccentricity and elliptic flow splittings between negatively and positively charged particles, it does result in a large axial charge dipole moment in the transverse plane even for quark matter of vanishing charge asymmetry $A_\pm = 0$. As shown in Fig. 5.3, the value is even larger than that

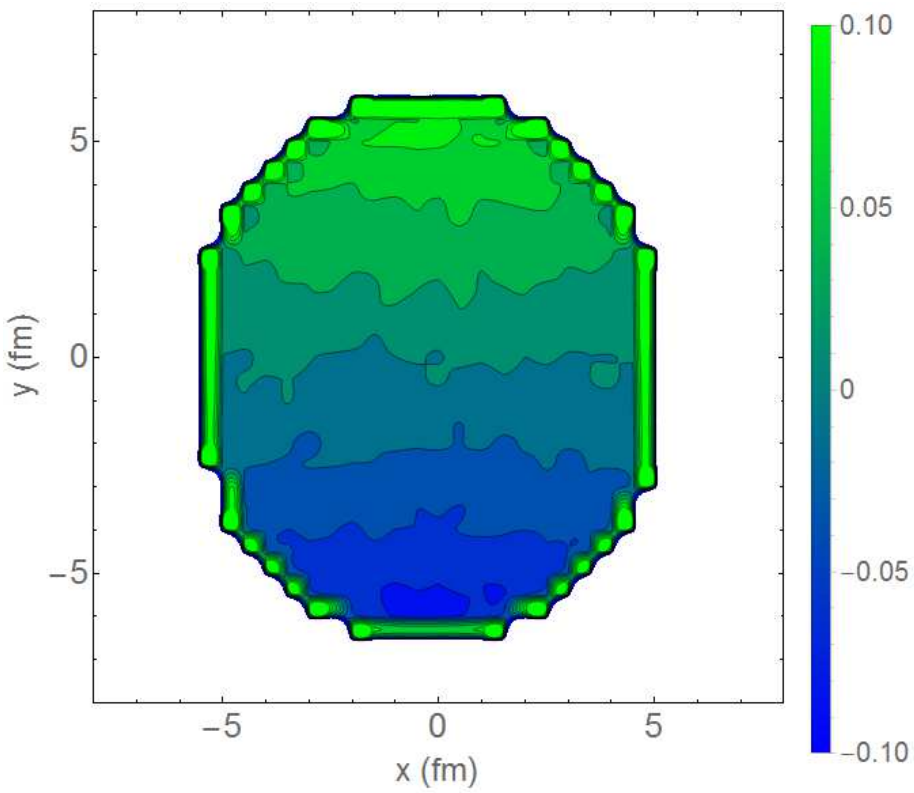

Figure 5.3: Axial charge chemical potential μ_5/T distribution in the transverse plane $z = 0$ at time $t = 5$ fm/c for partonic matter of zero charge asymmetry. Reprinted from Ref. [4]

shown in the previous chapter due to the CMW based on a magnetic field of strength $eB = 7m_\pi^2$. This can be understood from the axial charge current induced by the magnetic and vorticity fields [28]

$$\mathbf{j}_5 \propto \left(\frac{1}{6}T^2 + \frac{1}{2\pi^2}(\mu^2 + \mu_5^2)\right)\boldsymbol{\omega} + \frac{Q}{2\pi^2}\mu\mathbf{B}. \tag{5.5}$$

With $T = 0.3$ GeV, $\mu = \mu_5 = 0$, $\omega = 0.02$ GeV in the present study, the axial charge current is $0.0375/\text{fm}^3$, which is larger than the value $0.02/\text{fm}^3$ obtained with $\mu/T = 0.16$ and $QB = 3.5m_\pi^2$ used in the previous chapter at same temperature.

5.3.3 *Effect of vorticity field plus magnetic field with the Lorentz force*

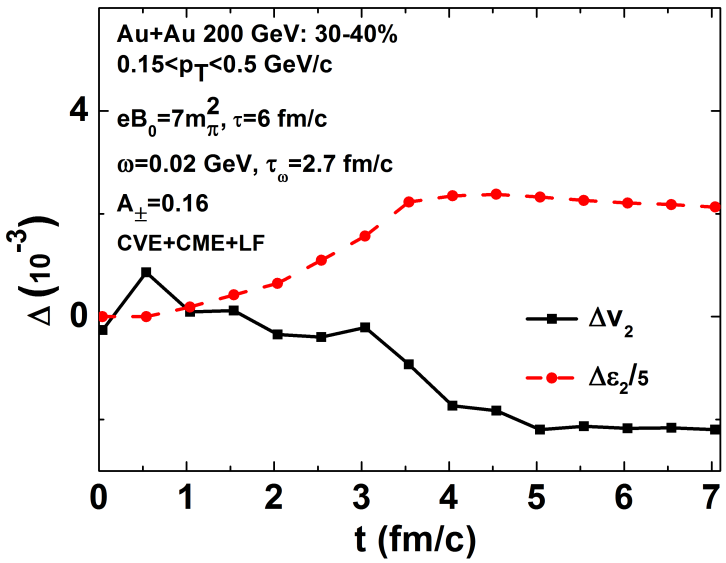

Figure 5.4: Eccentricity and elliptic flow differences between negatively and positively charged particles as a function of time for different scenarios of parton dynamics when the total charge asymmetry of the quark matter is $A_\pm = 0.16$. Reprinted from Ref. [4]

Including also the magnetic field, the time evolution of the eccentricity and elliptic flow differences between negatively and positively charged particles is shown in Fig. 5.4 for a partonic matter of charge asymmetry $A_\pm = 0.16$. It is seen that the eccentricity difference between negatively and positively charged particles with transverse momenta in the range $0.15 \leq p_T \leq 0.5$ GeV/c initially increases with time but decreases after reaching a maximum value. For the time evolution of the elliptic flow difference between negatively and positively charged particles, Fig. 5.4 shows that the combined effects of the vorticity and magnetic fields with the inclusion of the Lorentz force lead to an initial increase of the elliptic flow difference, which then

quickly decreases and becomes negative.

5.3.4 Effect of vorticity field plus magnetic field without the Lorentz force

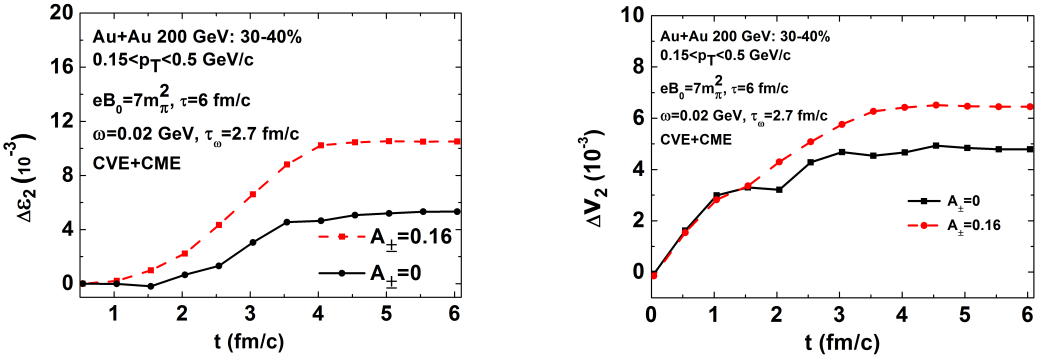

Figure 5.5: Eccentricity (left window) and elliptic flow (right window) difference between negatively and positively charged particles as a function of time for partonic matter of charge asymmetries $A_\pm = 0$ and $A_\pm = 0.16$. Reprinted from Ref. [4]

Including also the magnetic field but neglecting the Lorentz force in the chiral equations of motion, the time evolution of the difference between the eccentricities of negatively and positively charged particles is studied for partonic matter of charge asymmetries $A_\pm = 0$ and $A_\pm = 0.16$. Results for particles of momenta in the range $0.15 \leq p_T \leq 0.5$ GeV/c are shown in the left window of Fig. 5.5. It is seen that the eccentricity difference increases with time in both cases and is nonzero even for zero charge asymmetry, indicating that effects of the vorticity field and the magnetic field are not additive because the eccentricity difference is zero in both cases for zero charge asymmetry. The latter is due to the finite axial charge current induced by the vorticity field, which leads to an axial charge dipole moment in the transverse plane, characterized by positive and negative axial charge chemical potentials in the positive and negative y regions of the transverse plane, respectively. Because of the

chiral magnetic effect, there is a vector charge current along the magnetic field in the positive y region and opposite to the magnetic field in the negative y region. This then leads to a vector charge quadrupole moment in the transverse plane even when the charge asymmetry is zero.

Further shown in the right window of Fig. 5.5 is the time evolution of the elliptic flow difference between negatively and positively charged particles due to both the vorticity and the magnetic field but with the neglect of the Lorentz force for quark matter of charge asymmetries $A_\pm = 0$ and $A_\pm = 0.16$. A finite positive elliptic flow difference is seen for zero charge asymmetry as a result of the finite eccentricity difference shown in the left window of Fig. 5.5. Compared to the case of having only the magnetic field in the previous chapter, the elliptic flow difference in the present case of having also the vorticity field appears earlier in time, and this is because the vorticity field helps to generate different average velocities for negatively and positively charged particles more quickly, which is in contrast to the case with only the magnetic field, where this difference is proportional to the axial charge chemical potential and thus takes time to develop.

Compared with the results in the previous section with the Lorentz force, it is seen that the Lorentz force cancels the chiral effects due to the vorticity and magnetic fields shown in the right window of Fig. 5.5 and even leads to an opposite effect on the elliptic flow difference between negatively and positively charged particles.

5.3.5 Charge asymmetry dependence of the elliptic flow difference

Fig. 5.6 shows the charge asymmetry dependence of the elliptic flow difference between negatively and positively charged particles for different scenarios of parton dynamics. The dotted line shows that the elliptic flow difference is consistent with zero for the case when only the vorticity field is present (CVE), and this is because

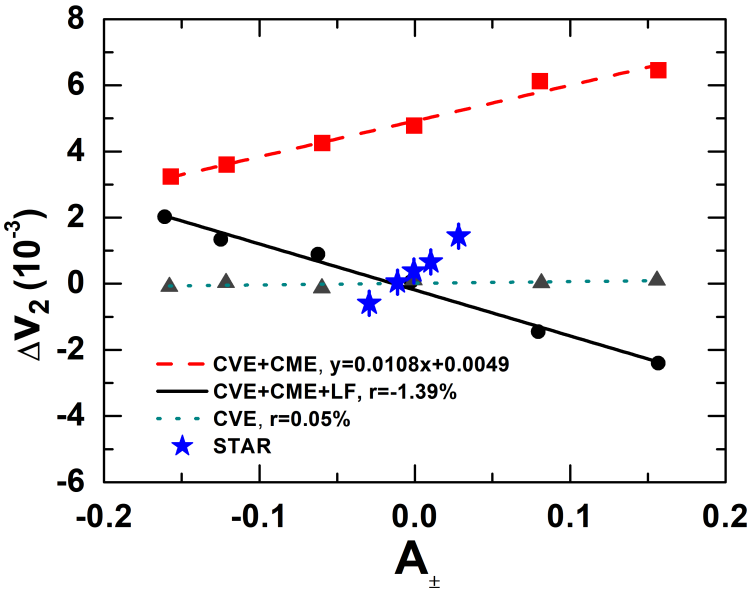

Figure 5.6: Elliptic flow difference as a function of charge asymmetry $A_{\pm}$ for different scenarios of parton dynamics. Experimental data (solid stars) are from Ref. [3]. Reprinted from Ref. [4]

the vorticity field has same effects on negatively and positively charged particles. When both the vorticity and the magnetic field are present but without including the Lorentz force (CVE+CME), the elliptic flow difference increases linearly with the charge asymmetry of the partonic matter with a slope of 0.0108, which is comparable to the results obtained in Refs. [54, 1] based on the CMW. However, the inclusion of the vorticity field leads to a finite intercept of 4.9×10^{-3} at zero charge asymmetry, and this is due to the fact that the axial charge dipole moment in the transverse plane generated by the vorticity field can subsequently induce by the magnetic field a vector charge quadrupole moment of different eccentricities for negatively and positively charged particles. With the inclusion of the Lorentz force, which is shown by the solid line, chiral effects due to the vorticity and magnetic fields disappear,

and the slope parameter in the charge asymmetry dependence of the elliptic flow difference becomes negative with a magnitude of 0.0139.

Using the realistic magnetic field obtained in Appendix D, the elliptic flow difference between negatively and positively charged particles is essentially zero in both cases of with and without the Lorentz force.

5.4 Summary

Based on the anomalous transport model, which includes the propagation of massless quarks and antiquarks according to the chiral equations of motion and the chirality-changing scattering, the elliptic flows of charged particles in non-central heavy ion collisions at relativistic energies have been studied. Using initial conditions from the Bjorken boost-invariant model and assuming the presence of only the vorticity field, which is modeled according to that from the AMPT model [112], it is found that the CVW does not lead to an elliptic flow splitting of negatively and positively charged particles when the charge asymmetry of the partonic matter is nonzero. On the other hand, including also a strong and long-lived magnetic field but neglecting the Lorentz force can lead to a splitting between the elliptic flows of negatively and positively charged particles. However, the slope parameter in the charge asymmetry dependence of the elliptic flow splitting is smaller than the experimental data, while the positive intercept at zero charge asymmetry is larger than the experimental value [3]. Unfortunately, as in the case of including only the magnetic field studied in the previous chapter, the inclusion of the Lorentz force cancels the chiral effects due to the magnetic and vorticity fields and leads instead to a negative slope parameter in the charge symmetry dependence of the elliptic flow splitting of negatively and positively charged particles, contrary to that observed in experiments. If one uses a magnetic field of realistic lifetime, then the signals from the chiral ef-

fects would be hardly seen. Understanding these experimental results in terms of the chiral effects thus remains a challenge.

6. LAMBDA HYPERON POLARIZATION IN THE ANOMALOUS TRANSPORT MODEL *

Because of the large orbital angular momentum in non-central collisions of two heavy nuclei at relativistic energies, the vorticity field in the produced quark-gluon plasma (QGP) can reach a very large value of 10^{21} s^{-1} [57, 58]. It has been argued that due to their spin-orbit interactions, quarks and antiquarks can be polarized along the direction of the orbital angular momentum by the vorticity field, and after hadronization, they then lead to the production of polarized Lambda (Λ) hyperons, which can be measured in experiments [30, 31]. Taking into consideration the non-uniformity of the vorticity field due to that in the spatial distribution of particles in the statistical-hydrodynamic approach [32, 33, 34] or the quantum kinetic approach [35], local structures in the polarization density can also be studied. Such effects have been included in many studies based on the hydrodynamical model [57, 58, 59, 60, 61, 62, 63, 64, 65, 66, 67, 68, 69, 70], and some of these studies can indeed quantitatively reproduce the polarization of Λ hyperons measured by the STAR Collaboration [7]. A similar study using the transport model [71] also gives a result that agrees with the experimental observation.

Although the time evolution of the vorticity field is included in both the hydrodynamic and transport studies, the spin polarization of hyperons is calculated from their equilibrium distribution in the final state and is therefore only determined by the final vorticity field in the produced matter. Moreover, these studies have not addressed the non-equilibrium effect on the polarization of Λ hyperons. To include

*Reprinted with permission from "Λ hyperon polarization in relativistic heavy ion collisions from a chiral kinetic approach"by Yifeng Sun and Che Ming Ko, 2017, Phys. Rev. C **96**, 024906, Copyright 2017 by APS.

the non-equilibrium effect on the spin polarizations of quarks and antiquarks in the partonic phase of heavy ion collisions, the chiral kinetic approach, which takes into account both the time evolution of the spins of quarks and antiquarks via their equations of motion and scatterings in the chiral limit [72, 75, 76, 121, 122, 123, 90, 102], is used in the present study. By converting quarks and antiquarks to hadrons using the coalescence model after the partonic phase [78, 79], the polarizations of Λ and $\bar{\Lambda}$ hyperons are also studied.

6.1 Anomalous transport model for chiral fermions in vorticity field

As discussed earlier, the chiral kinetic equations of motion for massless spin-$\frac{1}{2}$ particles in a vorticity field are given by

$$\dot{\mathbf{r}} = \frac{\hat{\mathbf{p}} + 2\lambda p(\hat{\mathbf{p}}\cdot\mathbf{b})\boldsymbol{\omega}}{1 + a\lambda p(\boldsymbol{\omega}\cdot\mathbf{b})}, \qquad \dot{\mathbf{p}} = 0. \tag{6.1}$$

The numerical factor a can be determined by considering the spin-polarization density as discussed below.

Besides modifying the equations of motion for massless fermions, the vorticity field also affects their distributions in phase-space by introducing the measure $\sqrt{G} = 1+a\lambda|\mathbf{p}|(\boldsymbol{\omega}\cdot\mathbf{b})$ [72, 75, 76, 121], which appears in the denominator of Eq. (6.1) if $a = 2$. Taking into account the modified phase-space measure changes the particle density in a fluid with non-zero vorticity field from $\int \frac{d^3\mathbf{p}}{(2\pi)^3} f(p^0)$ to $\int \frac{d^3\mathbf{p}}{(2\pi)^3}\sqrt{G} f(p^0)$ [124], where $p_0 = \gamma(|\mathbf{p}| - \mathbf{v}\cdot\mathbf{p})$ with $\gamma = \frac{1}{\sqrt{1-\mathbf{v}^2}}$ and $\mathbf{v}$ being the fluid velocity. In the local rest frame of the fluid and assuming an equilibrium Boltzmann distribution at temperature T, the average spin of massless spin-$\frac{1}{2}$ fermions is then

$$\mathbf{S} = \frac{\int \frac{d^3\mathbf{p}}{(2\pi)^3}\frac{\lambda}{2}\hat{\mathbf{p}}\sqrt{G} f(p)}{\int \frac{d^3\mathbf{p}}{(2\pi)^3}\sqrt{G} f(p)} = \frac{a}{6}\left(\frac{\lambda^2\boldsymbol{\omega}}{4T}\right), \tag{6.2}$$

which differs from the usual value by the factor $a/6$ as a result of the modified phase-space measure from the Berry curvature. This result shows that the vorticity field can lead to the spin polarization of a massless fermion along its direction, and the result agrees with that from the quantum kinetic approach [35] if the value of a is taken to be $a = 6$. In the present study, Eq. (6.1) is used with the numerical factor 2 in the denominator replaced by the numerical factor 6 to describe the motions of massless fermions in a vorticity field.

The above equations of motion and modified phase-space measure are for massless fermions. Since treating helicity as a good quantum number remains a good approximation for quarks of finite but small masses, their equations of motion can still be given by Eq. (6.1) after replacing $\hat{\mathbf{p}}$, p, and $\mathbf{b} = \frac{\hat{\mathbf{p}}}{2p^2}$ by $\frac{\mathbf{p}}{E_p}$, E_p and $\mathbf{b} = \frac{\hat{\mathbf{p}}}{2E_p^2}$, respectively [122].

To ensure that massless fermions reach the equilibrium distribution $\sqrt{G}f((p^0 - \mu)/T)$, where μ is the baryon chemical potential, from their collisions, the momenta $\mathbf{p_3}$ and $\mathbf{p_4}$ of two colliding fermions after a collision are determined by momentum conservation but with the probability $\sqrt{G(\mathbf{p_3})G(\mathbf{p_4})}$. This effect can be included in the calculation by randomly selecting their momenta after a collision in their center of mass frame according to momentum conservation and then Lorentz transforming to the fireball frame. The probability $\sqrt{G(\mathbf{p_3})G(\mathbf{p_4})}$ is then calculated and compared with a random number. This process is continued until the random number is less than $\sqrt{G(\mathbf{p_3})G(\mathbf{p_4})}$. Since the values of $\sqrt{G(\mathbf{p_3})}$ and $\sqrt{G(\mathbf{p_4})}$ can be negative, which is unphysical as a result of the approximation used in deriving the chiral vortical equation of motion, their values are set to one and these particles are then treated without including the effect due to the vorticity field. Also, the value of $\sqrt{G(\mathbf{p_3})G(\mathbf{p_4})}$ can be greater than one. In this case, the random number mentioned above is taken between 0 and 25. Because of the upper cutoff, particles of small

momentum are not affected by the modified phase-space measure. Since the number of such particles is small, increasing the value of the upper cutoff does not affect the results. As to the conditions for the collision, they can be determined by using the geometric method based on the scattering cross section as described in Ref. [107]. For the collision between a fermion and its antiparticle that have opposite helicities, their helicities can be flipped after the collision. This chirality changing scattering is included in the present study as in previous chapters.

6.2 Coalescence model for production of polarized Λ ($\bar{\Lambda}$) hyperon

To study the spin polarization of Λ ($\overline{\Lambda}$) hyperon, the coalescence model for hadron production [78] is used to convert polarized quarks and antiquarks to polarized baryons and antibaryons. In this model, the probability for u, d and s quarks (antiquarks) at phase-space points ($\mathbf{r}_1$, $\mathbf{p}_1$), ($\mathbf{r}_2$, $\mathbf{p}_2$), and ($\mathbf{r}_3$, $\mathbf{p}_3$), respectively, to form a Λ ($\overline{\Lambda}$) is given by the quark Wigner function of the Λ ($\overline{\Lambda}$) [79]:

$$f_\Lambda(\boldsymbol{\rho}, \boldsymbol{\tau}, \mathbf{k}_\rho, \mathbf{k}_\tau) = 8^2 g_C g_S e^{-\frac{\boldsymbol{\rho}^2}{\sigma_\rho^2} - \frac{\boldsymbol{\tau}^2}{\sigma_\tau^2} - \mathbf{k}_\rho{}^2\sigma_\rho^2 - \mathbf{k}_\tau{}^2\sigma_\tau^2}, \tag{6.3}$$

if the wave functions of the quarks (antiquarks) are taken to be those of a harmonic oscillator potential. In the above, $g_C = 1/27$ is the coalescence factor for colored u, d, and s quarks to form a colorless Λ, g_S is the coalescence factor for these polarized quarks to form a polarized Λ and will be discussed later. The relative coordinates

and momenta are defined as

$$\begin{aligned}
\boldsymbol{\rho} &= \frac{1}{\sqrt{2}}(\mathbf{r}'_1 - \mathbf{r}'_2), \quad \mathbf{k}_\rho = \sqrt{2}\frac{m_2\mathbf{p}'_1 - m_1\mathbf{p}'_2}{m_1+m_2}, \\
\boldsymbol{\tau} &= \sqrt{\frac{2}{3}}\left(\frac{m_1\mathbf{r}'_1 + m_2\mathbf{r}'_2}{m_1+m_2} - \mathbf{r}'_3\right), \\
\mathbf{k}_\tau &= \sqrt{\frac{3}{2}}\frac{m_3(\mathbf{p}'_1+\mathbf{p}'_2) - (m_1+m_2)\mathbf{p}'_3}{m_1+m_2+m_3},
\end{aligned} \tag{6.4}$$

where m_i is the mass of i-th quark, and $\mathbf{r}'_i$ and $\mathbf{p}'_i$ are its position and momentum in the center-of-mass frame of the three quarks after they are propagated to the time when the last quark freezes out. The width parameters σ_ρ and σ_τ in Eq. (6.3) are related to the oscillator frequency ω by $\sigma_\rho = 1/\sqrt{m_{12}\omega}$ and $\sigma_\tau = 1/\sqrt{m_{123}\omega}$, respectively, where the reduced masses are $m_{12} = \frac{2}{1/m_1+1/m_2}$ and $m_{123} = \frac{3/2}{1/(m_1+m_2)+1/m_3}$.

It can be shown that the oscillator frequency ω is related to the radius $\langle r^2\rangle_\Lambda$ of Λ [79],

$$\langle r^2\rangle_\Lambda = \frac{1}{2\omega}\frac{\sum_{(i,j)=(1,2),(2,3),(3,1)} m_i m_j(m_i+m_j)}{m_1m_2m_3(m_1+m_2+m_3)}. \tag{6.5}$$

Taking the root-mean-squared radius of Λ to have a value of 0.877 fm, similar to that of a proton as in Ref. [79], leads to $\sigma_\rho = 0.89$ fm and $\sigma_\lambda = 0.51$ fm if the masses of u, d and s quarks and antiquarks are taken approximately to be 3, 6, and 100 MeV, respectively [125]. It is noted that the spin polarization in a vorticity field does not depend on the mass of the particles in the statistical-hydrodynamic approach [32, 33, 34] and the quantum kinetic approach [35]. On the other hand, the mass correction to the CKE in the chiral kinetic approach leads to a decrease of the spin polarization with increasing mass. Since the latter is valid in the small

mass limit, including the mass correction for any values of mass needs to be further studied. On the other hand, since the spin polarization of a particle should not depend on its mass, one thus can still use the chiral kinetic approach to study the spin polarization of quarks even at $T = T_\chi$.

The spin coalescence factor g_S in Eq. (6.3) can be evaluated by noting the spin state of Λ is determined by the spin state of its constituent s quark, so its value is given by the probability for u and d quarks to form a spin-singlet state. Denoting the spin vectors of u and d quarks in the fireball frame by $\lambda_1\hat{\mathbf{p}}_1/2$ and $\lambda_2\hat{\mathbf{p}}_2/2$, respectively, where their respective momenta are $\mathbf{p}_1$ and $\mathbf{p}_2$ and their respective helicities are λ_1 and λ_2, the probability for u and d quarks to form a spin-singlet state is then

$$\begin{aligned} g_S &= |(1/\sqrt{2})(\langle\uparrow\downarrow| - \langle\downarrow\uparrow|)[\cos(\theta_1/2)\cos(\theta_2/2)|\uparrow\uparrow\rangle \\ &\quad + \cos(\theta_1/2)\sin(\theta_2/2)e^{i\phi_2}|\uparrow\downarrow\rangle \\ &\quad + \sin(\theta_1/2)\cos(\theta_2/2)e^{i\phi_1}|\downarrow\uparrow\rangle \\ &\quad + \sin(\theta_1/2)\sin(\theta_2/2)e^{i(\phi_1+\phi_2)}]|\downarrow\downarrow\rangle|^2 \\ &= \frac{1}{4}(1 - \cos\theta_1\cos\theta_2 - \sin\theta_1\sin\theta_2\cos(\phi_1 - \phi_2)) \\ &= \frac{1}{4}(1 - \lambda_1\lambda_2\hat{\mathbf{p}}_1\cdot\hat{\mathbf{p}}_2), \end{aligned} \tag{6.6}$$

where θ_1 (θ_2) and ϕ_1 (ϕ_2) are the azimuthal angles of the spin vector $\lambda_1\hat{\mathbf{p}}_1/2$ ($\lambda_2\hat{\mathbf{p}}_2/2$) of u (d) quark.

6.3 Initial conditions and the vorticity field

To study the effect of the vorticity field in relativistic heavy ion collisions based on the chiral kinetic approach, the string-melting version of AMPT model [126], with its parameters taken from Ref. [127], is used to generate the initial phase-space distri-

butions of quarks and antiquarks. Specifically, the values $a = 0.5$ and $b = 0.9$ GeV^{-2} are used in the Lund string fragmentation function. For the impact parameter, the value $b = 8.87$ fm is used to correspond to the centrality bin of $20 - 50\%$ in Au+Au collisions, which is obtained from the geometrical relation between the centrality bin and the impact parameter $c = \pi b^2/\sigma_{\rm in}$ with $\sigma_{\rm in} = 705$ fm^2 from Ref. [128]. The reason that the fireball model was used to study the elliptic flow splitting in the pervious section is because quark matter with large charge asymmetry in heavy ion collisions at $\sqrt{s_{NN}} = 200$ GeV is rare and is thus difficult to be generated from the AMPT model. Since the spin polarization does not depend on the charge asymmetry of the quark matter, the more relativistic AMPT model is used to generate the initial conditions for the present study. For the helicities of initial partons, they are taken to have random positive or negative values, corresponding to an initial state of vanishing axial charge density and spin polarization. The phase-space distributions of these quarks and antiquarks are then evolved in time according to the chiral equations of motion [Eq. (6.1)] and by scatterings with an isotropic and constant cross section of 10 mb before including the modification by the chiral effects described above until they freeze out or stop scattering.

The vorticity field $\boldsymbol{\omega}$ in Eq. (6.1) is related to the velocity field $\mathbf{v}(\mathbf{r}, t)$ of partons by $\boldsymbol{\omega} = \frac{1}{2}\boldsymbol{\nabla} \times \mathbf{u}$ with $\mathbf{u} = \gamma\mathbf{v}$ and $\gamma = \frac{1}{\sqrt{1-\mathbf{v}^2}}$. For the velocity field, it can be calculated from the average velocity of partons in a local cell, i.e., $\mathbf{v}(\mathbf{r}, t) = \frac{\sum_i \mathbf{p_i}/E_i}{\sum_i 1}$ with i running over all particles in this cell, similar to the velocity of the particle flow in Ref. [57]. In the present calculations, the whole volume of the collision system is divided into $61 \times 61 \times 61$ cells with spacing $\Delta x = \Delta y = \Delta z = 0.5$ fm. Although partons are produced with different formation times, they are all included in calculating the local fluid velocity.

6.4 Results

In this section, the chiral kinetic equations are solved for quarks and antiquarks from the AMPT model to obtain their average spin, $\mathbf{S} = \frac{\sum_i \frac{\lambda_i \hat{\mathbf{p}}_i}{2}}{\sum_i 1}$, and polarization along the y direction, $P_y = 2S_y$. An extended coalescence model is then used to convert these partons to Λ and $\bar{\Lambda}$ hyperons and study their polarizations. Quark coalescence is assumed to occur when quarks and antiquarks stop scattering when their mean-free path becomes comparable to the size of the quark matter. Since this corresponds approximately the critical energy for the chiral phase transition, Λ and $\bar{\Lambda}$ hyperons are thus formed at about $T = T_\chi$.

6.4.1 Polarization of light quarks and antiquarks

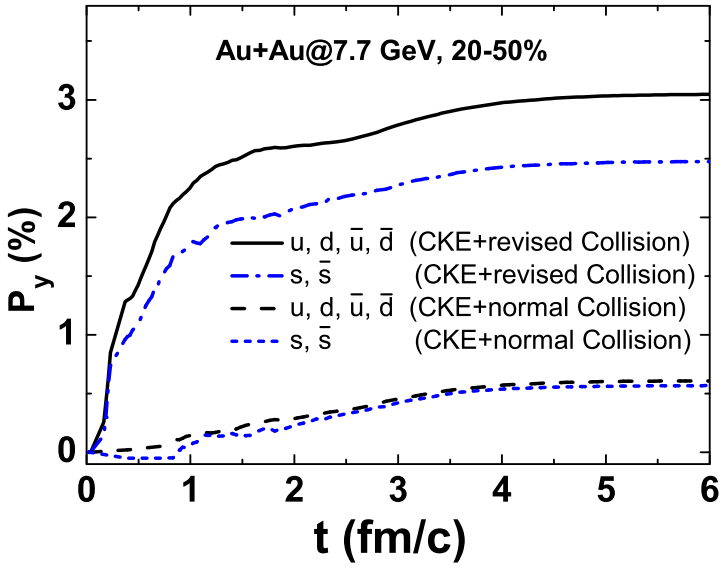

Figure 6.1: Time evolution of the spin polarization of light and strange quarks and antiquarks in midrapidity $|y| \leq 1$ along the total orbital angular momentum with (solid lines) and without (dashed lines) using a parton scattering cross section that includes the effect of the local vorticity field. Reprinted from Ref. [5]

As an illustration, Au+Au collisions at $\sqrt{s_{NN}} = 7.7$ GeV, which is the lowest energy in the beam energy scan (BES) program of the STAR Collaboration at RHIC, are first considered. Shown in Fig. 6.1 is the time evolution of the spin polarization along y direction P_y of light and strange quarks and antiquarks in midrapidity $|y| \leq 1$. Solid and dash-dotted lines are the respective results for light and strange quarks and antiquarks from using the chiral kinetic equations and the scattering cross section that includes the effect due to the modified phase-space measure. It is seen that the spin polarization of strange quarks and antiquarks is smaller than that of light quarks and antiquarks, and this is due to the larger strange quark mass compared to light quark mass and their different temporal and spatial distributions. As to their time dependence, the spin polarizations of both strange and non-strange quarks and antiquarks increase rapidly from zero during the first 1 fm/c and then gradually reach their respective constant values during $1 - 3.5$ fm/c. The initial rapid increase in the spin polarization is due to the fast approach of partons to their equilibrium distributions as a result of scatterings, while the slow increase in later times is because it takes a longer time to generate an axial charge dipole moment in the transverse plane from chiral kinetic motions, which is responsible for the generation of spin polarization [4]. This can be seen from the long- and short-dashed lines that the spin polarization increases much slower from zero to the maximum value if one uses an isotropic cross section instead of the non-isotropic one because of the modified phase-space measure due to the vorticity field.

6.4.2 Polarization of Λ *and* $\overline{\Lambda}$ *hyperons*

Shown in Fig. 6.2 is the transverse momentum dependence of the spin polarization of Λ and $\bar{\Lambda}$ hyperons at midrapidity ($|y| \leq 1$) in different directions at the collision energy $\sqrt{s_{NN}} = 7.7$ GeV. It is seen that its three components all show little depen-

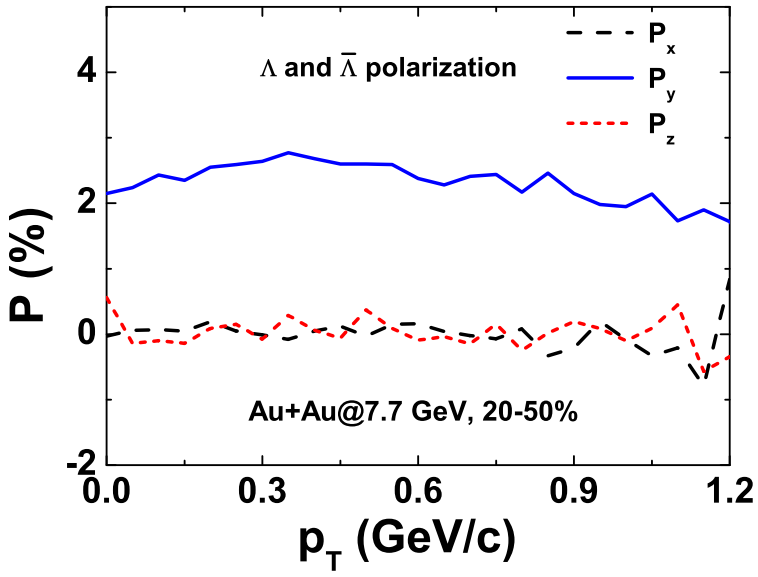

Figure 6.2: Transverse momentum dependence of the spin polarization of midrapidity ($|y| \leq 1$) Λ and $\bar{\Lambda}$ hyperons along different directions in Au+Au collisions at $\sqrt{s_{NN}} =$ 7.7 GeV. Reprinted from Ref. [5]

dence on transverse momentum. Although the values of the x- and z-components are consistent with zero, the total spin polarization in the y-direction, i.e., along the direction of total orbital angular momentum, has a value of 2.44%, which is slightly less than the spin polarization of strange quarks and antiquarks shown in Fig. 6.1.

The rapidity dependence of the spin polarization for Λ and $\overline{\Lambda}$ hyperons is shown in Fig. 6.3 at the same collision energy. Although the spin polarizations along the x-direction and the z-direction are consistent with zero for all rapidities, that along the direction of total orbital angular momentum peaks at zero rapidity and decreases with increasing magnitude of rapidity. The latter is due to the smaller number of scatterings for quarks and antiquarks at large rapidity.

Fig. 6.4 shows the collision energy dependence of the spin polarization of Λ and $\bar{\Lambda}$ hyperons along the direction of total orbital angular momentum at centrality 20-

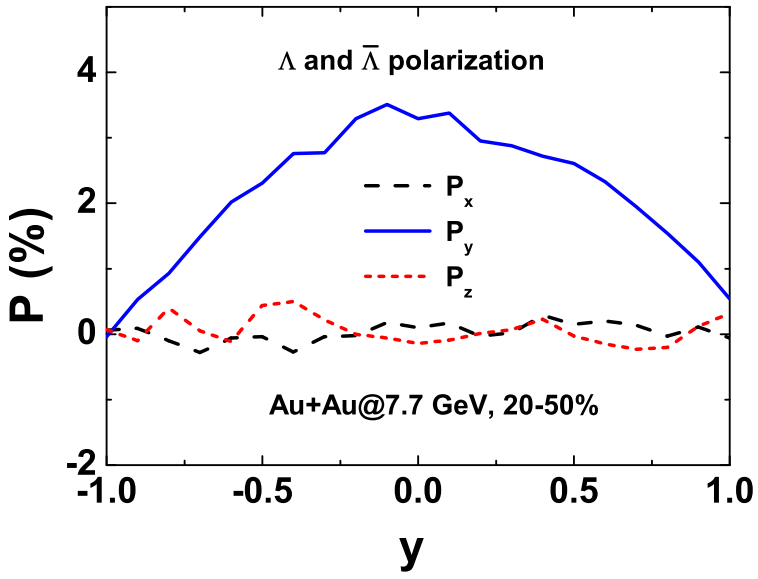

Figure 6.3: Rapidity dependence of the spin polarization of midrapidity ($|y| \leq 1$) Λ and $\bar{\Lambda}$ hyperons along different directions in Au+Au collisions at $\sqrt{s_{NN}} = 7.7$ GeV. Reprinted from Ref. [5]

50%. These results indicate that it decreases with increasing collision energy, and this is due to the decrease of the vorticity field in the partonic matter at freeze-out as a result of both the decrease of the initial vorticity field and the longer lifetime of the partonic phase, which leads to a decrease of the final vorticity field, with increasing collision energy [57, 58, 60]. These results are similar in both trend and value to the experimental data [7] and results from other studies based on the statistical model after a hydrodynamic or transport evolution of the produced matter [60, 71]. There are also feed-down corrections from resonance decays, which are not included in the present study. According to Refs. [60, 129, 130], including Λ and $\bar{\Lambda}$ from resonance decays reduces the polarization of Λ and $\overline{\Lambda}$ hyperons by 15% to 20%. One can see from Fig. 6.4 that including this effect is expected to bring our results into better agreement with the data.

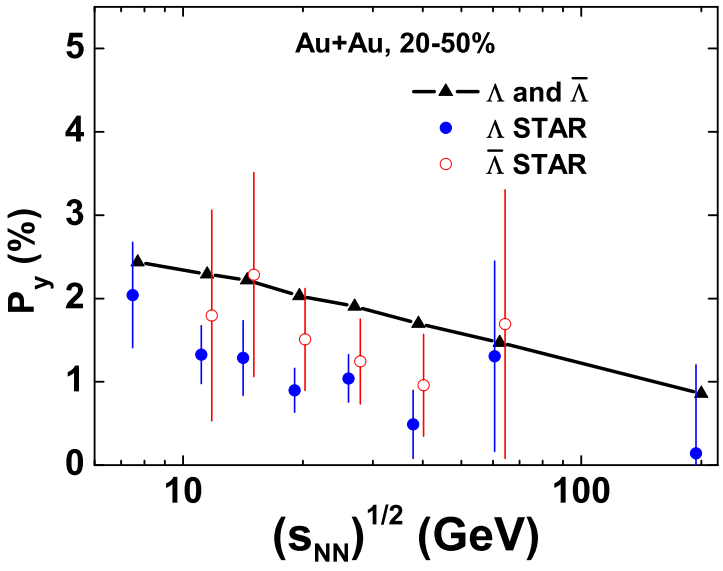

Figure 6.4: Energy dependence of the spin polarization of midrapidity ($|y| \leq 1$) Λ and $\overline{\Lambda}$ hyperons in Au+Au collisions at energies from 7.7 GeV to 200 GeV. Data with error bars are from the STAR Collaboration [6, 7]. Reprinted from Ref. [5]

6.5 Summary

The chiral kinetic equations have been used to study the spin polarizations of light and strange quarks and antiquarks based on the initial conditions from the AMPT model. They are found to have non-vanishing spin polarizations as a result of the chiral vortical effects on their equations of motion. Their polarizations are further increased by the modified collisions due to the modification of their phase-space distributions. Using the coalescence model to convert light and strange quarks and antiquarks to Λ and $\bar{\Lambda}$ hyperons after the partonic phase, it is further found that their spin polarizations, which are determined by those of strange quarks and antiquarks, are comparable to the experimental data. However, the effect of hadronic evolution on the Λ and $\bar{\Lambda}$ polarizations has not been included in the present study.

To study this effect requires a hadronic transport model that includes explicitly their spin degrees of freedom, such as in Refs. [131, 132, 133], and is beyond the present study. Also, Λ and $\bar{\Lambda}$ have the same polarization in present study because they are described by the same chiral kinetic equations of motion and modified collisions. The present study thus cannot explain the seemingly larger $\bar{\Lambda}$ than Λ polarization seen in the experimental data. Furthermore, only the global spin polarizations of Λ and $\bar{\Lambda}$ hyperons have been considered. Since the transport model includes non-equilibrium effects and the local structure of the vorticity field, it provides the possibility to study the local structure of the spin polarization [66] and other interesting features of this phenomenon.

7. SUMMARY

In this thesis, the chiral kinetic theory and resulting transport model have been used to study chiral effects on the quark-gluon plasma due to the large magnetic field and vorticity field present in non-central relativistic heavy ion collisions. These effects include the chiral magnetic effect (CME), chiral separation effect (CSE), chiral vortical effect (CVE), and the chiral vortical separation effect (CVSE) as well as the chiral magnetic wave (CMW) due to the interplay of CME and CSE, and the chiral vortical wave (CVW) due to the interplay of CVE and CVSE. The thesis starts with a review of these effects in an equilibrium system by considering its response to the magnetic and vorticity fields to obtain their dependence on the temperature, the vector and axial charge chemical potentials, and the masses of fermions.

The effect of CMW on the elliptic flow splitting between positively and negatively charged particles in heavy ion collisions is then studied. Using initial conditions from the Bjorken boost-invariant model and assuming the presence of a strong and long-lived magnetic field, an appreciable charge quadrupole moment in the transverse plane of the collision has been obtained as expected from the CMW, which then leads to different elliptic flows for particles of negative and positive charges as the system expands. The elliptic flow difference shows a linear dependence on the total charge asymmetry of the partonic matter with a slope that is negative and has a small magnitude when all effects are included (CKM+LF+CCS), in contrast to that measured in experiments with a positive and large magnitude of slope. Changing the lifetime of the magnetic field does not lead to a positive slope parameter.

Further studied is the effect of the CVW on the elliptic flow splitting of different charged particles in the presence of a vorticity field. Using the same initial conditions

from the Bjorken boost-invariant model and the vorticity field modeled according to that from the AMPT model, it is found that the CVW does not lead to an elliptic flow splitting of negatively and positively charged particles when the charge asymmetry of the partonic matter is nonzero. Including also a strong and long-lived magnetic field as in the case with only the magnetic field [1], the inclusion of the Lorentz force cancels the chiral effects due to the magnetic and vorticity fields and leads instead to a negative slope parameter in the charge symmetry dependence of the elliptic flow splitting of negatively and positively charged particles, contrary to that observed in experiments.

Using the chiral transport model, the effect of CVSE on the spin polarization of quarks is also studied. They are found to have non-vanishing spin polarizations as a result of the chiral vortical effect on their equations of motion. Their polarizations are further increased by the modified collisions due to the modification of their phase-space distributions. Using the coalescence model to convert light and strange quarks and antiquarks to Λ and $\bar{\Lambda}$ hyperons after the partonic phase, it is further found that their spin polarizations, which are determined by those of strange quarks and antiquarks, are comparable to the experimental data.

Results obtained in the present thesis thus indicate that it is a challenge to explain the splitting between the elliptic flows of negatively and positively charged particles seen in experiments if only chiral effects are included. Besides, the justification for the existence of a long-lived magnetic field in relativistic heavy ion collisions remains missing, although its strength is known to be sufficiently strong [119, 40, 109]. A calculation based on the AMPT model has shown that the lifetime of the magnetic field in heavy ion collisions at $\sqrt{s_{NN}} = 200$ GeV cannot exceed 0.1 fm/c no matter how one increases the conductivity by decreasing the partonic cross section. Using this magnetic field in heavy ion collisions, it is found that the signal of the chiral

effects is too small to be seen experimentally.

There are still other background effects that may contribute to the signal of the chiral effects [50, 51], such as local charge conservation and the viscous effects in hydrodynamics. Also, the similarities between the charge asymmetry dependence of the elliptic flow difference in p+Pb and Pb+Pb collisions at LHC seems to favor an explanation of the experimental data due to these background effects [52].

On the other hand, our results on the spin polarization of Λ and $\bar{\Lambda}$ based on the chiral transport model are comparable to the experimental data. It also provides the possibility to study the local structure of the spin polarization [66] and other interesting features of this phenomenon. However, the effect of hadronic evolution on the Λ and $\bar{\Lambda}$ polarizations has not been included in the present study. To study this effect requires a hadronic transport model that includes explicitly their spin degrees of freedom, such as in Refs. [131, 132, 133]. Further study is thus needed.

REFERENCES

[1] Y. Sun, C. M. Ko, F. Li, *Phys. Rev. C* **94**, 045204 (2016).

[2] J. Adams, *et al.*, *Phys. Rev. C* **72**, 014904 (2005).

[3] G. Wang, *Nuc. Phys. A* **904–905**, 248c (2013).

[4] Y. Sun, C. M. Ko, *Phys. Rev. C* **95**, 034909 (2017).

[5] Y. Sun, C. M. Ko, *Phys. Rev. C* **96**, 024906 (2017).

[6] B. I. Abelev, *et al.*, *Phys. Rev. C* **76**, 024915 (2007).

[7] L. Adamczyk, *et al.*, *Nature* **548**, 62 (2017).

[8] H. D. Politzer, *Phys. Rev. Lett.* **30**, 1346 (1973).

[9] D. J. Gross, F. Wilczek, *Phys. Rev. Lett.* **30**, 1343 (1973).

[10] Y. Nambu, G. Jona-Lasinio, *Phys. Rev.* **122**, 345 (1961).

[11] J. Adams, *et al.*, *Nucl. Phys. A* **757**, 102 (2005).

[12] K. Adcox, *et al.*, *Nucl. Phys. A* **757**, 184 (2005).

[13] I. Arsene, *et al.*, *Nucl. Phys. A* **757**, 1 (2005).

[14] B. B. Back, *et al.*, *Nucl. Phys. A* **757**, 28 (2005).

[15] K. Aamodt, *et al.*, *JINST* **3**, S08002 (2008).

[16] A. Belavin, A. Polyakov, A. Schwartz, Y. Tyupkin, *Physics Letters B* **59**, 85 (1975).

[17] R. Jackiw, C. Rebbi, *Phys. Rev. Lett.* **37**, 172 (1976).

[18] G. D. Moore, M. Tassler, *Journal of High Energy Physics* **2011**, 105 (2011).

[19] M. Mace, S. Schlichting, R. Venugopalan, *Phys. Rev. D* **93**, 074036 (2016).

[20] F. R. Klinkhamer, N. S. Manton, *Phys. Rev. D* **30**, 2212 (1984).

[21] P. Arnold, L. McLerran, *Phys. Rev. D* **36**, 581 (1987).

[22] D. E. Kharzeev, L. D. McLerran, H. J. Warringa, *Nuclear Physics A* **803**, 227 (2008).

[23] K. Fukushima, D. E. Kharzeev, H. J. Warringa, *Phys. Rev. D* **78**, 074033 (2008).

[24] D. E. Kharzeev, *Annals of Physics* **325**, 205 (2010).

[25] D. T. Son, A. R. Zhitnitsky, *Phys. Rev. D* **70**, 074018 (2004).

[26] M. A. Metlitski, A. R. Zhitnitsky, *Phys. Rev. D* **72**, 045011 (2005).

[27] Y. Burnier, D. E. Kharzeev, J. Liao, H.-U. Yee, *Phys. Rev. Lett.* **107**, 052303 (2011).

[28] D. T. Son, P. Surówka, *Phys. Rev. Lett.* **103**, 191601 (2009).

[29] Y. Jiang, X.-G. Huang, J. Liao, *Phys. Rev. D* **92**, 071501 (2015).

[30] Z.-T. Liang, X.-N. Wang, *Phys. Rev. Lett.* **96**, 039901 (2006).

[31] J.-H. Gao, *et al.*, *Phys. Rev. C* **77**, 044902 (2008).

[32] F. Becattini, F. Piccinini, J. Rizzo, *Phys. Rev. C* **77**, 024906 (2008).

[33] F. Becattini, F. Piccinini, *Annals of Physics* **323**, 2452 (2008).

[34] F. Becattini, V. Chandra, L. D. Zanna, E. Grossi, *Annals of Physics* **338**, 32 (2013).

[35] R.-h. Fang, L.-g. Pang, Q. Wang, X.-n. Wang, *Phys. Rev. C* **94**, 024904 (2016).

[36] S.-S. Chern, J. Simons, *Annals of Mathematics* **99**, 48 (1974).

[37] S. L. Adler, *Phys. Rev.* **177**, 2426 (1969).

[38] K. Fujikawa, *Phys. Rev. Lett.* **42**, 1195 (1979).

[39] V. D. Toneev, V. P. Konchakovski, V. Voronyuk, E. L. Bratkovskaya, W. Cassing, *Phys. Rev. C* **86**, 064907 (2012).

[40] W.-T. Deng, X.-G. Huang, *Phys. Rev. C* **85**, 044907 (2012).

[41] B. I. Abelev, *et al.*, *Phys. Rev. Lett.* **103**, 251601 (2009).

[42] B. I. Abelev, *et al.*, *Phys. Rev. C* **81**, 054908 (2010).

[43] B. Abelev, *et al.*, *Phys. Rev. Lett.* **110**, 012301 (2013).

[44] S. A. Voloshin, *Phys. Rev. C* **70**, 057901 (2004).

[45] A. Bzdak, V. Koch, J. Liao, *Phys. Rev. C* **83**, 014905 (2011).

[46] S. Schlichting, S. Pratt, *Phys. Rev. C* **83**, 014913 (2011).

[47] V. Khachatryan, *et al.*, *Phys. Rev. Lett.* **118**, 122301 (2017).

[48] D. E. Kharzeev, H.-U. Yee, *Phys. Rev. D* **83**, 085007 (2011).

[49] J. Adam, *et al.*, *Phys. Rev. C* **93**, 044903 (2016).

[50] A. Bzdak, P. Bozek, *Physics Letters B* **726**, 239 (2013).

[51] Y. Hatta, A. Monnai, B.-W. Xiao, *Phys. Rev. D* **92**, 114010 (2015).

[52] S. E. Park, *1704.06712* (2017).

[53] M. Hongo, Y. Hirono, T. Hirano, *1309.2823* (2013).

[54] H.-U. Yee, Y. Yin, *Phys. Rev. C* **89**, 044909 (2014).

[55] Y. Hirono, T. Hirano, D. E. Kharzeev, *Nuclear Physics A* **956**, 393 (2016).

[56] S. Shi, Y. Jiang, E. Lilleskov, Y. Yin, J. Liao, *1704.05531* (2017).

[57] W.-T. Deng, X.-G. Huang, *Phys. Rev. C* **93**, 064907 (2016).

[58] Y. Jiang, Z.-W. Lin, J. Liao, *Phys. Rev. C* **94**, 044910 (2016).

[59] F. Becattini, L. P. Csernai, D. J. Wang, *Phys. Rev. C* **88**, 034905 (2013).

[60] I. Karpenko, F. Becattini, *The European Physical Journal C* **77**, 213 (2017).

[61] Y. L. Xie, M. Bleicher, H. Stöcker, D. J. Wang, L. P. Csernai, *Phys. Rev. C* **94**, 054907 (2016).

[62] Y. Xie, D. Wang, L. P. Csernai, *Phys. Rev. C* **95**, 031901 (2017).

[63] L. P. Csernai, V. K. Magas, D. J. Wang, *Phys. Rev. C* **87**, 034906 (2013).

[64] L. P. Csernai, D. J. Wang, M. Bleicher, H. Stöcker, *Phys. Rev. C* **90**, 021904 (2014).

[65] F. Becattini, *et al.*, *The European Physical Journal C* **75**, 406 (2015).

[66] L.-g. Pang, H. Petersen, Q. Wang, X.-N. Wang, *Phys. Rev. Lett.* **117**, 192301 (2016).

[67] A. Aristova, D. Frenklakh, A. Gorsky, D. Kharzeev, *Journal of High Energy Physics* **2016**, 29 (2016).

[68] M. Baznat, K. Gudima, A. Sorin, O. Teryaev, *Phys. Rev. C* **88**, 061901 (2013).

[69] O. Teryaev, R. Usubov, *Phys. Rev. C* **92**, 014906 (2015).

[70] Yu. B. Ivanov, A. A. Soldatov, *1701.01319* (2017).

[71] H. Li, L.-G. Pang, Q. Wang, X.-L. Xia, *1704.01507* (2017).

[72] M. A. Stephanov, Y. Yin, *Phys. Rev. Lett.* **109**, 162001 (2012).

[73] D. T. Son, N. Yamamoto, *Phys. Rev. Lett.* **109**, 181602 (2012).

[74] D. T. Son, N. Yamamoto, *Phys. Rev. D* **87**, 085016 (2013).

[75] J.-H. Gao, Z.-T. Liang, S. Pu, Q. Wang, X.-N. Wang, *Phys. Rev. Lett.* **109**, 232301 (2012).

[76] J.-W. Chen, S. Pu, Q. Wang, X.-N. Wang, *Phys. Rev. Lett.* **110**, 262301 (2013).

[77] C. Manuel, J. M. Torres-Rincon, *Phys. Rev. D* **90**, 076007 (2014).

[78] V. Greco, C. M. Ko, P. Lévai, *Phys. Rev. Lett.* **90**, 202302 (2003).

[79] C. M. Ko, T. Song, F. Li, V. Greco, S. Plumari, *Nuclear Physics A* **928**, 234 (2014).

[80] X.-l. Sheng, D. H. Rischke, D. Vasak, Q. Wang, *1707.01388* (2017).

[81] J. Erdmenger, M. Haack, M. Kaminski, A. Yarom, *Journal of High Energy Physics* **2009**, 055.

[82] N. Banerjee, *et al.*, *JHEP* **01**, 094 (2011).

[83] M. Torabian, H.-U. Yee, *Journal of High Energy Physics* **2009**, 020.

[84] I. Amado, K. Landsteiner, F. Pena-Benitez, *Journal of High Energy Physics* **2011**, 81 (2011).

[85] K. Landsteiner, E. Megías, F. Pena-Benitez, *Phys. Rev. Lett.* **107**, 021601 (2011).

[86] D. E. Kharzeev, H. J. Warringa, *Phys. Rev. D* **80**, 034028 (2009).

[87] X.-G. Huang, *Sci. Rep.* **6**, 20601 (2016).

[88] M. N. Chernodub, *Journal of High Energy Physics* **2016**, 100 (2016).

[89] N. Yamamoto, *Phys. Rev. Lett.* **115**, 141601 (2015).

[90] J.-Y. Chen, D. T. Son, M. A. Stephanov, H.-U. Yee, Y. Yin, *Phys. Rev. Lett.* **113**, 182302 (2014).

[91] D. Xiao, J. Shi, Q. Niu, *Phys. Rev. Lett.* **95**, 137204 (2005).

[92] D. Xiao, M.-C. Chang, Q. Niu, *Rev. Mod. Phys.* **82**, 1959 (2010).

[93] C. Duval, Z. Horváth, P. A. Horváthy, L. Martina, P. C. Stichel, *Phys. Rev. Lett.* **96**, 099701 (2006).

[94] J. Wess, B. Zumino, *Physics Letters B* **37**, 95 (1971).

[95] E. Witten, *Nuclear Physics B* **223**, 422 (1983).

[96] M. Stephanov, H.-U. Yee, Y. Yin, *Phys. Rev. D* **91**, 125014 (2015).

[97] J. Xu, T. Song, C. M. Ko, F. Li, *Phys. Rev. Lett.* **112**, 012301 (2014).

[98] J. Xu, C. M. Ko, F. Li, T. Song, *Nucl. Phys. Rev.* **32**, 146 (2014).

[99] J. Xu, C. M. Ko, *Phys. Rev. C* **94**, 054909 (2016).

[100] J.-Y. Chen, D. T. Son, M. A. Stephanov, H.-U. Yee, Y. Yin, *Phys. Rev. Lett.* **113**, 182302 (2014).

[101] J.-h. Gao, S. Pu, Q. Wang, *Phys. Rev. D* **96**, 016002 (2017).

[102] J.-Y. Chen, D. T. Son, M. A. Stephanov, *Phys. Rev. Lett.* **115**, 021601 (2015).

[103] C.-Y. Wong, *Phys. Rev. C* **25**, 1460 (1982).

[104] D. Satow, H.-U. Yee, *Phys. Rev. D* **90**, 014027 (2014).

[105] C. Manuel, J. M. Torres-Rincon, *Phys. Rev. D* **92**, 074018 (2015).

[106] G.-L. Ma, *Phys. Lett. B* **735**, 383 (2014).

[107] G. F. Bertsch, S. Das Gupta, *Phys. Rept.* **160**, 189 (1988).

[108] G. Başar, D. E. Kharzeev, V. Skokov, *Phys. Rev. Lett.* **109**, 202303 (2012).

[109] L. McLerran, V. Skokov, *Nuc. Phys. A* **929**, 184 (2014).

[110] K. Tuchin, *Phys. Rev. C* **91**, 064902 (2015).

[111] V. D. Toneev, V. P. Konchakovski, V. Voronyuk, E. L. Bratkovskaya, W. Cassing, *Phys. Rev. C* **86**, 064907 (2012).

[112] Z.-W. Lin, C. M. Ko, B.-A. Li, B. Zhang, S. Pal, *Phys. Rev.* **C72**, 064901 (2005).

[113] Y. Nambu, G. Jona-Lasinio, *Phys. Rev.* **122**, 345 (1961).

[114] S. Ghosh, T. C. Peixoto, V. Roy, F. E. Serna, G. Krein, *Phys. Rev. C* **93**, 045205 (2016).

[115] U. Heinz, R. Snellings, *Ann. Rev. Nucl. Part. Sci.* **63**, 123 (2013).

[116] B.-A. Li, C. M. Ko, *Phys. Rev. C* **52**, 2037 (1995).

[117] C. M. Ko, T. Song, F. Li, V. Greco, S. Plumari, *Nucl. Phys. A* **928**, 234 (2014).

[118] J. Xu, L.-W. Chen, C. M. Ko, Z.-W. Lin, *Phys. Rev. C* **85**, 041901(R) (2012).

[119] V. Voronyuk, *et al.*, *Phys. Rev. C* **83**, 054911 (2011).

[120] V. D. Toneev, *et al.*, *Phys. Rev. C* **85**, 034910 (2012).

[121] D. T. Son, N. Yamamoto, *Phys. Rev. Lett.* **109**, 181602 (2012).

[122] J.-W. Chen, J.-y. Pang, S. Pu, Q. Wang, *Phys. Rev. D* **89**, 094003 (2014).

[123] C. Manuel, J. M. Torres-Rincon, *Phys. Rev. D* **90**, 076007 (2014).

[124] J. hua Gao, Q. Wang, *Physics Letters B* **749**, 542 (2015).

[125] C. Patrignani, *et al.*, *Chin. Phys. C* **40**, 100001 (2016).

[126] Z.-W. Lin, C. M. Ko, B.-A. Li, B. Zhang, S. Pal, *Phys. Rev. C* **72**, 064901 (2005).

[127] J. Xu, C. M. Ko, *Phys. Rev. C* **84**, 014903 (2011).

[128] W. Broniowski, W. Florkowski, *Phys. Rev. C* **65**, 024905 (2002).

[129] Z. Qiu, *1308.2182* (2013).

[130] F. Becattini, I. Karpenko, M. Lisa, I. Upsal, S. Voloshin, *1610.02506* (2016).

[131] J. Xu, B.-A. Li, *Phys. Lett. B* **724**, 346 (2013).

[132] Y. Xia, J. Xu, B.-A. Li, W.-Q. Shen, *Phys. Rev. C* **89**, 064606 (2014).

[133] Y. Xia, J. Xu, B.-A. Li, W.-Q. Shen, *Nucl. Phys. A* **955**, 41 (2016).

[134] M. V. Berry, *Proc. Roy. Soc. Lond. A* **392**, 45 (1984).

[135] A. Puglisi, S. Plumari, V. Greco, *Phys. Rev. D* **90**, 114009 (2014).

APPENDIX A

CMW AND CVW FROM HYDRODYNAMICS

A.1 CMW from magnetohydrodynamics

For a system in thermal equilibrium, the velocity of the CMW induced by a magnetic field can be found using the magnetohydrodynamics [48, 27] as reproduced below. Defining $\mathbf{J}_R = (\mathbf{J}^V + \mathbf{J}^A)/2$, $\mathbf{J}_L = (\mathbf{J}^V - \mathbf{J}^A)/2$, $\mu_R = \mu + \mu_5$, and $\mu_R = \mu - \mu_5$, then Eqs.(2.2) and (2.3) for the CME and CSE lead to

$$\mathbf{J}_{R,L} = \pm \frac{Q^2 \mu_{R,L}}{4\pi^2} \mathbf{B}, \tag{A.1}$$

where the " $+$ " is for particles and antiparticles of right chirality, and the " $-$ " is for particles and antiparticles of left chirality. In the case that the electric field and the magnetic field are perpendicular, the vector charge of right chirality and left chirality are conserved separately, which leads to

$$\frac{\partial \rho_{R,L}}{\partial t} + \boldsymbol{\nabla} \cdot \left(\pm \frac{Q^2 \mathbf{B} \mu_{R,L}}{4\pi^2} \right) = 0.$$

For a small fluctuation of chemical potential, one has

$$\frac{\partial \delta\rho_{R,L}}{\partial t} + \boldsymbol{\nabla} \cdot \left(\pm \frac{Q^2 \mathbf{B} \delta\mu_{R,L}}{4\pi^2} \right) = 0.$$

Using the relation $\delta\rho = Q\frac{\partial n}{\partial \mu}\delta\mu = Q\alpha\delta\mu$, where $\alpha = \partial n/\partial\mu$ with n being the density difference between particles and antiparticles or the net particle density, one can

show

$$\frac{\partial \delta\mu_{R,L}}{\partial t} \pm \frac{Q\mathbf{B}}{4\pi^2\alpha} \cdot \boldsymbol{\nabla}\delta\mu_{R,L} = 0.$$

A.2 CVW from hydrodynamics

From charge conservation and the CVE and CVSE, the time evolution of charge density fluctuation is given by

$$\frac{\partial \delta\rho_{R,L}}{\partial t} + \boldsymbol{\nabla} \cdot \left(\pm \frac{\boldsymbol{\omega}\mu_{R,L}\delta\mu_{R,L}}{2\pi^2} \right) = 0. \tag{A.2}$$

For small density fluctuation, this leads to

$$\frac{\partial \delta\mu_{R,L}}{\partial t} \pm \frac{\boldsymbol{\omega}\mu_{R,L}}{2\pi^2\alpha} \cdot \boldsymbol{\nabla}\delta\mu_{R,L} = 0, \tag{A.3}$$

where $\delta\rho = \alpha\delta\mu$ has been used.

APPENDIX B

CHIRAL KINETIC EQUATIONS AND BERRY CURVATURE

The Lagrangian of a massless particle of positive helicity is given by $\mathcal{L} = (\mathbf{p} + Q\mathbf{A}) \cdot \dot{\mathbf{x}} - p - Q\phi - \mathbf{a_p} \cdot \dot{\mathbf{p}}$, where $\mathbf{a_p} = \mathrm{Im}(\phi_+^\dagger \boldsymbol{\nabla}_\mathbf{p} \phi_+)$ and $\boldsymbol{\sigma} \cdot \mathbf{p}\phi_+ = p\phi_+$. From the method of variation,

$$\frac{d}{dt}\left(\frac{\partial \mathcal{L}}{\partial \dot{p}^i}\right) - \frac{\partial \mathcal{L}}{\partial p^i} = 0, \qquad \frac{d}{dt}\left(\frac{\partial \mathcal{L}}{\partial \dot{x}^i}\right) - \frac{\partial \mathcal{L}}{\partial x^i} = 0, \tag{B.1}$$

one has

$$-\dot{a}^i_\mathbf{p} - \dot{x}^i + \frac{p^i}{p} + \dot{p}^j \frac{\partial a^j_\mathbf{p}}{\partial p^i} = 0, \qquad \dot{p}^i + Q\dot{A}^i - Q\dot{x}^j \frac{\partial A^j}{\partial x^i} + \frac{\partial \phi}{\partial x^i} = 0, \tag{B.2}$$

i.e.,

$$\begin{aligned} \dot{x}^i &= -\frac{\partial \dot{a}^i_\mathbf{p}}{\partial p^j}\dot{p}^j + \frac{p^i}{p} + \dot{p}^j \frac{\partial a^j_\mathbf{p}}{\partial p^i} = \epsilon_{ijk}\dot{p}^j(\epsilon_{klm}\partial_l a^m_\mathbf{p}) + \frac{p^i}{p}, \\ \dot{p}^i &= -Q\frac{\partial A^i}{\partial t} - Q\dot{x}^j \frac{\partial A^i}{\partial x^j} + Q\dot{x}^j \frac{\partial A^j}{\partial x^i} - Q\frac{\partial \phi}{\partial x^i} = Q(E^i + \epsilon_{ijk}\dot{x}^j B^k), \end{aligned} \tag{B.3}$$

or the chiral kinetic equations of motion,

$$\dot{\mathbf{x}} = \hat{\mathbf{p}} + \dot{\mathbf{p}} \times \mathbf{b}, \qquad \dot{\mathbf{p}} = Q(\mathbf{E} + \dot{\mathbf{x}} \times \mathbf{B}), \tag{B.4}$$

where $\mathbf{b} = \nabla \times \mathbf{a_p}$.

Following Ref. [134], one has

$$\mathbf{b} = \mathrm{Im}\boldsymbol{\nabla} \times (\phi_+^\dagger \boldsymbol{\nabla}\phi_+) = \mathrm{Im}\boldsymbol{\nabla}\phi_+^\dagger \times \boldsymbol{\nabla}\phi_+ = \mathrm{Im}\sum_\lambda \boldsymbol{\nabla}\phi_+^\dagger \phi_\lambda \times \phi_\lambda^\dagger \boldsymbol{\nabla}\phi_+, \qquad \text{(B.5)}$$

where the identity $I = \sum_\lambda |\lambda\rangle\langle\lambda|$ has been used. Since $\phi_+^\dagger \boldsymbol{\nabla}\phi_+$ is purely imaginary, then $\mathbf{b} = \mathrm{Im}\boldsymbol{\nabla}\phi_+^\dagger\phi_- \times \phi_-^\dagger \boldsymbol{\nabla}\phi_+$. Further using

$$\begin{aligned} E_+\phi_-^\dagger \boldsymbol{\nabla}\phi_+ &= \phi_-^\dagger \boldsymbol{\nabla}(H\phi_+) = \phi_-^\dagger(\boldsymbol{\nabla}H)\phi_+ + \phi_-^\dagger H\boldsymbol{\nabla}\phi_+ \\ &= \phi_-^\dagger(\boldsymbol{\nabla}H)\phi_+ + E_-\phi_-^\dagger\boldsymbol{\nabla}\phi_+, \end{aligned} \qquad \text{(B.6)}$$

one gets

$$\phi_-^\dagger \boldsymbol{\nabla}\phi_+ = \frac{\phi_-^\dagger(\boldsymbol{\nabla}H)\phi_+}{E_+ - E_-},$$

and thus

$$\mathbf{b} = Im\frac{\phi_+^\dagger(\boldsymbol{\nabla}H)\phi_- \times \phi_-^\dagger(\boldsymbol{\nabla}H)\phi_+}{(E_+ - E_-)^2}. \qquad \text{(B.7)}$$

Using the explicit form of

$$\phi_+ = \begin{pmatrix} \cos(\frac{\theta}{2}) \\ \sin(\frac{\theta}{2})e^{i\phi} \end{pmatrix}, \qquad \phi_- = \begin{pmatrix} -\sin(\frac{\theta}{2})e^{-i\phi} \\ \cos(\frac{\theta}{2}) \end{pmatrix}$$

where θ and ϕ are the azimuthal angles of $\mathbf{p}$ as well as $H = \boldsymbol{\sigma}\cdot\mathbf{p}$, one has

$$\begin{aligned} &\phi_+^\dagger(\boldsymbol{\nabla}H)\phi_- = \phi_+^\dagger\boldsymbol{\sigma}\phi_- \\ &= \left(\cos^2\frac{\theta}{2} - \sin^2\frac{\theta}{2}e^{-2i\phi}, -i\left(\cos^2\frac{\theta}{2} + \sin^2\frac{\theta}{2}e^{-2i\phi}\right), -\sin\theta e^{-i\phi}\right). \end{aligned} \qquad \text{(B.8)}$$

Since

$$
\begin{aligned}
&(\phi_+^\dagger(\boldsymbol{\nabla}H)\phi_- \times \phi_-^\dagger(\boldsymbol{\nabla}H)\phi_+)_x \\
&= i(\cos^2\frac{\theta}{2} + sin^2\frac{\theta}{2}e^{-2i\phi})\sin\theta e^{-i\phi} + i(\cos^2\frac{\theta}{2} + \sin^2\frac{\theta}{2}e^{2i\phi})\sin\theta e^{-i\phi} \\
&= i(\sin\theta e^{i\phi} + \sin\theta e^{-i\phi}) \\
&= 2i\sin\theta\cos\phi, \qquad \text{(B.9)} \\
&(\phi_+^\dagger(\boldsymbol{\nabla}H)\phi_- \times \phi_-^\dagger(\boldsymbol{\nabla}H)\phi_+)_y \\
&= -(\cos^2\frac{\theta}{2} - \sin^2\frac{\theta}{2}e^{2i\phi})\sin\theta e^{-i\phi} + (\cos^2\frac{\theta}{2} - \sin^2\frac{\theta}{2}e^{-2i\phi})\sin\theta e^{i\phi} \\
&= (\sin\theta e^{i\phi} - \sin\theta e^{-i\phi}) \\
&= 2i\sin\theta\sin\phi, \qquad \text{(B.10)} \\
&(\phi_+^\dagger(\boldsymbol{\nabla}H)\phi_- \times \phi_-^\dagger(\boldsymbol{\nabla}H)\phi_+)_z \\
&= i(\cos^2\frac{\theta}{2} - \sin^2\frac{\theta}{2}e^{-2i\phi})(\cos^2\frac{\theta}{2} + \sin^2\frac{\theta}{2}e^{2i\phi}) \\
&+i(\cos^2\frac{\theta}{2} + \sin^2\frac{\theta}{2}e^{-2i\phi})(\cos^2\frac{\theta}{2} - \sin^2\frac{\theta}{2}e^{2i\phi}) \\
&= 2i(\cos^4\frac{\theta}{2} - \sin^4\frac{\theta}{2}), \\
&= 2i\cos\theta. \qquad \text{(B.11)}
\end{aligned}
$$

the Berry curvature is thus given by $\mathbf{b} = \frac{2\hat{\mathbf{p}}}{4p^2} = \frac{\hat{\mathbf{p}}}{2p^2}$.

For particles (antiparticles) with negative helicity, calculations similar to the above gives $\dot{\mathbf{x}} = \hat{\mathbf{p}} - \dot{\mathbf{p}} \times \mathbf{b}$. The chiral kinetic equations derived from the Lagrangian therefore include the first-order quantum correction.

APPENDIX C

CMW AND CVW IN CHIRAL KINETIC THEORY

C.1 CMW in chiral kinetic theory

Because charge is separately conserved for particles and antiparticles of right chirality and left chirality, one can consider right chirality particles and antiparticles as an illustration. The Boltzmann equation for these particles is

$$\frac{\partial f_\pm}{\partial t} + \dot{\mathbf{x}} \cdot \frac{\partial f_\pm}{\partial \mathbf{x}} + \dot{\mathbf{p}} \cdot \frac{\partial f_\pm}{\partial \mathbf{p}} = \mathcal{C}_\pm[f_+, f_-], \tag{C.1}$$

where the plus and minus are for positive helicity particles and negative helicity antiparticles, respectively, and the right hand side is the collision term. In the presence of a magnetic field, the equations of motion are $\sqrt{G}\dot{\mathbf{x}} = \hat{\mathbf{p}} + Q\frac{\mathbf{B}}{2p^2}$ and $\sqrt{G}\dot{\mathbf{p}} = \pm Q\hat{\mathbf{p}} \times \mathbf{B}$ with $\sqrt{G} = 1 + Q\frac{\mathbf{B}\cdot\mathbf{p}}{2p^3}$, as given in Chapter 3. From Section 3.4, one then has

$$\frac{\partial \sqrt{G} f_\pm}{\partial t} + \frac{\partial \sqrt{G}\dot{\mathbf{x}} f_\pm}{\partial \mathbf{x}} + \frac{\partial \sqrt{G}\dot{\mathbf{p}} f_\pm}{\partial \mathbf{p}} = \sqrt{G}\mathcal{C}_\pm[f_+, f_-], \tag{C.2}$$

and thus

$$\begin{aligned} &\frac{\partial \sqrt{G}(f_+ - f_-)}{\partial t} + \frac{\partial \sqrt{G}\dot{\mathbf{x}}(f_+ - f_-)}{\partial \mathbf{x}} + \frac{\partial \sqrt{G}\dot{\mathbf{p}}(f_+ - f_-)}{\partial \mathbf{p}} \\ &= \sqrt{G}(\mathcal{C}_+[f_+, f_-] - \mathcal{C}_-[f_+, f_-]). \end{aligned} \tag{C.3}$$

Integrating both sides over the momentum, i.e., $\int \frac{d^3\mathbf{p}}{(2\pi)^3}$, the right hand side is zero because the conservation of right chirality charge guarantees that the number differ-

ence between positive helicity particles and negative helicity antiparticles is always conserved no matter what the distribution function is. Also, the third term on the left hand side is zero because the distribution is zero at large magnitude of momenta.

For an equilibrium system with chemical potential μ and temperature T, changing its chemical potential modifies its distribution function. For a small change of μ to $\mu + \delta\mu$, one can use the relation $f_+ = f(p - (\mu + \delta\mu)) = f(p - \mu) - \frac{\partial f_+}{\partial p}\delta\mu$ and $f_- = f(p + (\mu + \delta\mu)) = f(p + \mu) + \frac{\partial f_-}{\partial p}\delta\mu$ to obtain

$$\begin{aligned}
&\frac{\partial}{\partial t}\int \frac{d^3\mathbf{p}}{(2\pi)^3}\sqrt{G}(f_+ - f_-) \\
&= \frac{\partial}{\partial t}\int \frac{d^3\mathbf{p}}{(2\pi)^3}[\sqrt{G}f(p-\mu) - \sqrt{G}f(p+\mu) - \sqrt{G}\delta\mu(\frac{\partial f_+}{\partial p} + \frac{\partial f_-}{\partial p})] \\
&= \frac{\partial}{\partial t}[\rho_0 + \delta\mu\frac{\partial \rho}{\partial \mu}], \qquad \text{(C.4)} \\
&\frac{\partial}{\partial \mathbf{x}}\int \frac{d^3\mathbf{p}}{(2\pi)^3}\sqrt{G}\dot{\mathbf{x}}(f_+ - f_-) = \frac{\partial}{\partial \mathbf{x}}\int \frac{d^3\mathbf{p}}{(2\pi)^3}(\hat{\mathbf{p}} + Q\frac{\mathbf{B}}{2p^2})(f_+ - f_-) \\
&= \frac{\partial}{\partial \mathbf{x}}[\frac{Q\mathbf{B}(\mu + \delta\mu(f_+(0)) + f_-(0))}{4\pi^2}]. \qquad \text{(C.5)}
\end{aligned}$$

One then has

$$\frac{\partial \delta\mu}{\partial t} + \frac{Q\mathbf{B}}{4\pi^2\frac{\partial\rho}{\partial\mu}} \cdot \frac{\partial \delta\mu}{\partial \mathbf{x}} = 0, \qquad \text{(C.6)}$$

which is the same as that obtained in Section 2.1.4. The above equation can be solved by introducing the Fourier transformation $\delta\mu(\mathbf{x}, t) = \int d\omega d^3\mathbf{k} h(\mathbf{k}, \omega) e^{i(\omega t - \mathbf{k}\cdot\mathbf{x})}$, and one obtains from the resulting equation the dispersion relation $\omega = \mathbf{k} \cdot \frac{Q\mathbf{B}}{4\pi^2\alpha}$ for the CMW.

C.2 CVW in chiral kinetic theory

As in the previous section for the case of magnetic field, one has a similar equation for the case of the vortical field,

$$\frac{\partial\sqrt{G}(f_+ - f_-)}{\partial t} + \frac{\partial\sqrt{G}\dot{\mathbf{x}}(f_+ - f_-)}{\partial \mathbf{x}} + \frac{\partial\sqrt{G}\dot{\mathbf{p}}(f_+ - f_-)}{\partial \mathbf{p}} = \sqrt{G}(\mathcal{C}_+[f_+, f_-] - \mathcal{C}_-[f_+, f_-]).$$

Following similar discussions as in Section 3.5, one obtains the dispersion relations $\omega_1 = \mathbf{k_1} \cdot \frac{3\mu\boldsymbol{\omega}}{\pi^2 T^2}$ and $\omega_1 = \mathbf{k_1} \cdot \frac{\mu\boldsymbol{\omega}}{2T^2}$ for the CVW for the cases of using the Fermi-Dirac and Boltzmann distributions, respectively.

APPENDIX D

TIME EVOLUTION OF THE MAGNETIC FIELD IN RELATIVISTIC HEAVY ION COLLISIONS

In studying the CMW effect in Chapters 5 and 6, it is assumed that the magnetic field produced in Au+Au collisions at $\sqrt{s_{NN}} = 200$ GeV at RHIC has a long lifetime of 6 fm/c. In the literature, there is a large uncertainty on the lifetime of the magnetic field. For example, it has been shown in Ref. [109] that for a static QGP with a constant conductivity, the lifetime of a decaying magnetic field, such as that produced in relativistic heavy ion collisions, is about 0.1 fm/c if the conductivity is chosen to be that from the lattice QCD calculations. The lifetime can increase to several fm/c only if the conductivity is increased by a unrealistic large factor of 1000. According to Ref. [40], an even larger (infinite) conductivity is required to make the magnetic field to decrease with time as $1/t$ when one takes into account the longitudinal expansion of the QGP.

Shown in this appendix are results on the time evolution of the magnetic field obtained from the string melting version of the AMPT model for Au+Au collisions at $\sqrt{s_{NN}} = 200$ GeV and impact parameter $b = 10$ fm. In this model, the system before collisions, i.e., $t < 0$ fm/c, consists of only nucleons with their momenta along the z direction. After collisions, while the spectator nucleons continue to travel with their initial momenta, the participant nucleons are slowed down and lead to the production of a dense partonic matter consisting of partons produced at different times and positions with various momenta. For hadrons before and after collisions, since they travel with constant velocity, one can use the standard Lienard-Wiechert potentials to calculate the resulting time and spatial dependent electric and magnetic

fields. In particular, the space is divided into cells and the electromagnetic field from these hadrons is stored in each cell at various times to be treated as an external field. For produced partons, they are first propagated back in time to $t = 0$ as free particles and then allow them to collide and move under the influence of the electromagnetic field from both the spectator nucleons and the partons themselves. Although these partons undergo collective expansion, the flow velocity is small compared to the speed of light. So one can neglect the retardation effect on the electromagnetic field and use simply Coulomb's law and the Biot-Savart law to calculate the electromagnetic field produced by these partons, which move under the influence of the electromagnetic field due to the Lorentz force and change their directions due to scatterings. By varying the magnitude of the parton scattering cross section, one can simulate the effect of the QGP electric conductivity on the lifetime of the magnetic field produced in non-central heavy ion collisions.

Shown in Fig. D.1 is the time evolution of the magnetic field at the center of produced partonic matter at different times. The black line represents the background contribution from the spectator nucleons only. it is found that the magnetic field initially has a very large magnitude of about $7m_\pi^2$ but decreases quickly with time. Including the contribution from partons by using an isotropic and constant scattering cross section of 3 mb only increases the magnitude of the magnetic field after 0.2 fm/c with its magnitude remaining very small compared to the initial magnetic field shown by the red line.

Also shown is the result from using a zero cross section for parton scattering, which corresponds to an infinite conductivity since it behaves as $\frac{1}{T\sigma}$ according to the relaxation time calculation of Ref. [135] for massless particles. It is seen that the results in this case, shown by the green line in Fig. D.1, are essentially the same as in the case for a cross section of 3 mb. These results thus show that increasing the

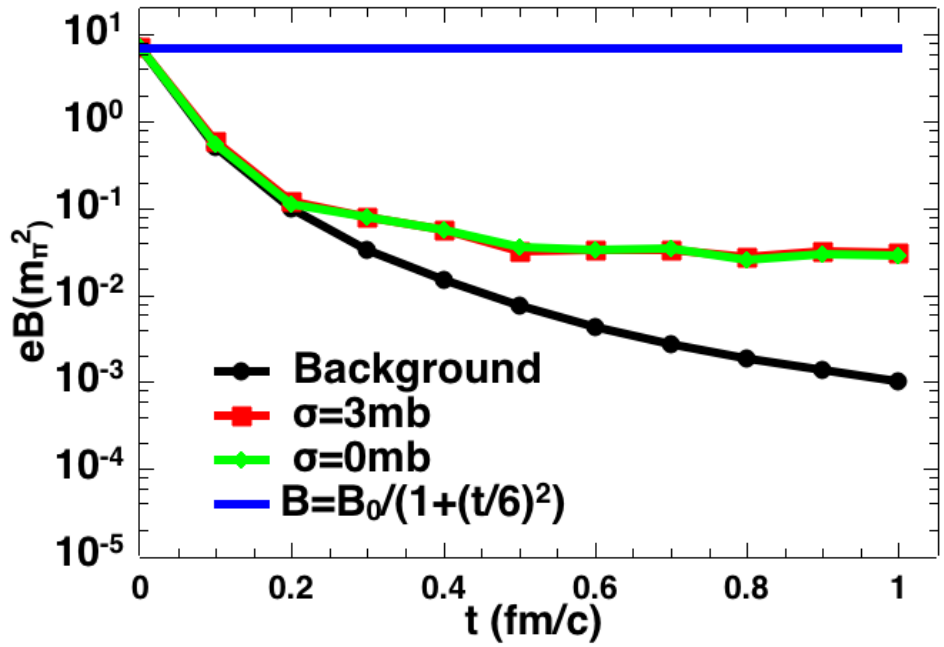

Figure D.1: Time evolution of the magnetic field for different choices of cross sections.

conductivity of the quark matter does not increase the lifetime of the magnetic field, indicating that the medium response to the electromagnetic field changes very little with the scattering cross section. The time dependence of the magnetic field from the transport model study thus deviated significantly from the magnetic field lifetime of 6 fm/c used in Chapters 4 and 5, which is shown by the blue line in Fig. D.1.

To understand our result, a box simulation to study the medium response to an electric field has been carried out. The medium consists of only massless u, d, and s quarks at a temperature of 0.3 GeV in a box of $6\times6\times6$ fm^3. A static uniform electric field with strength $eE = 0.02$ GeV^2 is applied to study how the charge current is generated. Because the charges of u, d, and s quarks are $\frac{2e}{3}, -\frac{e}{3}$, and $-\frac{e}{3}$ separately, the electric conductivity of the partonic matter is expected to be $\frac{4\pi\alpha}{9T\sigma}$ according to the relaxation time calculation. It is found that the result from our simulation is

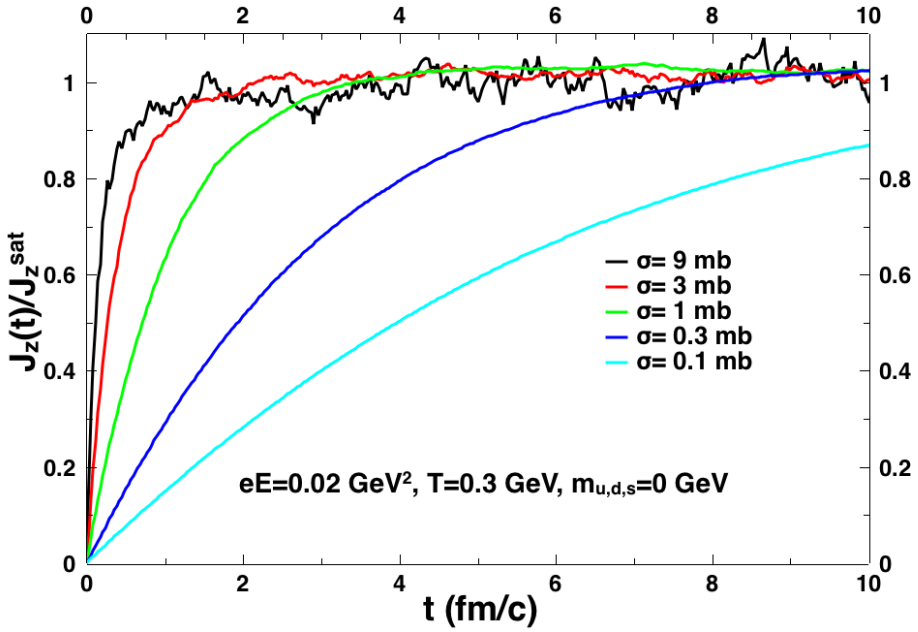

Figure D.2: Time evolution of the normalized charge current in response to a static uniform electric field in z direction.

close to this value when the cross section σ is larger than 1 mb, which corresponds to a conductivity of 13.2 MeV. The conductivity deviates from the above value if the cross section is further decreased. The reason for this is because the maximum velocity a particle can achieve is the speed of light, so the charge current density has a maximum value $J^{\max} = \frac{4ne}{9}$, where n is the number density of all quarks.

Shown in Fig. D.2 is the time evolution of the normalized charge current density given by its ratio to the saturation vale $J^{\rm sat}$, which is generally smaller than $J^{\max}$. The current density is seen to approache the saturation value during a timescale of about the relaxation time, which is $\frac{3}{2n\sigma}$ [135]. Since the electromagnetic field is strong only during the time interval of about 0.1 fm/c from Fig. D.1, thus all charged particles propagate under the influence of the Lorentz force with essentially no scattering during this time interval. Further decreasing the parton scattering

cross section thus does not affect the current density in the medium.

The above results are in contradiction with those obtained from solving the Maxwell equations and assuming Ohm's law $\mathbf{J} = \sigma\mathbf{E}$ [109, 40]. They thus cast doubt on the validity of Ohm's law when the lifetime of the electromagnetic field is comparable to the relaxation time of the medium. In this case, one needs to take into consideration the spatial and temporal dependence of the electromagnetic field and study the frequency and wave vector dependence of the medium's electric conductivity.